UNIVERSITÉ DE SHERBROOKE
Faculté de génie
Département de génie civil

EXPERIMENTAL INVESTIGATION ON LAP SPLICING OF GFRP BUNDLED BARS IN CONCRETE

ÉTUDE EXPÉRIMENTALE SUR LE CHEVAUCHEMENT DE BARRES D'ARMATURE EN PRFV GROUPÉES DANS LE BÉTON

Thèse de doctorat
Spécialité : Génie Civil

Alireza ASADIANARDAKANI

Sherbrooke (Québec) Canada

Mai 2019

MEMBRES DU JURY

Brahim BENMOKRANE, Prof.
Directeur

Mathieu NUTH, Prof.
Rapporteur et Évaluateur

P. V. VIJAY, Prof.
Évaluateur

Hany TOBBI, PhD
Évaluateur

ABSTRACT

In recent years, glass-fiber-reinforced-polymer (GFRP) rebars have seen a substantial rise in popularity owing to their inherent characteristics, such as an outstanding corrosion resistance, high electromagnetic transparency, and light weight. As with many industrial products, GFRP bars must be subjected to various experimentations in order to verify different aspects of their structural characteristics. However, the splice strength of bundled GFRP bars has received less attention in the past studies, despite the fact that splicing of bundled GFRP bars is inevitable in practice. The lack of the knowledge about this subject has led to the scarcity of relevant design provisions. Thus, the current study was conducted to investigate the strength of spliced bundled GFRP bars and the influencing parameters, such as staggering, number of bars within a bundle, confinement provided by clear cover and transverse reinforcement, splice length, and bar diameter. In this regard, a total of 22 full-scale reinforced concrete beams, measuring 5200 *mm* in length with a rectangular cross section of 300×450 *mm*, were tested under a four-point bending set-up to failure. Three different diameters of sand-coated GFRP bars (No. 4, No. 5, No. 8) were used as a longitudinal reinforcement. The test specimens were cast using a normal-weight ready-mixed concrete with a target compressive strength of 35 *MPa*.

The results indicated that staggering could increase the splice strength and reduce the maximum crack width particularly in the case of three-bar bundles. In addition, the splice strength decreased as the number of bars in a bundle increased, while the general behavior of individual bars within a bundle remained similar to that of single bars. Moreover, increasing the splice length could result in enhancing both the reinforcement stress and force at ultimate load. Furthermore, the larger the bar diameter was, the longer the splice length required to fully develop a given bar stress was. It was also proven that providing transverse reinforcement along the splice zone improved both cracking and failure loads and was very effective in increasing the failure reinforcement stress. Providing transverse reinforcement

was also found to be an effective means of reducing the average crack width within the flexural span regardless of its yield strength. Based on the experimental results, it was recommended that, in lieu of the length-modifier factors available in CSA S806-12 and until more experimental results become available, the design-stress amplification factors of 1.2 and 1.33 could be used for two- and three-bar bundles, respectively. Based on the regression analysis of the experimental results, a semi-empirical model was also derived to predict the contribution of transverse reinforcement to the total splice strength of bundled GFRP bars. Finally, it has been shown that the moment–curvature analysis could provide a reliable prediction of the experimental strain values of reinforcement and concrete.

Keywords: Splice length, bond strength, bundled bars, GFRP bars, reinforced concrete, staggering effect, moment-curvature analysis, flexural deformation, confinement.

RÉSUMÉ

Ces dernières années, l'utilisation des barres d'armature en polymère renforcé de fibres de verre (PRFV) a considérablement augmenté en raison de leurs propriétés intrinsèques telles que leur grande résistance à la corrosion, leur transparence électromagnétique élevée et leur légèreté. À l'instar de nombreux produits industriels, les barres en PRFV doivent faire l'objet de divers essais afin de vérifier différents aspects de leurs propriétés structurales. Cependant, la résistance du chevauchement de barres en PRFV groupées a moins retenu l'attention dans les études précédentes, bien que le chevauchement de barres en PRFV groupées soit inévitable dans la pratique. Le manque de connaissances sur ce sujet a conduit au manque de dispositions de conceptions appropriées. La présente étude a ainsi été menée pour étudier la résistance du chevauchement des barres en PRFV groupées dans du béton et les paramètres qui l'influencent tels que le décalage, le nombre de barres groupées, le confinement fourni par l'enrobage et les armatures transversales, la longueur de chevauchement et le diamètre des barres. À cet effet, un total de 22 poutres pleine grandeur, mesurant 5200 mm de long, de section transversale rectangulaire de 300 × 450 mm, ont été testées en flexion quatre points jusqu'à la rupture. Trois différents diamètres de barres en PRFV recouvertes de sable fin (barres ayant 13 mm, 15 mm et 25 mm de diamètre) ont été utilisés comme armatures longitudinales. Les poutres ont été fabriquées avec un béton normal prêt à l'emploi ayant une résistance à la compression projetée de 35 MPa.

Les résultats ont montré que le décalage pourrait augmenter la résistance du chevauchement et réduire l'ouverture maximale des fissures, en particulier dans le cas de trois barres groupées. De plus, la résistance du chevauchement diminuait à mesure que le nombre de barres groupées augmentait, tandis que le comportement général de barres individuelles d'un groupe restait similaire à celui d'une barre unique. Par ailleurs, l'augmentation de la longueur de chevauchement contribue à l'augmentation de la contrainte dans les armatures et de la force correspondante à l'ultime. En outre, plus le diamètre de la barre était grand, plus la

longueur de chevauchement requise pour développer une contrainte donnée dans la barre était élevée. Il a également été montré que la présence d'armatures transversales le long de la zone de chevauchement améliorait à la fois les charges de fissuration et de rupture et était très efficace pour augmenter la contrainte à la rupture des armatures. La présence d'armatures transversales s'est également révélée comme un moyen efficace pour réduire l'ouverture moyenne des fissures dans la travée en flexion. Sur la base des résultats expérimentaux, il a été recommandé d'utiliser les coefficients d'amplification de contrainte de calcul de 1,2 et 1,3 respectivement pour les groupes de deux et de trois barres au lieu des coefficients de modification de longueur disponibles dans la norme CSA S806-12. Sur la base d'une analyse de régression des résultats expérimentaux, un modèle semi-empirique a également été élaboré pour prédire la contribution des armatures transversales à la résistance totale de chevauchement des barres en PRFV groupées. Enfin, il a été démontré que l'analyse moment-courbure pourrait fournir une prévision fiable des valeurs expérimentales de déformations des barres d'armature et du béton.

Mots clés: Longueur de chevauchement, résistance d'adhérence, barres groupées, barres de PRFV, béton armé, effet de décalage, analyse moment-courbure, déformations en flexion, confinement.

Acknowledgments

First and foremost, I would like to offer my sincerest gratitude to my supervisor, Prof. Brahim BENMOKRANE, for his great wisdom, expert guidance, extensive encouragement and constructive criticism during the course of my PhD at the University of Sherbrooke.

I am very thankful to all of those who I have had the pleasure to work with during this research project. I would like to thank Dr. Abolfazl ESLAMI for his assistance with laboratory work, for extended discussions during preparation of journal papers, and for his willingness to help in every possible way. I would also like to acknowledge Dr. Ahmed FARGHALY for his expert advice and assistance during testing of the specimens and for his valuable comments and suggestions during drafting the papers. I am also very grateful to the members of my thesis committee, Prof. Mathieu NUTH, Prof. P. V. VIJAY and Dr. Hany TOBBI, for their valuable comments and suggestions on my PhD thesis.

Special thanks to the technicians of our research group, Marc DEMERS, Jérôme LACROIX and Steven MACEACHERN, for their help and technical assistance during casting and testing of the specimens.

Je souhaite transmettre mes sincères remerciements aux professeurs de langue française au centre des langues de l'Université de Sherbrooke, particulièrement Vicky POIRIER, Marie-Maude CAYOUETTE PAPINEAU, Catherine DUMONT et Julie BABIN de m'avoir aidé à réaliser mon rêve de maîtriser le français et de m'avoir beaucoup appris sur le Québec et la culture québécoise. Ces personnes m'ont inspiré pour atteindre un niveau de français supérieur à celui auquel j'aspirais. Je me sens extrêmement privilégié d'avoir été leur élève.

I would like to thank all my Sherbrooke friends, Yulia, Eli, Mojgan, Bahar, Yasin, Mahdi, Sahar, Bahman, Amir and Girish, for their love, laughter, encouragement, and understanding; for all our coffee breaks, drinks, conversations, long nights; and for simply being there for me whenever I needed a friend. These people supported me all the way

through my PhD and became a big part of my life. I am also grateful to Jacob and Paul, my French speaking buddies, for encouraging me to learn French. I would also like to send my thanks to all my Iranian friends scattered around the world. Thank you for your thoughts, well-wishes, prayers, phone calls, texts and visits.

Most importantly, I owe a dept of gratitude to my family – my parents, my sister, my brother, my brother-in-law and my niece – whose infallible love and continuous encouragement are with me in whatever I pursue. This accomplishment would not have been possible without my parents. They are the most important people in my world, and I dedicate this thesis to them.

TABLE OF CONTENTS

LIST OF TABLES

LIST OF FIGURES

CHAPTER 1 INTRODUCTION

1.1. General Background

The corrosion resistance of FRP composites has resulted in a significant boost in their application in construction industry, particularly in Canadian environment. Apart from being corrosion resistant, FRP bars offer other inherent advantages such as a high electromagnetic transparency and light weight. The former has introduced them as a superior reinforcement in certain buildings such as magnetic resonance imaging (MRI) units in hospitals, while the latter has led to lower labor cost by facilitating and expediting the construction. Constraints in the reinforcement bar length due to transportation, demand overlapping of reinforcing bars in practice. Moreover, arrangement of heavy reinforcement necessitates bundling of rebars within a section. To provide reinforced concrete (RC) structural integrity, the section where rebars are spliced needs to provide a strength equal to or greater than that outside the spliced zone. This is possible by providing an adequate lap splice length to sustain the design stress of reinforcement developed at the critical section (i.e. end of the spliced zone). Estimating the adequate length, requires profound understanding of the bond mechanism between a reinforcing bar and concrete as well as the major parameters affecting this mechanism. Moreover, the bond strength of reinforcing bars in concrete environment is a critical parameter that controls the serviceability, cracking behavior, and ultimate capacity of RC members.

Despite the necessity of bundling in practice and the importance of bond between reinforcing bars and surrounding concrete, only one study —conducted by Aly et al. (2006a)— investigated the bond behavior of spliced bundled FRP bars. Their study comprised nine full-scale beam specimens reinforced with bundled bars spliced in the same section. Based on their results, the development length of individual bars within a bundle might be equal to

that of a single bar, increased by 60% for a two-bar bundle, and 100% for a three-bar bundle (Aly et al., 2006a). This conclusion raised questions regarding the reliability of the current provisions stipulated in CSA S806-12 (Canadian Standards Association, 2012) and the applicability of the steel-reinforcing-bar provisions specified in ACI 318-14 (ACI Committee 318, 2014) to FRP bars. Nonetheless, the splice arrangement adopted by Aly et al. (2006a) did not comply with code provisions, as all the bars were spliced in the same section. Moreover, as only No. 3 CFRP bars were tested, it is not clear whether or not the conclusions can be appropriate for GFRP bars and other bar sizes. It should also be noted that, to the best of the author's knowledge, no other experimental studies on the bond strength of bundled FRP bars have yet been reported in the technical literature. Moreover, the literature contains no studies on the effect of staggering and confinement provided by transverse reinforcement and concrete cover on the splice strength of GFRP bars.

Therefore, this study was conducted to fill the current gap of knowledge and to provide more information about the splice strength of staggered and non-staggered bundled GFRP bars. Moreover, the results of moment–curvature analysis in terms of the neutral-axis depth as well as reinforcement and concrete strains were compared to the experimental measurements and observations. Furthermore, a relationship was suggested to account for the contribution of transverse reinforcement to the overall bond strength of tension lap splices of bundled GFRP bars.

1.2. Objectives and Scopes

The main focus of this project was to elaborate on the bond behavior of lap-spliced bundled GFRP bars. This was achieved through conducting a total of 22 full-scale beam-splice tests on lap splicing of bundled GFRP bars. The experimental program was comprised of different parameters including splice length, bar diameter, confinement, and bar staggering. The results were analyzed and described in terms of strain in the reinforcing bars, crack width, number of cracks within the splice zone, cracking pattern, maximum load capacity, and mid-span deflection in the companion specimens. A number of specific research objectives are listed below.

1. To investigate the effects of staggering on the bond strength of bundled GFRP bars.
2. To scrutinize the effect of number of bars in bundle on the splice strength.
3. To provide more insight into how the length of splice can affect its performance.
4. To evaluate the effect of bar size on the behaviour of splices of bundled GFRP bars.
5. To investigate and quantify the effect of transverse reinforcement along the length of splice on its strength.
6. To investigate the accuracy of available code provisions and to provide possible modifications to improve their accuracy and safety.
7. To investigate the accuracy of moment-curvature analysis in estimating the reinforcement and concrete strains compared to the experimental measurements.

1.3. Organization of the Dissertation

- CHAPTER 1 provides an outline of the thesis with a brief description of the contents of each chapter
- CHAPTER 2 covers a comprehensive review on the background and past studies conducted to investigate the bond behavior of single and bundled bars. The current code provisions regarding bundled GFRP and steel rebars are also summarized in this chapter.
- CHAPTER 3 presents the geometry and reinforcement details, fabrication procedure, instrumentation details, and testing procedure of the specimens.
- CHAPTER 4 (1st article) evaluates the strength of spliced bundled GFRP bars and the influencing parameters, such as staggering, number of bars in a bundle, and bar size. In addition, the reliability of the design provisions prescribed by CSA S806-12 and the applicability of those recommended in ACI 318-14 for steel reinforcement to GFRP bars are assessed by comparison with the experimental findings. Moreover, the recommendations are made for the splice strength of bundled GFRP bars that could be included in the future versions of design codes for GFRP-reinforced concrete structures.
- CHAPTER 5 (2nd article) provides more insights into the effect of splice length and bar diameter on the splice strength of bundled GFRP bars in unconfined concrete.

The bond behavior of spliced single bars is also compared to that of bundled bars, and a recommendation is made for the design purposes. In addition, the results of moment–curvature analysis in terms of the neutral-axis depth as well as reinforcement and concrete strains are compared to the experimental measurements and observations.

- CHAPTER 6 (3rd article) assesses the influence of confinement provided by transverse reinforcement and concrete cover on the splice strength of bundled GFRP bars. In this regard, comparisons are made in terms of failure mode, crack pattern and width, ultimate load, general load-deflection behavior and splice strength. Moreover, a relationship is suggested to account for the contribution of transverse reinforcement to the overall bond strength of tension lap splices of bundled GFRP bars.
- CHAPTER 7 presents the summary of this study, conclusions, and recommendation for future research.

CHAPTER 2 LITERATURE REVIEW

In order to elaborate on the state-of-the-art of the lap splicing of bundled GFRP bars and to highlight the existing gap in the knowledge, this chapter provides a comprehensive review of the background of bond strength and the technical literature regarding the bond mechanism of bundled bars. In the following, at first the concepts of bond strength including the basics and the nature of bond mechanism, expected failure modes, and lap splice mechanism are introduced. Subsequently, past studies pertaining to the lap splicing of single and bundled FRP reinforcing bars along with those conducted on bundled steel rebars are reviewed in detail. The testing methods, influential parameters, and expected behaviors are also described. The literature presented in each subsection is in ascending chronological order. Finally, a summary of the design recommendations regarding bundled GFRP reinforcement as well as those provided for steel reinforcement in the current versions of the major design codes and guidelines are presented.

2.1. Concepts of bond strength

2.1.1. Bond strength-basics

There must be an appropriate force transfer or bond mechanism between different materials, reinforcement and concrete, in order for them to stick properly together while carrying tensile forces. In other words, bond stress needs to exist when force in reinforcement changes between two points along the bar length. Considering the free body diagram between two points presented in Figure 2-1, where $f_{s2} > f_{s1}$ and summing horizontal forces acting along reinforcement direction results in:

$$(f_{s2} - f_{s1})\frac{\pi d_b^2}{4} = \mu_{avg}(\pi d_b)l \tag{2-1}$$

where, d_b is the bar diameter, l is the bar length, and μ_{avg} is the average bond stress (Wight & MacGregor, 2011). Substituting $(f_{s2} - f_{s1})$ with Δf_s and rearranging Eq. (2-1) give:

$$\mu_{avg} = \frac{\Delta f_s d_b}{4l} \tag{2-2}$$

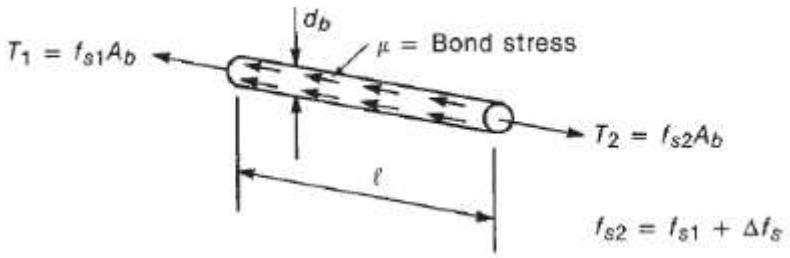

Figure 2-1: Relationship between change in bar stress and average bond stress (Wight & MacGregor, 2011)

Considering Eq. (2-2) for an infinitesimally distance, $l = dx$, the slope of reinforcement force diagram at any point can be expressed as:

$$\frac{df_s}{dx} = \frac{4\mu}{d_b} \tag{2-3}$$

where μ is the true bond (Wight & MacGregor, 2011).

2.1.2. Nature of bond stress in a reinforced concrete flexural member

The tensile force, T, in reinforcement located at flexural crack is calculated as:

$$T = \frac{\mathrm{M}}{\mathrm{jd}} \tag{2-4}$$

where M is the moment at the cracked section and jd is the internal moment arm. For single bar located between the two consecutive flexural cracks along the member (as shown in Figure 2-2), where $T_2 > T_1$ and $M_2 > M_1$, the difference in tensile forces can be determined by:

$$\Delta T = T_2 - T_1 = \frac{M_2}{\mathrm{j}d_2} - \frac{M_1}{\mathrm{j}d_1} \tag{2-5}$$

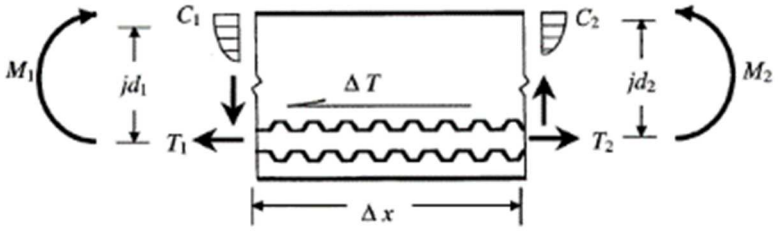

Figure 2-2: Variation in bar force due to change in moment in a flexural member (ACI 408 Committee 2003)

The force equilibrium along the reinforcing bar direction similar to Eq. (2-1) gives:

$$\Delta T = \mu_{avg}(\pi d_b)\,\Delta x. \tag{2-6}$$

Assuming a negligible change in moment arm in section 1 and 2 ($\mathrm{j}d_2 = \mathrm{j}d_1 = \mathrm{jd}$ in Eq. (2-5)) results in:

$$\Delta T = \frac{\Delta \mathrm{M}}{\mathrm{jd}}. \tag{2-7}$$

Substitution of Eq. (2-6) into Eq. (2-7) gives:

$$\frac{\Delta \mathrm{M}}{\Delta x} = \mu_{avg}(\pi d_b)\mathrm{jd}. \tag{2-8}$$

Therefore, average bond stress between the two cracks in a beam can be expressed as:

$$\mu_{avg} = \frac{\mathrm{V}}{(\pi d_b)\mathrm{jd}}. \tag{2-9}$$

and thus:

$$\mathrm{U} = \frac{\mathrm{V}}{\mathrm{jd}} \tag{2-10}$$

in which V is the shear acting on the section and U is the bond force (ACI 408 Committee, 2003; Wight & MacGregor, 2011). In Eq. (2-9), if there are more than one bar acting in tension, bundled bars, the term (πd_b) may be replaced by sum of exposed perimeters of reinforcing bars, $\sum o$, as presented by:

$$\mu_{avg} = \frac{\mathrm{V}}{\sum o\,\mathrm{jd}} \tag{2-11}$$

Eqs. (2-9) and (2-10) indicate that the average bond stress or bond force is proportional to the amount of shear acting on a section. The bond force in Eq. (2-10) was used in the design of RC flexural members for many years (ACI 408 Committee, 2003).

As mentioned earlier, the amount of tensile force in reinforcement at flexural cracks can be determined using Eq. (2-4). At the points between these cracks, however, forces are shared between uncracked concrete and reinforcement. Consequently, interpreting bond force as a proportion of shear force acting on section is inaccurate. At these points, the bond force is a function of tension force variation along the reinforcement bar, $U = dT/dl$ (ACI 408 Committee, 2003). Adopting this concept, actual bond force changes in amount and even in direction from point to point in-between flexural cracks as depicted in Figure 2-3 (ACI 408 Committee, 2003; Darwin et al., 2011).

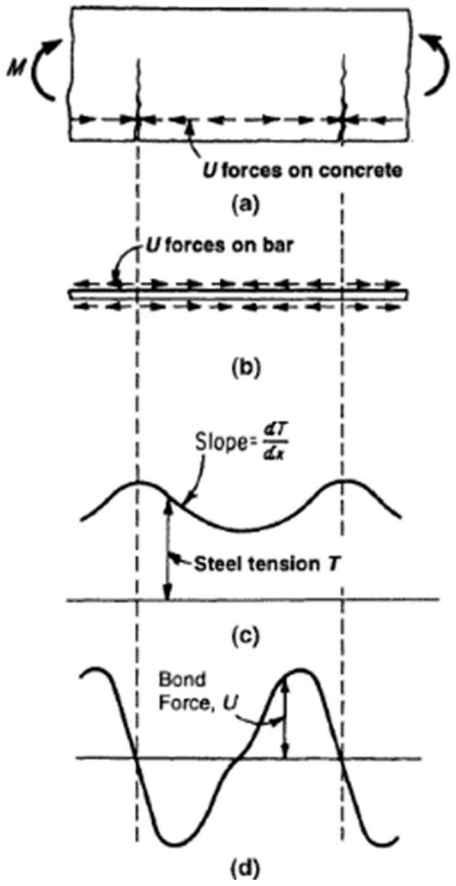

Figure 2-3: The real distribution of bond forces along the length of a bar: (a) cracked concrete section; (b) bond stress acting on bar; (c) variation of tensile force; and (d) variation of bond force along bar (Darwin et al., 2011)

Until the 1971 versions of ACI 318 Building Code, bond stress, u, was calculated as the average bond force, U, per unit perimeter of reinforcing bar:

$$\mathrm{u} = \frac{\mathrm{U}}{\sum o} = \frac{\Delta \mathrm{T}}{\Delta l \sum o} = \frac{\Delta f_s A_b}{\Delta l \sum o} = \frac{\Delta f_s d_b}{4\Delta l} \tag{2-12}$$

where A_b is the area of bars and Δf_s is the change in the bar stress along the length of Δl (ACI 408 Committee, 2003). Taking Δf_s as the yield stress, f_y, and Δl equal to the development length, l_d, of steel reinforcing bars, Eq. (2-12) can be re-written as Eq. (2-13) and be used for the design purposes.

$$\mathrm{u} = \frac{f_y d_b}{4 l_d} \tag{2-13}$$

The maximum permitted bond force, in SI units, according to ACI 318-63 (ACI Committee 318, 1963) may be determined as (ACI 408 Committee, 2003):

$$u = 20\frac{\sqrt{f_c'}}{d_b} \leq 5.52\ MPa\ (in\ SI\ units). \tag{2-14}$$

Replacing Eq. (2-14) into Eq. (2-13), rearranging it and considering incremental factor of 1.2 to account for the reduced bond strength of closely spaced bars which is attributed to the interaction of splitting cracks, results in:

$$l_d = 0.019 A_b \frac{f_y}{\sqrt{f_c'}}\ (in\ SI\ units). \tag{2-15}$$

This equation was then used for calculation of the development length in ACI building code from 1971 to 1995 (ACI 408 Committee, 2003). In 1995 and succeeding versions, however, ACI building code committee utilized a semi-empirical equation which better represents the bond behavior of rebars (ACI 408 Committee, 2003).

2.1.3. Bond mechanism

In general, in deformed bars, there are three mechanisms that provide the bond force transfer between reinforcement and surrounding concrete: a) chemical adhesion between the bar and surrounding concrete, b) friction forces caused by the roughness of the interface and bar-

concrete slip, and c) mechanical interaction or bearing arising from the textures or profile of the reinforcing bar surface as illustrated in Figure 2-4 (ACI 408 Committee, 2003).

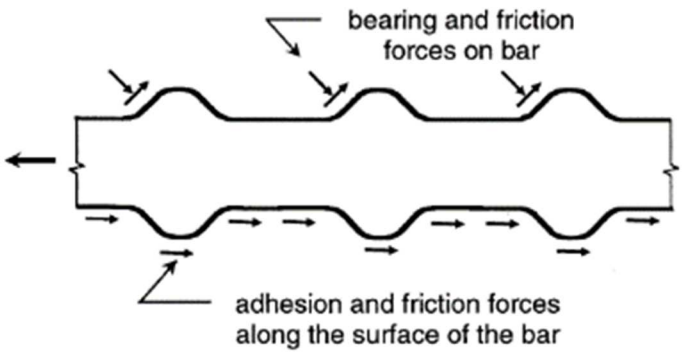

Figure 2-4: Mechanisms for bond force transfer between reinforcement and surrounding concrete (ACI 408 Committee, 2003)

When a plain bar is loaded in tension, its diameter decreases slightly depending on its Poisson's ratio. Consequently, the chemical adhesion and friction which play the most important roles in the bond strength of plain bars are lost (Wight & MacGregor, 2011). That is why plain bars are not permitted to be used as flexural reinforcement.

The force transfer between a deformed bars and concrete is somehow different than that of a plain bar. Once slip occurs between a deformed bar and concrete, the chemical adhesion is lost. Afterward, the bearing forces play the most important role in bond transfer mechanism. Although the friction force can also be considered as a major component in force transfer, its contribution would be reduced by increasing the slip (ACI 408 Committee, 2003). As a result of stress transfer from deformed bars to concrete by interlocking mechanism (bearing forces), the resultant force is exerted to the concrete at an inclined angle with respect to the bar axis (Figure 2-5 (b)). This inclined force may cause two force components acting on concrete, a longitudinal and a radial (Figure 2-5(c)). The former component acts along the bar length which secure the bar from being pulled out of the concrete while the latter component acts perpendicular to bar length which can eventually cause splitting of the surrounding concrete (Figure 2-5 (d)).

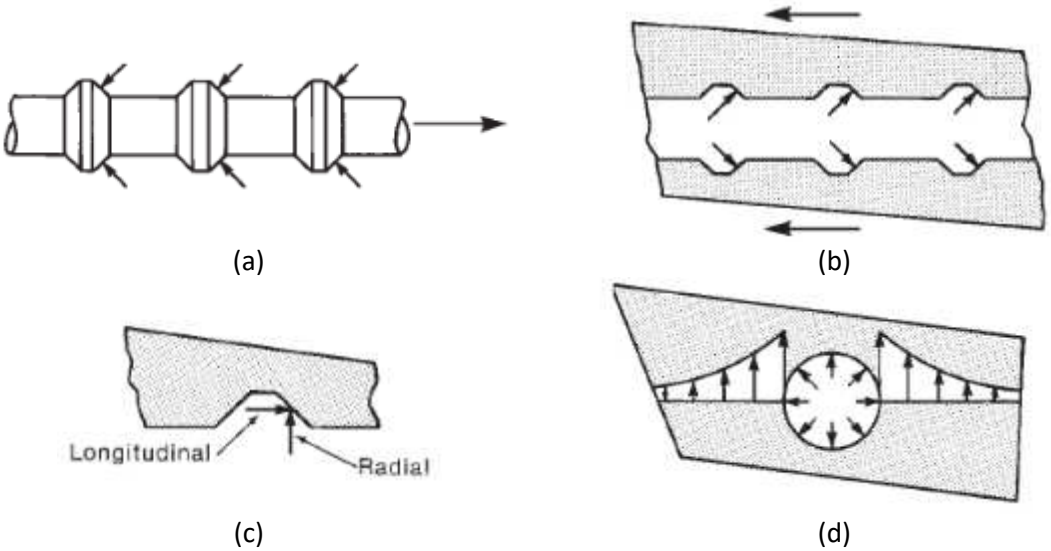

Figure 2-5: Inclination of bond forces in interlocking bond transfer mechanism: (a): inclined forces on bar; (b) inclined forces on concrete; (c) radial and longitudinal components of force on concrete; and (d) Radial component on concrete and splitting stresses on a section through the bar (Source: (Wight & MacGregor, 2011) rearranged).

If adequate confinement is provided to allow the longitudinal component to be larger than the shear capacity of concrete located between successive deformations on bar, the reinforcement may be pulled out of the concrete. On the other hand, if this component exceeds the shear capacity of reinforcement, which can be the case for FRP bars, the deformations or coating may be peeled off as shown in Figure 2-6 (Retika et al., 1997). However, if the radial force exceeds the tensile resistance providing by the surrounding concrete, splitting cracks may appear and propagate in-between the bars and concrete cover (Tepfers, 1982; Tepfers & De Lorenzis, 2003).

The FRP surface deformation peeling was observed in most of the pullout tests performed in the literature (Larralde & Silva-Rodriguez, 1993; Pecce et al., 2001; Achillides & Pilakoutas, 2004). A combination of the surface deformation peeling and concrete shearing was reported in the splitting failure of GFRP RC specimens (Mazaheripour et al., 2013), in the pullout test of GFRP bars (Tepfers et al., 1998), and in beam-splice specimens with progressive pullout failure (Harajli & Abouniaj, 2010). No damage on the surface of FRP bars was observed after splitting failure in the research conducted by Pay et al. (2014).

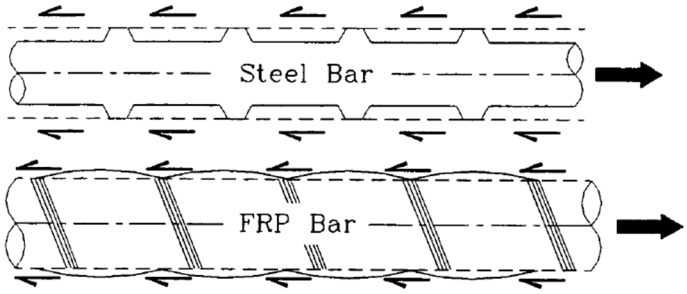

Figure 2-6: Pullout failure in steel and FRP bars (dashed lines shows shearing either concrete or surface of FRP bars (Retika et al., 1997)

2.1.4. Modes of failure

It could be interpreted from the previous section that there can be two general modes of bond failure: a) the pullout mode of failure as a result of high longitudinal force, and b) the splitting mode of failure attributed to the high radial force. The latter is the most probable mode of failure in structural members (ACI 408 Committee, 2003).

Normally, splitting cracks tend to develop along the shortest distances. Thus, the splitting mode of failure can occur with different formations depending on the side and bottom cover thicknesses (C_s and C_b, respectively) and bar spacing ($\acute{S} = 2C_s$) as shown in Figure 2-7. In the case where $C_b > C_s$, the splitting cracks develop along a horizontal plane at the level of the bars. This failure is categorized as "side splitting failure". In the case where $C_s > C_b$, longitudinal cracks form vertically through the concrete cover before development of splitting cracks along the horizontal plane at the level of the bars. This failure is categorized as "face-and-side splitting failure". When $C_s \gg C_b$, the longitudinal cracks form prior to inclined cracks which form "V-notch failure" (Orangun et al., 1975). In lap splices, the failure mode and splitting cracks are identical to those for single bars except that the hypothetical cylinder would be oval shape as indicated in Figure 2-8 (Orangun et al., 1975). Examples of face- and side-splitting modes of failure observed by Mosley et al. (2008) for lap-spliced FRP bars are shown in Figure 2-9.

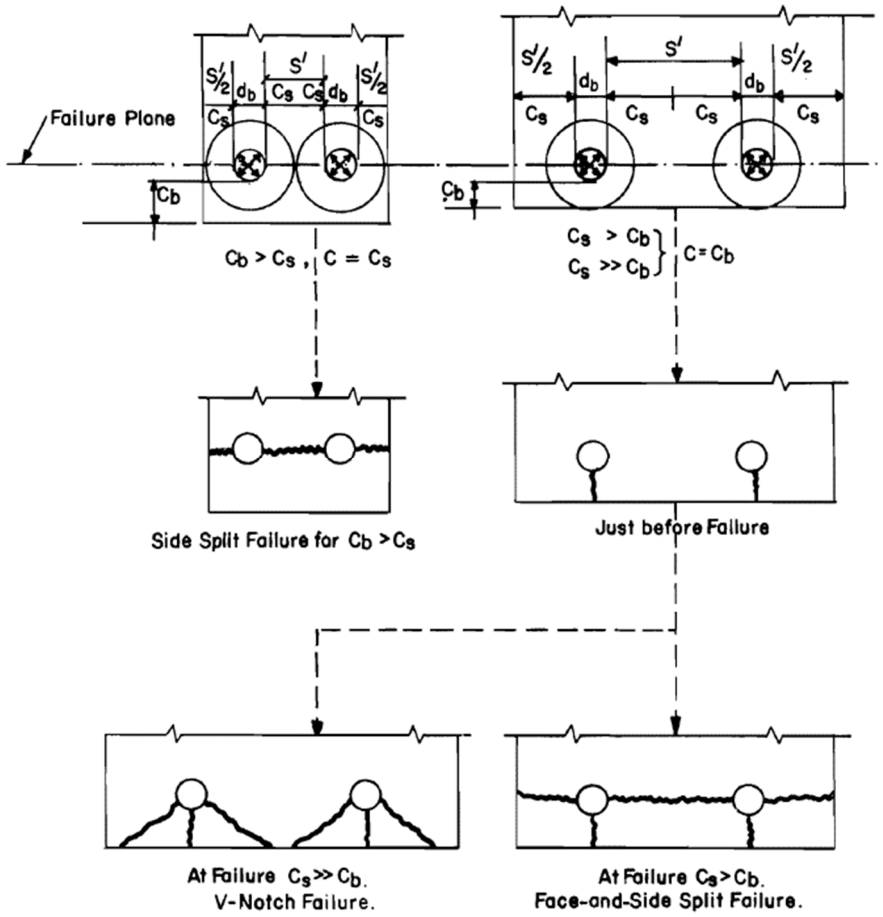

Figure 2-7: Different splitting mode of failure (Orangun et al., 1975)

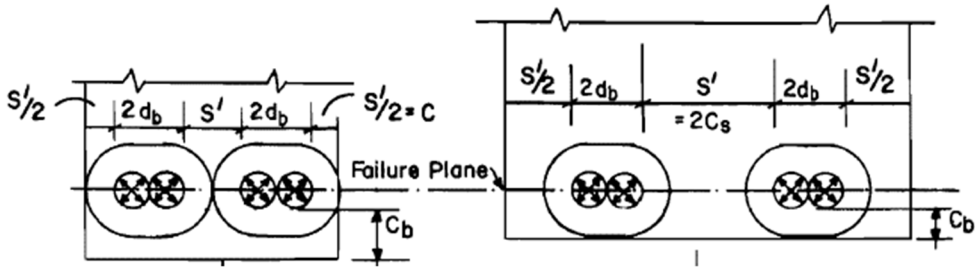

Figure 2-8: Oval shape hypothetical cylinder for lap-spliced bars (Orangun et al., 1975)

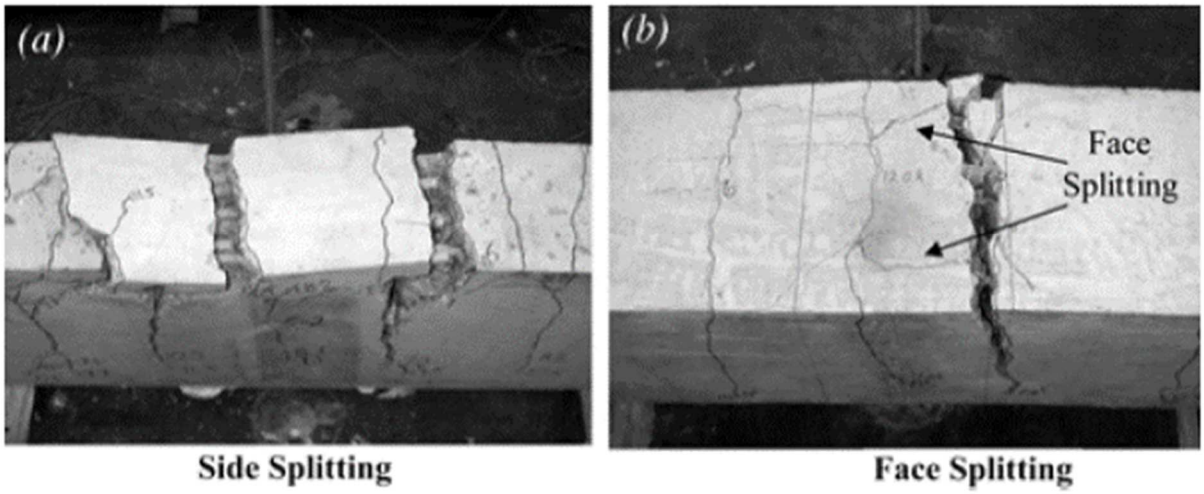

Figure 2-9: The face- and side-splitting modes of failure observed by Mosley et al. (2008)

2.1.5. Analysis of bond splitting load

A simple analytical approach can be utilized to describe the influential factors in splitting loads. As discussed earlier, the radial component of bond force, acting on hypothetical concrete pipe thickness (shown in Figure 2-10), is opposed by the tensile strength of the effective cover (pipe thickness). A free body diagram of tensile stress affecting this hypothetical concrete pipe is depicted in Figure 2-10 (b). The concrete non-linear tensile stress distribution on either side of the bar balances the pressure caused by radial component of bond force. This non-linear stress distribution may be simplified to a linear one as shown in Figure 2-10 (c) (Wight & MacGregor, 2011). Balance between forces along a length of l of the free body diagram shown in Figure 2-10 gives:

$$\frac{p d_b l}{2} = K\left(c_b - \frac{d_b}{2}\right) f_{ct} l \tag{2-16}$$

where p is the vertical pressure due to the radial component of bond stress, f_{ct} is the concrete tensile strength, and K is the average to maximum concrete tensile strength ratio ($K = 0.5$ for triangular distribution). Therefore:

$$\mathrm{p} = \left(\frac{c_b}{d_b} - \frac{1}{2}\right) f_{ct} \tag{2-17}$$

Assuming an inclination angle of $45°$ for the interlocking bond forces shown in Figure 2-5 (b) and (c), the value of vertical and horizontal components of bond stress are equal, thereby the average bond stress ($\mu_{avg,u}$) equals vertical pressure (p). By replacing $f_{ct} = 6\sqrt{f_c'}(in\ psi)$ in Eq. (2-17) average bond stress could be determined as:

$$\mu_{avg,u} = 6\sqrt{f_c'}\left(\frac{c_b}{d_b} - \frac{1}{2}\right) \tag{2-18}$$

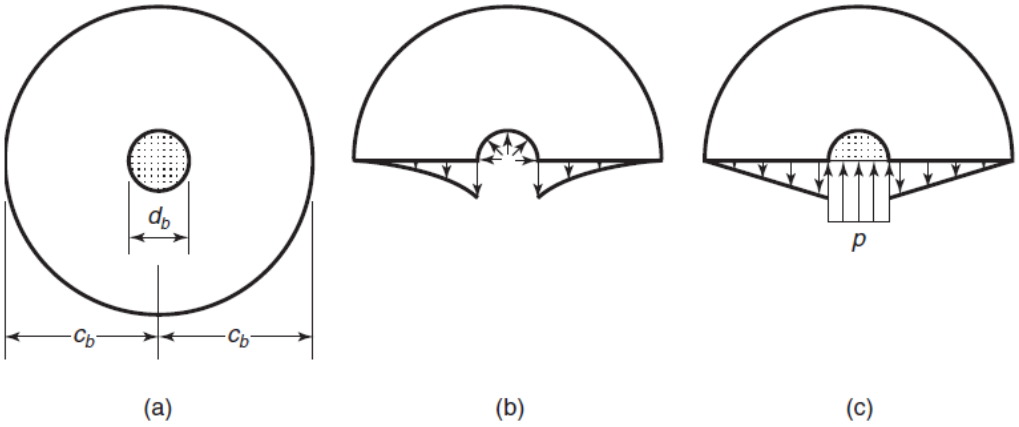

Figure 2-10: Hypothetical concrete cylinder subjected to bond stress (Wight and MacGregor 2011)

Rearranging Eq. (2-13) and substituting $\mu_{avg,u}$ with u in Eq. (2-18), the development length, l_d, can be determined as:

$$l_d = \frac{f_y d_b}{24\sqrt{f_c'}\left(\frac{c_b}{d_b} - \frac{1}{2}\right)} \tag{2-19}$$

It is worth mentioning that in derivation of Eq. (2-19), the following simplifications were made: 1) triangular tensile strength distribution in the concrete, 2) inclination angle of 45°for bearing force, 3) evenly distribution of forces over development length instead of concentric forces at the bar deformation, and 4) using average bond stress instead of real one with in-and-out bond stresses (Wight & MacGregor, 2011).

2.1.6. Introduction to lap splices

In construction practice, splicing of bars is made by overlapping two discontinuous bars (in the case of single bar splice) where the bars are placed either in contact together or not. In such case, the concrete between two adjacent bars convey force in-between them. The force transfer mechanism between lap-spliced bars and the zigzag cracking pattern as a result of this force transfer are illustrated in Figure 2-11 (Wight & MacGregor, 2011).

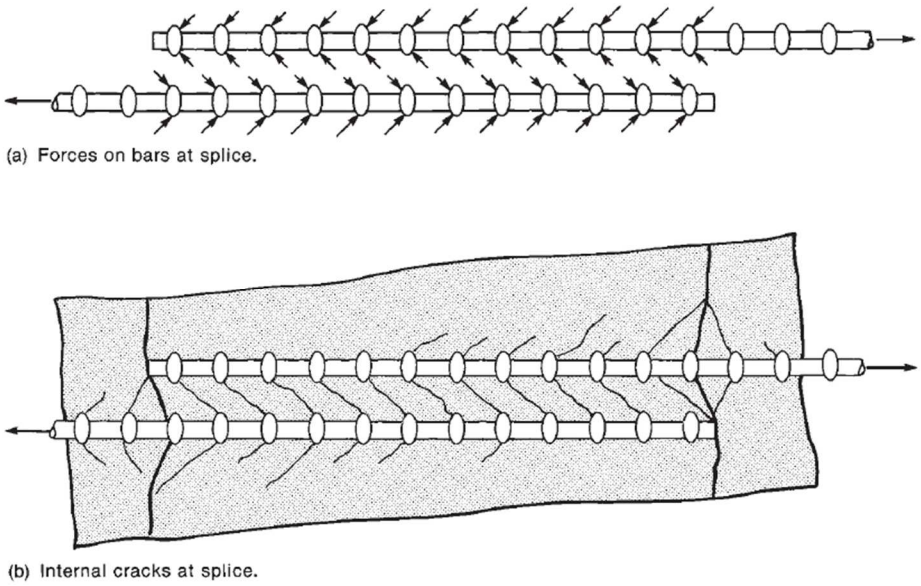

Figure 2-11: Force transfer mechanism between lap-spliced bars (Wight and MacGregor 2011)

2.2. Experimental studies on lap splicing of single FRP reinforcing bars

Different test methods have been used in the previous studies to evaluate the bond strength of reinforcing bars. They include the pullout, the notched beam, the hinged beam, the beam end, and the beam-splice test. Since the nature of bond response is different in each test method, each method may lead to a different bond strength. The pros and cons of these test methods are the decisive factors in selecting the appropriate one.

Although the pullout test is easy, quick and inexpensive to perform, the state of stresses in concrete cannot represent the level of stress in real flexural members. This is mainly attributed to the fact that in the pullout test, the concrete around reinforcing bar is under compression while the reinforcing bar is in tension. Additionally, this test method cannot signify the curvature effects in real structural members. Therefore, it can overestimate the bond strength. In the beam-splice test method, however, concrete around the bar sustain the same stress state as real application while the effects of curvature are also considered. However, performing this test on large-scale specimens is expensive in comparison with other test methods. Since beam-splice test method has been successfully used by other researchers in the past, this test method is adopted herein. This section provides a review of the technical literature related to the bond strength of single FRP rebars performed using the beam-splice test method.

Tighiouart et al. (1998) performed 16 large-scale beam-splice tests to investigate the effects of bar diameter and splice length on the bond strength of GFRP rebars. Their experimentation comprises two different bar diameters (12.7 and 15.9 *mm*) and five splice lengths. The specimens were tested under four-point bending setup with a shear and moment spans of 1000 *mm*. All specimens were confined within the splice region using 11.3 *mm* plain steel stirrups provided at 80 *mm* intervals. To check the applicability of the provisions stipulated in ACI 318-95 for the development length of steel reinforcement to FRP rebars, different splice length as a portion of the development length were investigated in their experimental tests. The obtained results indicated that the development length recommended by ACI 318-95 should be increased by 30% to be used for GFRP rebars. They also observed that the ultimate capacity of GFRP reinforced beams was achieved in specimens with splice length of 1.6 times ACI 318-95 development length. Moreover, it was indicated that increasing the splice length would lead to reducing the average bond stress.

Aly et al., (2006b) reported twelve full scale beam-splice tests to scrutinize the influence of splice length and bar diameter on the bond strength of confined GFRP and CFRP rebars. Their reinforcing bars consisted of 9.5 and 12.7 *mm* sand-coated CFRP and 15.9 and 19.1 *mm* sand-coated GFRP rebars. All beams were $250 \times 400\ mm$ in cross-section and 4200

mm in length, with a moment span of 3600 *mm*. The dimensions of their specimens along with an illustration of a specimen is shown in Figure 2-12. A number of strain gages were attached at two ends and along the splice length to measure strain values in FRP bars.

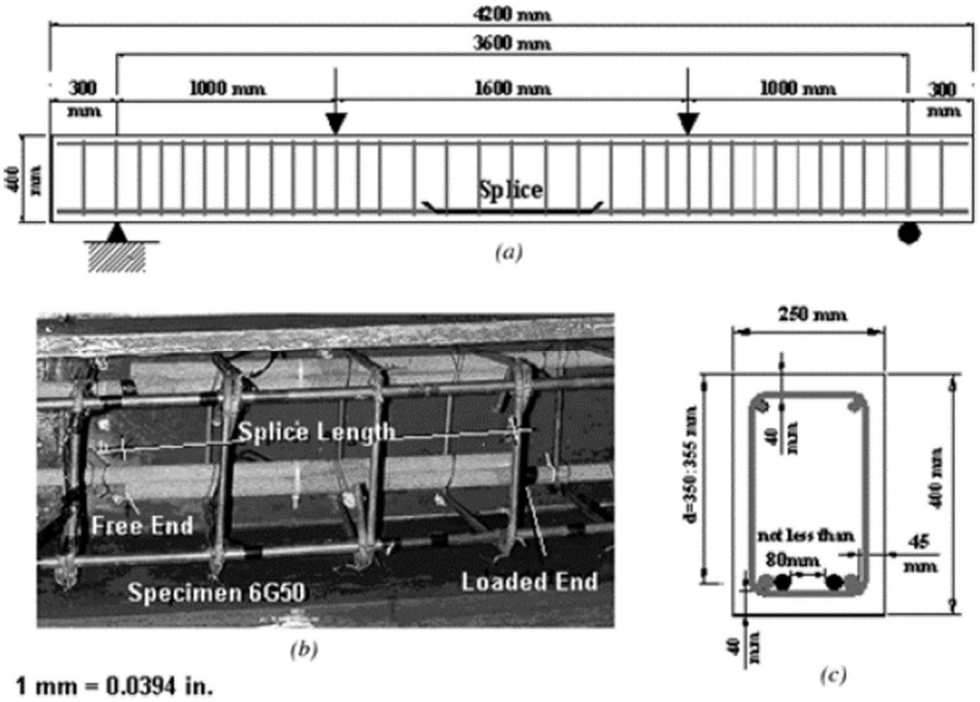

Figure 2-12: Splice beam test set-up (Aly et al., 2006b)

Based on their experimental observations, the bar stress was concentrated at the loaded ends at early stages of loading while it was eventually distributed linearly over the confined splice length. Consequently, they concluded that the bond stress distributes evenly through the confined splice region just before failure. This finding is in contrast whit what reported by Aly (2005) for the splices of the unconfined specimens. Moreover, it was found that the ultimate strength analysis could be used to predict the stresses at the end of splices. They also recommended that appropriate space should be provided between the end of splice length and concentrated load to avoid shear failure. Their experimental results confirmed the rupture of tensile reinforcement in No.3 CFRP, No.5 GFRP, and No.6 GFRP reinforced specimens with 800 *mm*, 500 and 700 *mm*, and 1100 *mm* splice lengths, respectively. Analyzing the maximum theoretical stress in FRP reinforcement, calculated based on maximum moment recorded during test, showed that the maximum bar stress at the end of

splice length would increase linearly by increasing in splice length. Therefore, it was stated that the critical splice length can be calculated using limited number of tests as the relationship between splice length and tensile stress in reinforcement is linear. As a result, they recommended the splice lengths of $70d_b$, $90d_b$, $40d_b$, and $50d_b$ for No.3 CFRP, No.4 CFRP, No.5 GFRP, and No.6 GFRP rebars, respectively.

The effects of reinforcement type, bar spacing, and splice length on the bond strength of spliced reinforcements in beam were also studied by Mosley et al. (2008). Their experimental program was comprised of a total of 12 specimens categorized in three series. Four types of No.5 (16 *mm*) reinforcing bar including two types of GFRP, one type of AFRP as well as the conventional steel rebar were utilized. The splice lengths were 457 *mm* and 305 *mm*. As their intention was to evaluate the lower bond strength, all of their specimens were without transverse reinforcement in the splice region. Figure 2-13 provides the geometric and reinforcement details of the test specimens while their test setup is shown in Figure 2-14.

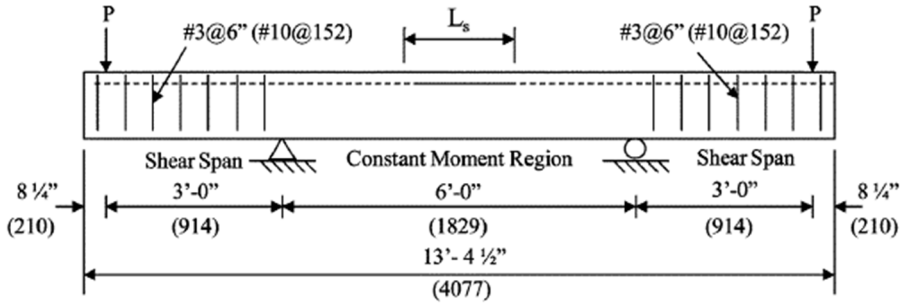

Figure 2-13: The geometric dimensions and reinforcement details of beam specimens tested by (Mosley et al. 2008)

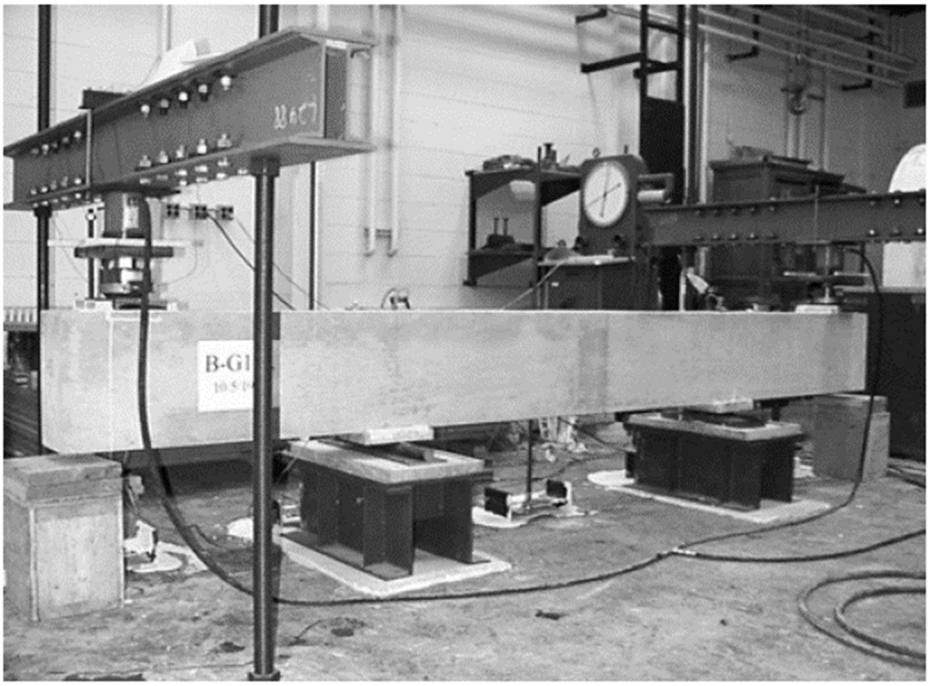

Figure 2-14: Test setup used by (Mosley et al. 2008)

Based on their experimental observation, the crack depths and widths in FRP reinforced sections were larger than those of steel reinforced sections with the same reinforcement ratio. This was found to be attributed to the lower elastic modulus of FRP reinforcements. They also stated that the cracked section analysis method was an accurate approach to calculate the neutral axis depth of FRP reinforced section. Moreover, no correlation was found between the average crack width and type of reinforcement. In addition, they deduced that the enhancement in the average bond stress was proportional to the square root of increment in the splice length independent of reinforcement material (22% increase in average bond stress achieved in specimen with 50% longer splice length). They also concluded that increasing the clear spacing was more influential in achieving a higher average bond stress for FRP reinforced than steel reinforced members. Comparing relative bond strengths between companion specimens, Mosley et al. (2008) inferred that there was a correlation between the bar stiffness, particularly the elastic modulus, and the average bond stress. From their results, FRP reinforcement could attain approximately 50% of the average bond stress developed by its corresponding steel bar. Moreover, they stated that the surface condition of FRP rebars is an ineffectual parameter in the average bond strength and crack width. Finally,

to evaluate the accuracy of the design guidelines, they compared the results obtained from their experimental program with those calculated by the provisions specified in ACI 318-08 (ACI Committee 318, 2014) and ACI 440.1R-06 (ACI Committee 440, 2006). Based on their evaluation, the safety margins provided by both codes were dependent on the development length and was decreased as the splice length increased. Accordingly, they noted that the design equations suggested in ACI 440.1R-06 could result in an unconservative splice length for FRP rebars with higher splice lengths.

Harajli and Abouniaj (2010) carried out an experimental investigation to examine the effects of surface condition (thread wrapped and ribbed), concrete cover (15 and 25 *mm*), splice length ($15, 20, and\ 30d_b$), and cross-sectional area of transverse reinforcement within the splice length on the bond strength of 12 *mm* GFRP bars. Toward this, a total of 12 GFRP RC specimens were tested using the beam-splice test method. Four additional companion steel specimens were also included for comparison purposes. Their test setup, geometric dimensions, and reinforcement details are shown in Figure 2-15. Two concrete compressive strengths of 48 and 52 *MPa* were used in their experimentation. In order to verify the maximum bar forces, a series of strain gages were attached to the reinforcement at both ends of the splice length outside the splice region in the constant moment zone. The bar stresses were also calculated by cracked section analysis. The authors also performed a number of pullout tests to investigate the bond stress-slip response of GFRP bars.

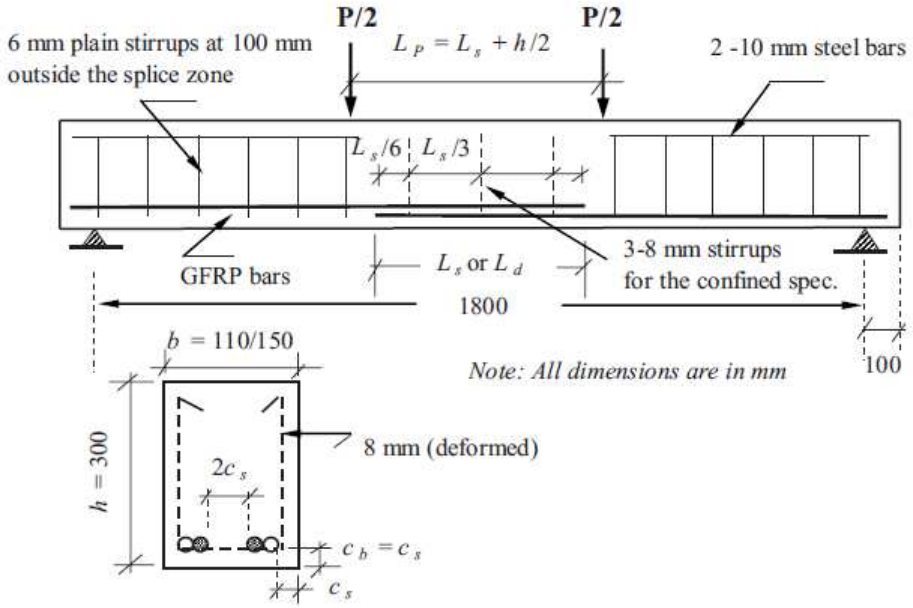

Figure 2-15: Test setup, geometric dimensions, and reinforcement details of specimens tested by (Harajli and Abouniaj 2010)

Two different types of bond failure were observed depending on the surface condition regardless of the splice length and concrete cover. All of the ten specimens reinforced with ribbed bars as well as four companion steel beams experienced a sudden splitting failure while all of the six specimens reinforced with thread wrapped GFRP bars sustained a progressive pullout failure. Based on their experimental results, ribbed GFRP rebars resisted 42-67% of their maximum tensile strength while thread wrapped GFRP bars resisted 27-36%. In addition, the confinement had a significant effect in increasing the bond strength of FRP bars. For the ribbed GFRP bars, implementing confinement could lead to a 31% increase in the maximum bond force. Likewise, the maximum bond force of the thread wrapped GFRP bars in the confined specimens was enhanced by 13%. Moreover, increasing the concrete cover from 1.25 to $2d_b$ slightly improved the bond strength of the ribbed GFRP bars, while it had no effect on the bond strength of the thread wrapped bars. On the contrary, the same increase in the concrete cover for the steel rebars resulted in a 30% increase in the bond strength. Consequently, they stated that the bond strength of steel rebars was more dependence on c/d_b than GFRP rebars.

To evaluate the bond strength of GFRP bars in unconfined concrete Choi et al. (2012) performed the beam-splice test for 29 beams and 10 one-way slabs. Among them, one beam and one slab were cast without splice, and four beams were reinforced with conventional steel rebars for comparison purposes. The concrete compressive strength ranged from 23 to 30 *MPa* and from 26.5 to 33.2 *MPa* for beam and slab specimens, respectively. Four types of GFRP bars, manufactured in USA, Canada, and Korea used in their beam specimens while all slap specimens were built utilizing only one type of GFRP, manufactured in Korea. The GFRP bars had a diameter of 12.7 *mm*, whereas their companion steel reinforcement had a diameter of 13 *mm*. Two cross-sectional dimensions of $300 \times 400\ mm$ and $240 \times 320\ mm$ with 2 to 5 bars spliced at the middle were investigated in the beam specimens. All slab specimens had an identical cross-section of $750 \times 250\ mm$ with 5 or 9 spliced bars. Splice lengths ranged from $10\ to\ 70d_b$ and $45\ to\ 75d_b$ in beam and slab specimens, respectively. Strain gauges were applied at both ends of the splices in all specimens while strain distribution along the splice length was only investigated in four steel specimens.

As expected, Choi et al. (2012) observed that the bond strength of GFRP rebars was lower than that of companion steel rebars. Moreover, they have reported that an increase in the splice length led to a decrease in the average bond stress. They also concluded that using a smaller cover or bar spacing could reduce the average bond strength. Additionally, they concluded that changing the surface conditions of GFRP rebars had no considerable effects on the bond stress. Their experimentation also indicated that the bond strength of GFRP rebars was more dependence on c/d_b for larger splice lengths. Moreover, their experimental results in terms of tensile force of rebars and neutral axis depth agreed well with the results calculated from the theoretical cracked section analysis. Based on their experimental results, it was also shown that ACI 440-1R-06 (ACI Committee 440, 2006) overestimated the bond stress of GFRP bars by 15%. Finally, they proposed two equations for the average bond strength of GFRP bars in unconfined concrete. One of which was derived by adopting the basic bond strength relationship suggested by Orangun et al. (1977), while the other was expanded based on the model suggested by Darwin et al. (1996). By comparing the results of the Orangun-based equation with those of equation stipulated in ACI 440.1R-06, they

concluded that ACI 440-1R-06 might provide unconservative results for the unconfined splices with cover thickness smaller than $2.5d_b$.

In another experimental study conducted by Esfahani et al. (2013), the bond strength of GFRP bars was investigated performing 13 beam-splice tests. The specimens were reinforced with three different diameters of 10, 12 and 16 *mm* with two surface configurations of either sand coated or ribbed GFRP bars. The beams were tested with the splice length ranging from $18 \text{ to } 33.3\mathrm{d_b}$. Two target concrete compressive strengths of 40 and 70 *MPa* were used in their experimental program. All beams were $150 \times 200\ mm$ in cross-section and 2300 *mm* in length with the shear and moment span of 700 and 600 *mm*, respectively. Conventional 6 *mm* steel stirrups with intervals of 80 *mm* were provided as shear reinforcement throughout the shear span in all specimens. In confined specimens, 8 mm stirrups were also added within the constant-moment span. Confinement stirrups were spaced at 20 and 80 *mm* in the sand-coated and at 50, 100, and 150 *mm* in the ribbed GFRP RC specimens. In both cases, one specimen was cast without transverse reinforcement within the constant-moment span.

Esfahani et al. (2013) calculated the average bond stresses. Based on their results, the bond strength was not considerably changed when the concrete compressive strength increased from 41 to 70 *MPa* (Esfahani et al., 2013). Moreover, their results showed a decrease in bond strength with an increase in bar diameter for specimens reinforced with the ribbed bars and a splice length of 400 *mm*. They concluded that the effect of transverse reinforcement was contingent on the surface treatment. While the transverse reinforcement could increase the bond strength of ribbed bars, it had no noticeable effect on the bond strength of sand coated bars. This phenomenon was attributed to the different relative rib area of these surface deformations, akin to that found by Darwin et al. (1996) for steel reinforcements. However, Esfahani et al. (2013) observed that in specimens reinforced with sand-coated GFRP rebars, the failure mode changed from the splitting in a specimen without transverse reinforcement to pullout in the companion specimens with transverse reinforcement.

Esfahani et al. (2013) have implemented Monte Carlo method to determine a reduction coefficient for ACI 440.1R-06 equation for bond strength. To augment their database, results

of the unconfined specimens failed by splitting in preceding studies (Aly, 2005; Mosley et al., 2008; Harajli & Abouniaj, 2010), were also used and this coefficient was calculated to be around 0.59. The same method was then used to determine a coefficient for contribution of transverse reinforcement in bond strength. Towards this, all confined specimens from preceding studies (Tighiouart et al., 1998; Aly, 2005; Harajli & Abouniaj, 2010) failed by splitting were utilized to evaluate transverse reinforcement contribution factor (f_R) depending on surface condition. Finally, the derived relationship was compared with the design equation of ACI 440.1R-06. Accordingly, it was found that ACI 440.1R-06 equation could result in an unconservative development length for members with a small amount of transverse reinforcement or without transverse reinforcement while it could be conservative for those with a large amount of transverse reinforcement.

Pay et al. (2014) carried out 41 beam-splice tests on a variety of reinforcing bars. They evaluated the influences of different variables including splice length, surface condition, modulus of elasticity (E), axial rigidity (AE), and bar casting position on bond strength. In their experimental study, the cross-sectional depth was kept constant at 406 *mm*, while the cross-sectional width was designed to keep the clear spacing of 25.4 *mm* and top and bottom clear cover of 38 *mm* within the splice region in all specimens. No transverse reinforcement was provided within splice region, while No.3 steel stirrups were provided throughout the shear span. Their GFRP bars had two different sizes of 15.9 *mm* (No.5) and 25.4 *mm* (No.8) with three different surface conditions (fabric texture, sand and wrapped, and sand coated). All of their CFRP bars had a diameter of 15.9 *mm* (No.5) with two different surface conditions (fabric texture and sand coated) while deformed steel reinforcements of 15.9 *mm* and 25.4 *mm* were also included. To distinguish between the effects of elastic modulus and axial rigidity, No.8 (25.4 *mm*) hollow steel bar with the same contact surface area and elastic modulus were also included. Specimens comprised a broad range of splice lengths (12 to $86d_b$) and concrete compressive strength varied from 27.7 to 37.7 *MPa*. Three strain gages were attached at the ends of the splice in sixteen specimens, while no strain gages were applied in the rest of FRP reinforced specimens as the theoretical strain values were in good agreement with the experimental measurements. Therefore, the reinforcement stresses at failure, f_{test}, calculated using crack section analysis were used to determine the average

bond stress throughout the splice length. Bar stresses were normalized by the forth root of the compressive strengths, as endorsed by ACI 408R-03 (ACI 408 Committee, 2003).

Based on the obtained results of Pay et al. (2014), it was observed that the specimens reinforced with rebars possessing a greater elastic modulus could reach a higher loading capacity with a lower deflection at failure. Consequently, the effects of splice length on the bond strength were found to be a function of elastic modulus of reinforcement. This was because, for the same increment in splice length, steel reinforcements exhibited more improvement in the bond strength followed by CFRP and GFRP rebars. In addition, for No.5 and No.8 bars with the same splice lengths, the relationship between reinforcement force at failure and axial rigidity followed approximately a linear trend. As an important conclusion, they noted the dependence of the splice length on the axial rigidity of reinforcement. Based on this conclusion, they stated that a unified development length equation could be developed irrespective of reinforcement material (steel or FRP). According to their findings, the modulus of elasticity is an important parameter in bond strength as it increased linearly by modulus of elasticity. Moreover, according to their experimental outcome, the difference between the bond stress values among different surface conditions were relatively small, confirming negligible influence of surface conditions of GFRP rebars.

Based on Pay et al. (2014), the bond strengths decreased on average by 7% in top-casted specimens in comparison with their companion bottom-casted specimens (equivalent to a top bar factor of 1.08). However, the bond strength decreased by 22% in No.5 specimens with short splice length of 305 *mm* (equivalent to a top bar factor of 1.28). Therefore, they recommended a top bar factor of 1.3 for FRP reinforcement and stated that the current factor of 1.5 advised by ACI 440.1R-06 is unduly very conservative. Furthermore, the current equation of ACI 440.1R-06 for development length of GFRP bars was found to be unconservative even by considering the current top bar factor of 1.5 particularly for longer splices. It is also interesting to note that, in their closure in discussion paper by Martí-Vargas, (2015), Pay et al. stated that average bond stress was not an appropriate measure to evaluate the bond strength of rebars and, therefore, they have utilized bond strength (maximum bar force or bar stress) in their calculations.

In another experimental study, Zemour et al. (2018) carried out 11 full-scale beam-splice tests on GFRP and steel reinforcing bars to evaluate the influences of different parameters including splice length ($20d_b$ and $40d_b$), concrete type (normal and self-consolidating concrete (SCC)) and material type (GFRP and steel) on the bond strength. The beams measured 4300 *mm* in length, with a cross-sectional width of 250 *mm*, and a cross-sectional height of either 400 or 600 *mm*. The clear testing shear span was 1100 *mm*, and the constant-moment span was 1500 *mm*.

Zemour et al. (2018) stated that the moment-curvature analysis can be used to predict the bar stress at the end of splices. Based on their experimental results, the concrete type (NC and SCC) had negligible effect on the load capacity, crack pattern, failure mode, and load–deflection response of GFRP RC beam. The bond strength of reinforcing bars in SCC was slightly (on average 5%) lower compared to normal concrete. Beam height had no effect on the splice strength on GFRP bars with relatively long splice length. They have also found that the average bond strength decreased with increasing splice length. At early loading stages, the distribution of reinforcement strain along the splice length was nonlinear. Similar to other researchers, the bond strength of GFRP reinforcement was found to be lower than steel reinforcement (by 26%). Finally, they assed the accuracy of current code provisions available for splice strength of GFRP bars in concrete and concluded that the JSCE-97 (Japan Society of Civil Engineers, 1997) provisions could result in the highest safety margin, while those of CSA S6-14 (Canadian Standards Association, 2014a) could yield nonconservative predictions in the majority of their specimens. Therefore, they suggested that the bar-surface factor provide by CSA S6-14 might need revision and suggested the value of 1.4 for this factor.

2.3. Previous studies on bundled FRP reinforcement

Very limited research is available on the bond behavior of spliced bundled FRP bars. To the best of the author's knowledge, the only study on the bond behavior of spliced bundled CFRP reinforcing bars was performed in the Department of Civil Engineering at University of Sherbrooke, QC, CA by Aly et al. (2006a). Their variables were type of bundle and splice

length. Their experimental program consisted of nine large-scale concrete beams tested under four-point loading. The concrete compressive strength at the time of testing ranged from 41 to 49 MPa. All of their specimens were reinforced with 9.5 *mm* sand coated CFRP bars with a bottom clear cover of 40 *mm*. In addition, 8 *mm* steel transverse reinforcement spaced at 150 *mm* was provided throughout the splice length. All beams were $160 \times 480\ mm$ in cross-section and 4200 *mm* long with the shear and moment spans of 1000 and 1600 *mm*, respectively. Strain gages were attached on rebars at the end of splices in all specimens as well as through the splice length in some specimens to measure the strain variations in FRP bars. Figure 2-16 demonstrates the geometric and reinforcement details of their test specimens.

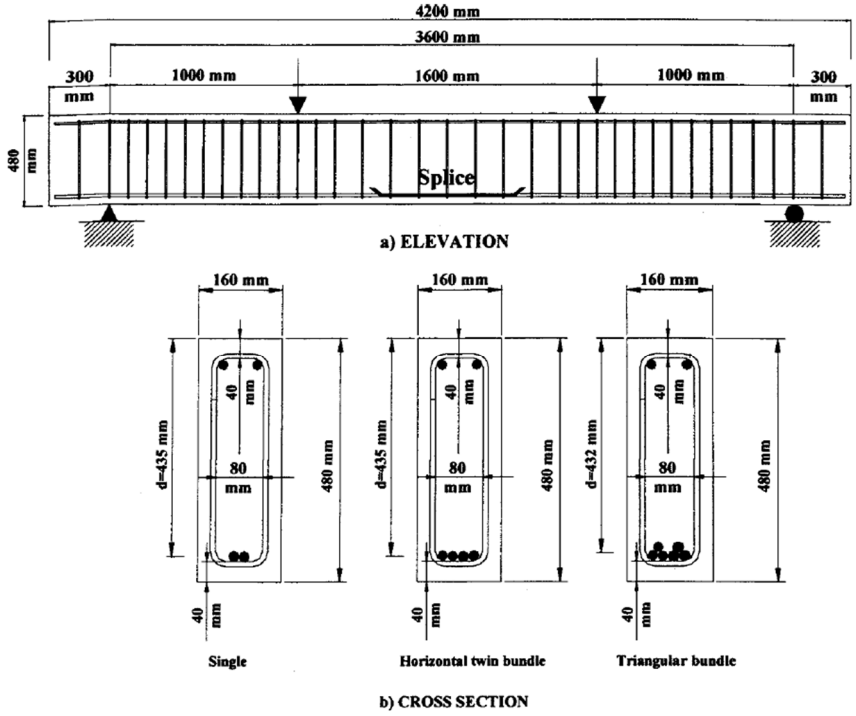

Figure 2-16. Test setup and geometric dimensions of specimens tested by (Aly et al., 2006a)

Based on their experimental observations, they deduced that there was a linear relationship between the maximum bar stress at the end of splice length and splice length. Accordingly, they proposed a procedure for calculating the critical splice length of FRP bars requiring at least one experimental test. Similar to Aly et al. (2006b) for confined spliced GFRP bars, they noticed the concentration of bar strain at loaded end at early stages of loading and

approximately linear distribution of strain over the splice length of bundled CFRP bars just prior to failure. Based on their findings, the ultimate strength method was accurate in calculation of bar stresses, concrete strain, and neutral axis depth at the end of splices. Their experimental observations also confirmed the formation of cracks started at the ends of splices. They also pointed out that the average critical bond stresses over critical splice length for single, horizontal twin, and triangular bundles of 9.5 *mm* CFRP bars are 5.55, 4.9, and 4.65 MPa, while their critical splice lengths were estimated to be around $75d_b$, $90d_{be}$, and $95d_{be}$, respectively. In the calculated critical splice length, d_b was the diameter of single FRP bar and d_{be} was the equivalent bar diameter of bundled bars. According to Aly et al. (2006b), the average critical bond strength of GFRP bars was inversely proportional to the equivalent bar diameter for bundled bars. Moreover, they pointed out that for 9.5 *mm* sand coated CFRP bars, the development length of individual bars within a bundle might be equal to that of the single bar, increased by 60% for two-bar bundles, and 100% for three-bar bundles.

2.4. Previous studies on bundled steel reinforcement

This section provides a brief summary of the studies performed to investigate the behavior of bundled steel rebars, providing additional information on general concepts of the bond behavior of bundled bars regardless of the material type of bars.

As early as 1952, Hadley (1952) discussed the advantages and feasibility of using bundled steel bars in RC sections. Successful and satisfactory results were reported on the application of bundled bars. In addition, some successful examples of practical application of bundled bars were explained, while considering some precautions was recommended for marine applications. Moreover, the satisfactory performance of utilizing bundle bars was reported in the precast members.

Hanson and Reifenstuhl (1958) scrutinized the crack width, stress distribution, deflection and ultimate strength of three-bar bundles of No.9 and four-bar bundles of No.6 and No.8 rebars. Their experimental program comprised 10 large-scale beams, including five specimens with bundled as well as five companion specimens with the same reinforcement

but equally spaced rebars as demonstrated in Figure 2-17. Among them six specimens were reinforced with intermediate grade steel while the rest with high strength reinforcing steel bars. The beams were cast so that the tension reinforcing bars were located at the top during one-week curing. Afterwards, all beams were stored upside down until the testing. Crack widths were measured at the axis of longitudinal reinforcement. Eight strain gages were attached to the reinforcement in each beam (as shown in Figure 2-17) to measure strain distributions during the test. Figure 2-18 shows their test setup used for beam test. The ultimate strength and feasibility of splicing bundled bars in columns were also investigated in their study.

According to Hanson & Reifenstuhl (1958), all beams reinforced with intermediate grade steel failed by tension (yielding of the tension reinforcement) with no sign of bond failure. For the specimens reinforced with high strength steel, one reinforced with single bar failed due to yielding of tension reinforcement but after the bar slippage whereas the remainder eventuated by bond failure. Measured steel stresses and deflections through the beam length at different load levels were similar in companion specimens. Based on their calculation, the calculated ultimate loads based on ACI 318-56 were on average by 13% higher than the measured ones in all specimens. No considerable differences were found in the ultimate flexural strength and crack width amongst companion specimens reinforced with bundle and equally spaced single bars. Furthermore, no discrepancies were found between the ultimate bond stresses developed by the bundle and spaced bars when ultimate bond stress was calculated based on the exposed perimeter. Overall, the authors concluded that utilizing bars in bundle had no adverse impact providing a) not more than four bars in contact in each bundle; b) bond stress based on exposed perimeter of bar was not higher than permitted value; c) all bars within bundle were deformed and individually well anchored; and d) transverse reinforcement was used in the area of high bond stress. Accordingly, bundling was a satisfactory detailing procedure for beam-column members.

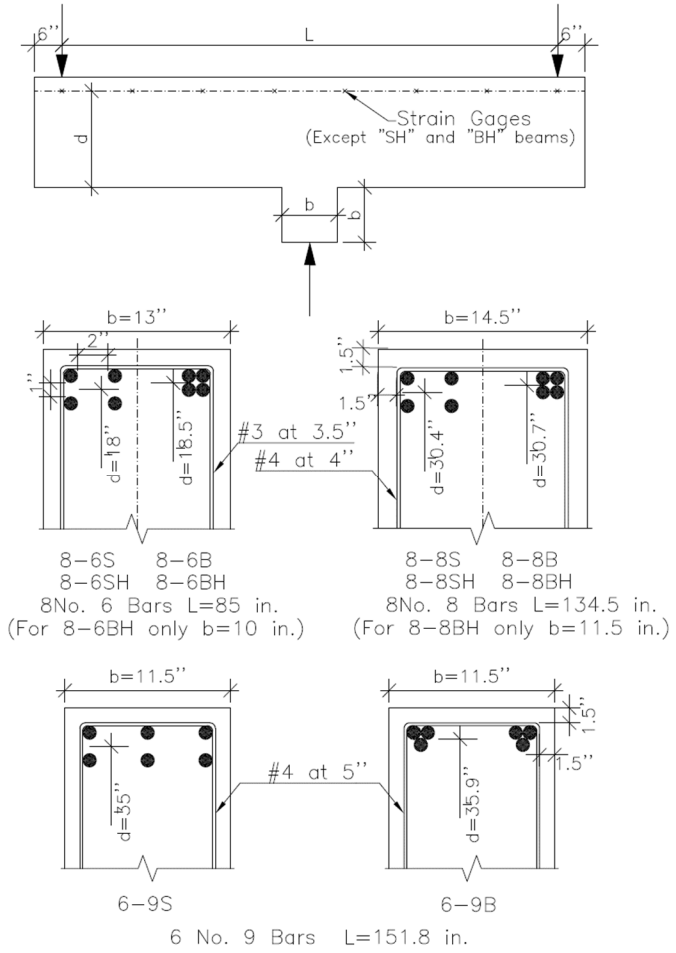

Figure 2-17: Beam sections, reinforcement and loading details (redraw) (Hanson and Reifenstuhl 1958)

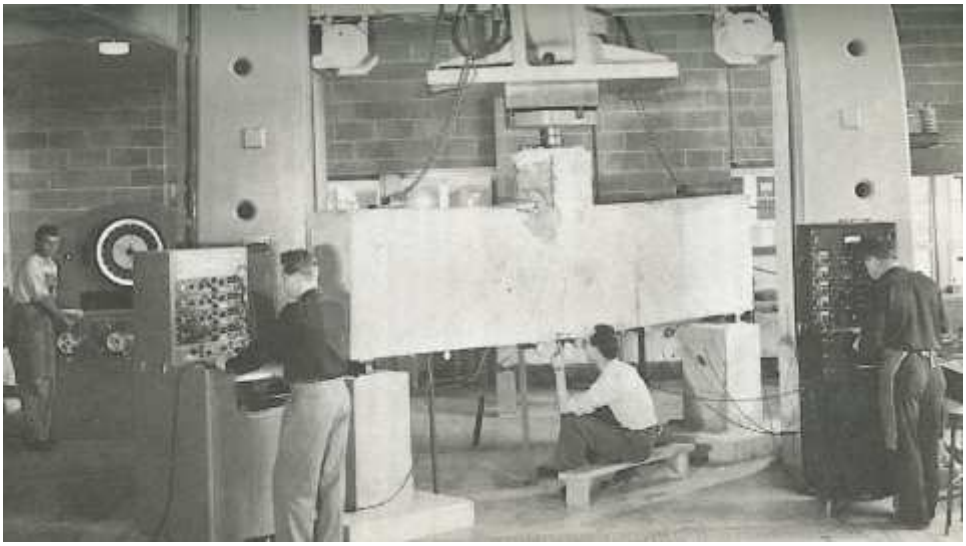

Figure 2-18 Test setup (Hanson and Reifenstuhl 1958)

In another experimental study, Jirsa et al. (1995) explored the effect of several parameters such as casting position, equivalent bar area, number of bars in bundle, and transverse reinforcement on the bond strength and development length of multiple bar bundles arranged in one or two layers. They also investigated the accuracy of calculating development length of bundled bars based on equations developed for single bars. As a common approach in bond evaluation of steel bars, all of their specimens were designed so that bond failure precedes yielding of reinforcement.

Their experimental investigation showed that, in specimens where bars arranged in two layers, the stress in the outer layer was approximately 20% higher than that in the inner layer before peak load. However, after peak load and cracking, the stress in outer layer decreased and transferred to inner layer. After cracking the load began to decrease as stress was transferred from the outer layer to the inner layer. During experimentation, bond failure was observed in both inner and outer planes. Failure mechanisms in both planes were due to splitting forces produced by tension in the anchored bars. Moreover, it was observed that the group of bars in bundle acted as a single unit as evidenced by no relative displacement between bars in bundle after failure. The mean top cast position ratio (bond strength of bottom cast specimens over that of the top cast specimens) of 1.23 with high variation was also calculated for bundle bars which was attributed to weak quality of concrete below top-casted bars. Consequently, they proposed a value of 1.3 or 1.4 as the top casting factor.

Furthermore, they introduced the concept of maximum and minimum exposed perimeter of bundled bars and investigated the accuracy of using each one in average bond strength calculation. Figure 2-19 shows the maximum and minimum perimeters defined by Jirsa et al. (1995). The values correspond to each concept for two, three, and four-bar bundles as a function of the bar diameter (d_b) are presented in Table 2-1. They drew a comparison between the measured bond stresses based on either maximum or minimum perimeter and predicted bond stresses ($u_{test}/u_{Orangun}$). Predicted bond stresses were calculated based on equation provided by Orangun et al. (1977) considering reduction factor of 1.3 for the top-casted bars. Jirsa et al. (1995) also reported that using a maximum and a minimum perimeter for calculating measured bond stress could lead to on average, 15% and 43% higher bond

stresses, respectively. As a noteworthy conclusion, they stated that using a maximum perimeter could better represent the predicted values.

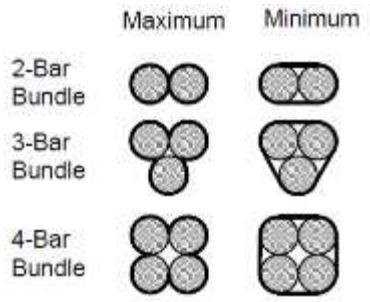

Figure 2-19: Maximum and minimum exposed perimeter introduced by Jirsa et al. (1995)

Table 2-1: Maximum and minimum exposed perimeter as a function of d_b

Bundle size	Maximum perimeter	Minimum perimeter	Dia. of equivalent-bar with same cross-sectional area	Perimeter of equivalent bar	Perimeter of equally spaced bars
2-bar bundle	$2\pi d_b$	$\pi d_b + 2d_b$	$1.41d_b$	$1.41\pi d_b$	$2\pi d_b$
3-bar bundle	$2.5\pi d_b$	$\pi d_b + 3d_b$	$1.73d_b$	$1.73\pi d_b$	$3\pi d_b$
4-bar bundle	$3\pi d_b$	$\pi d_b + 4d_b$	$2d_b$	$2\pi d_b$	$4\pi d_b$

Based on the test results, Jirsa et al. (1995) noted that the presence of a secondary reinforcement could increase the ultimate bond stress by a value ranging from 33% to 107%. They also observed that the equivalent bar, a hypothetical bar with the same cross-sectional area as group of bars in bundle, experienced approximately from 30% to 80% higher ultimate bond stress in comparison with the companion bundled bar. Therefore, it was concluded that use of equivalent bars to evaluate the bond behavior would lead to unconservative results. Furthermore, their experimental results for the three and four-bar bundles showed no consistent trend in stress distribution between bars in bundle placed at the same depth in the section. For the two-bar bundles, however, the stress was distributed evenly between the bars. In the three-bar bundles, they noticed that the average stress recorded in the outer bars was about 16% to 19% lower than that in the inner bars which was not in agreement with expected value form strain compatibility considering higher depth of outer layer. In this regard, they explained that this trend was contributed to the higher confinement provided for the inner bar due to the larger clear spacing and cover provided in the level of inner bars. For the four-bar bundles without transverse reinforcement, however, their recorded stress agreed well with that expected from strain compatibility.

Bashandy (2009) performed 16 four-point bending beam-splice tests aimed at providing a better understanding of bond behavior of bundled bars under tension. In particular, the splice strength of two, three, and four-bar bundles, where all bars were spliced at the same section in the constant-moment span, were compared with their companion specimens reinforced with equivalent rebars. The equivalent rebar had approximately a same cross-sectional area as the group of bars in bundle. Variables included in his experiments were the number of bars in bundle, splice length, total area of bars in bundle, concrete cover thickness, and confinement. All beams have a clear span of 1500 *mm* and top section width of 240 *mm*. The bottom section width was designed to keep side cover, bottom cover, and half of the clear spacing (c) constant in all companion specimens. The dimensions of his test specimens and the test setup are presented in Figure 2-20, while the reinforcement arrangement in cross-sections is schematically shown in Figure 2-21.

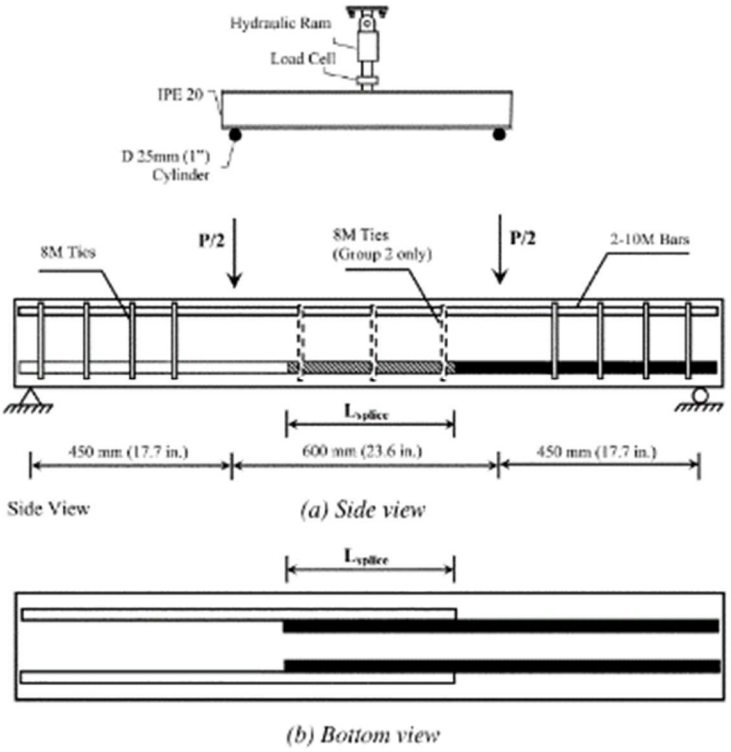

Figure 2-20: Longitudinal reinforcement and loading details of specimens tested by (Bashandy, 2009)

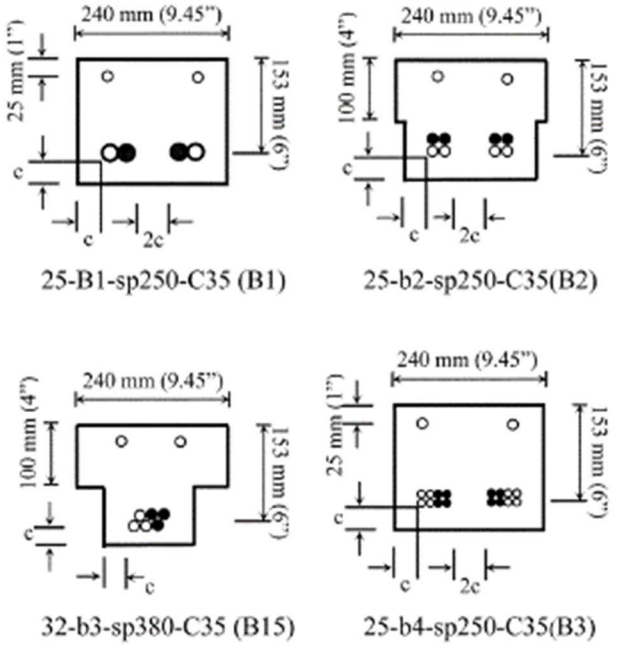

Figure 2-21: Cross-sectional detail of specimens tested by (Bashandy, 2009)

The cross-sectional area of reinforcement in each group of specimens was approximately identical. The specimens in the first four groups were reinforced with two splices of either single No.25, two-bar bundle No.18 or four-bar bundle No.12. However, specimens of the fifth group were reinforced with splice of a pair of either single No.32, two-bar bundle No.22, or three-bar bundle No.18. The steel stirrups of 8 *mm* diameter were also placed at spacing of 10 *mm* in shear span. In order to investigate each variable independently, most of the specimens were designed without stirrups in splice region and all of the bars were spliced at the same section. In the experimental investigation, the spliced lengths were selected to be 10, 12 and 15 times the equivalent bar diameter. The concrete compressive strengths at the time of testing were 28 and 29 *MPa*. Bar stresses were measured by attaching strain gages at the ends and along the splice length.

Based on his experimental results, the cracking and failure pattern were similar between the specimens with bundled bars and those with equivalent single bars. Since every bar in a bundle had the same displacement after failure, it was deduced that the group of bars in bundle could act as a single unit. Although it was not permitted by the design codes, Bashandy (2009) noted that splicing of all bars in a bundle at the same section can be more

practical. Moreover, the stress distribution along splice length at failure followed a similar trend for bundled bars and equivalent bars specimens. Besides, the tendency of stress distribution between bars at the same level in four-bar bundles was not clear, while the stress was equally distributed between bars at the same level in two-bar bundles. As this unclear tendency had also been previously reported by other researchers (Jirsa et al., 1995), it was concluded that flexural test is not appropriate to investigate stress distribution within bars in bundle. It should be noted that a good agreement was observed between the bar stresses measured by strain gages and those calculated by linear cracked section analysis (less that 6% difference). Bashandy (2009) also noticed that bond strength of a group of bars in bundle was similar to that of equivalent single bar meaning that an increase in the exposed perimeter of bundled bars could not improve the bond strength. Furthermore, based on his experimental outcomes, the number of bars in bundle had no significant effect on the maximum load at failure.

His results also confirmed that increasing the splice length by 50% could raise failure loads by 39, 64, and 38% for two-bar bundle, four-bar bundle, and their companion equivalent specimens, respectively. Moreover, increasing the clear cover by 40% could result in failure loads increased by 43, 31, and 29% for the two-bar bundle, four-bar bundle, and their companion equivalent specimens, respectively. When the transverse reinforcement was provided, the failure load increased by from 54 to 60%. Consequently, it was deduced that the effect of splice length, concrete cover, and transverse reinforcement on maximum load at failure was similar for bundled bars and single bars. Moreover, Bashandy (2009) noted that calculation of the required splice length of bars in bundle based on the diameter of single bar was not accurate and an equivalent diameter should be utilized instead. Furthermore, it was observed that bundling had no considerable effect on the maximum load to center deflection ratio which represents beam stiffness.

Cairns (2013) tested 10 large-scale beams to investigate the performance of two and three-bar bundles and to scrutinize the accuracy of ACI 318-08 provisions for lap splice of bundled bars. All of his beams were 3550 *mm* in length and simply supported under four-point loading with a shear and a constant-moment span of 1150 and 1000 *mm*, respectively. All of

the reinforcing bars were staggered within the splice zone, except for those in the two reference beams. Specimens were reinforced with either 12, 16 or 20 *mm* rebars with a splice length of 20 times the bar diameter. Figure 2-22 and Figure 2-23 show the reinforcement layout and test setup details, respectively. Moreover, the 8 *mm* stirrups provided within the splice length (as schematically shown in Figure 2-22) and spaced 300 *mm* on center outside the splice region.

No strain gages were utilized to measure the bar strains. The average stresses at the peak load (f_{su}) at the end of the splice zone were, therefore, calculated using a rectangular stress block for concrete according to Eurocode 2 (BS EN 1992-1-1:2004 2004) considering safety factors of 1.0. The ultimate bond strength (f_{bu}) was also calculated as follows:

$$f_{bu} = \frac{f_{su}}{4(l_b/d_b)} \tag{2-20}$$

where l_b/d_b is the ratio of splice length to the diameter of the single bar.

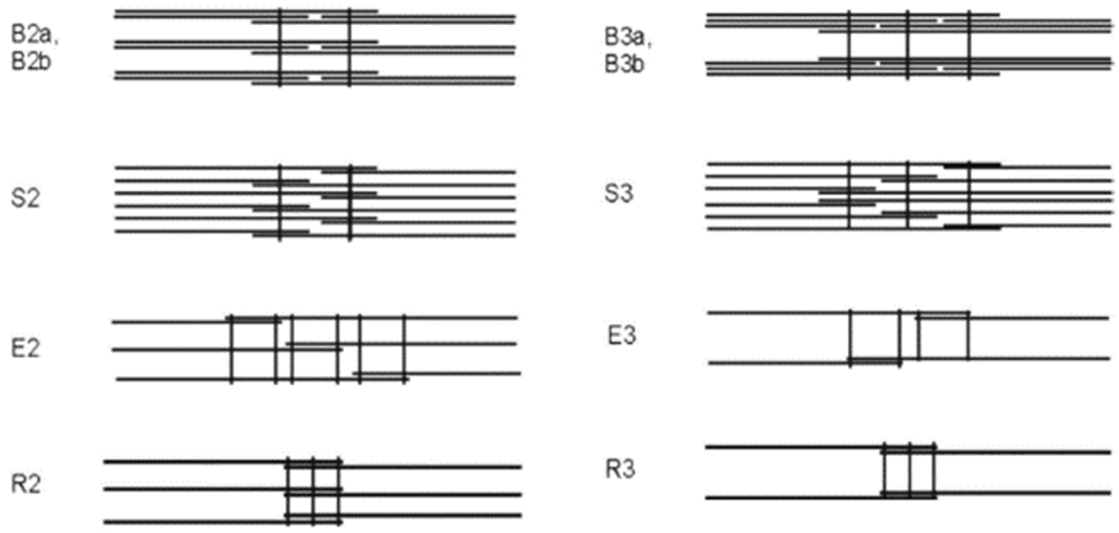

Figure 2-22: Reinforcement layout of the specimens tested by Cairns (2013)

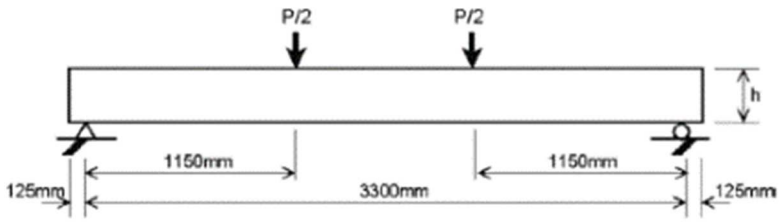

Figure 2-23: Test Setup used by Cairns (2013)

Comparison of the bond strength (average bond stress along the splice length) of individual bar within a bundle (average value of (b2a, b2b) and (b3a, b3b) in Figure 2-22) and that of individually spaced bars in companion specimens with the same amount and size of reinforcement (S2 and S3 in Figure 2-22) revealed that the bond strength of individual bar within a bundle was similar to the spaced bars. Based on the obtained experimental results, Cairns also deduced that the bond strength ratio - the ratio of experimental bond strength to that calculated based on Darwin et al. (2005)- increased as the portion of bars spliced at the same section decreased. Moreover, the deformability index decreased by increasing the percentage of bar staggered at a section. It was also concluded that staggering could reduce the bond strength whether or not bars were bundled. In addition, Cairns noted that the strength of lap splice was not correlated to exposed area of bars in the bundle, yet, controlled by resistance to cracking force due to bond action. Therefore, it was pointed out that underlying concept of ACI 318 provision for increasing splice length due to a reduction in the exposed perimeter might not be justified.

2.5. Bundled bars in design codes

2.5.1. Bundled bars in design codes of FRP RC structures

The corrosion resistance of FRP composites has resulted in a significant boost in their application in construction industry, particularly in Canadian environment. Although inevitable in real practice, there is a scarcity of the available test data on the bond behavior of lap-spliced bundled FRP reinforcing bars. Available experimentations for splice length are restricted to individual FRP bars spliced at the same section which are reviewed in section 2.3. This lack of experimental data has led to the paucity of design provisions in most of international design codes and guidelines (Japan Society of Civil Engineers, 1997; Canadian Standards Association, 2014a; ACI Committee 440, 2015). Only CSA S806-12 (Canadian Standards Association, 2012) stipulates some recommendations for the bundled GFRP bars which are mostly similar to those for the steel bars despite the differences in their inherent behavior.

2.5.1.1. CSA S806-12 (Canadian Standards Association 2012)

According to Clause 9.3.4 of CSA S806-12 (Canadian Standards Association, 2012), the development length of each individual bar within a bundle may be provided by the manufacturer. This clause also restricts the number of bars in a bundle to three. In addition, Clause 9.3.5 of this code states that the diameter of each individual bar within a bundle may not be greater than 25 mm for GFRP and 20 mm for AFRP and CFRP bars. Furthermore, Clause 9.3.6 points out that "*individual bars in a bundle cut off within the span of flexural members shall terminate at different points at least 45 times bar diameter apart*". This criterion is similar to Clauses 7.4.2.3 of CSA A23.3-14 and 25.6.1.4 of ACI 318-14, except that the steel design codes demand at least $40d_b$ stagger. Similar to Clause 25.6.1.6 of ACI 318-14, Clause 9.3.7 notes that "*where spacing limitation and clear concrete cover are based on bar size, a unit of bundled bars shall be treated as a single bar with a diameter giving an area equal to the total area of the bundle under consideration"*. Although according to Clause 9.3.4 of CSA S806-12, the development length of individual bars within a bundle shall be provided by the manufacturer, Clause 9.10.4 notes that "*lap splices of bundled bars shall be based on the lap splice length required for individual bars within a bundle (1.3 times of development length based on Clause 9.10.3), increased by 20% for a two-bar bundle and 30% for a three-bar bundle. Individual bar splices within a bundle shall not overlap"*.

2.5.2. Bundled bars in steel RC structures design codes

2.5.2.1. ACI 318-14 (ACI Committee 318 2014)

According to Clause 25.6.1.1 of ACI 318-14, "*groups of parallel reinforcing bars bundled in contact to act as a unit shall be limited to four in any one bundle*". Based on this criterion only two- and three-bar bundles can be spliced, in this way four bars or less would be in contact within the splice length. This clause was intended to prevent bundling more than two bars in the same plane (ACI Committee 318, 2014). Consequently, the typical shapes in cross-section are triangular, L-shaped, or square-shaped patterns for three or four-bar bundles as commentated in clause R25.6.1.1. Moreover, Clause 25.6.1.3 of this code states

that "*bars larger than No. 11 (35M) shall not be bundled in beams*". The latter restriction is a practical limit for application to building size members as commentated in Clause R25.6.1.3. In addition, Clause 25.6.1.4 points out that "*individual bars within a bundle terminated within the span of flexural members shall terminate at different points with at least* $40d_b$ *stagger*". This criterion is based on bond research by ACI Committee 408 (ACI Committee 318, 2014). In addition, Clause 25.6.1.5 of ACI 318-14 states that the development length of bundled bars shall be at least equal to that of individual bars being developed increased by 20% for the bundle of three and 33% for the bundle of four. As stated in Clause 25.4.10.1 of ACI 318-14, the development length of bundled FRP bars can be reduced by ($A_{f,required}/A_{f,provided}$) where reinforcement in a flexural member exceeds that required by analysis, except where anchorage or development for design strength is specifically required for the reinforcement.

According to Clause 25.6.1.7, lap splice length of bundled bars may be equal to that of individual bars within bundle increased according to Clause 25.6.1.5. This provision was aimed at considering reduction in exposed perimeter of bars when making part of bundle as commentated in R25.6.1.7. Taking into account these provisions, lap splice length of bundled bars may be at least equal to that of individual bars increased by 20% and 33% for two- and three-bar bundle (which comprise, respectively, a total of three and four bars in touch within splice length), respectively. Additionally, an equivalent diameter of the entire bundle derived from total area of bars may be used for determining the spacing and cover values. As noted in clause 25.6.1.6, "*a unit of bundled bars shall be treated as a single bar with an area equivalent to that of the bundle and a centroid coinciding with that of the bundle. The diameter of the equivalent bar shall be used for* d_b *in (a) through (e): (a) Spacing limitations based on* d_b*; (b) Cover requirements based on* d_b*; (c) Spacing and cover values in 25.4.2.2; (d) Confinement term in 25.4.2.3; and (e)* ψ_e *factor in 25.4.2.4"*. Furthermore, according to Clause 25.5.2.1 of ACI-318-14, in all cases in which more than 50% of bars are spliced at a section the splice length should be increased by at least 30 percent.

2.5.2.2. AASHTO LRFD-12 (AASHTO-LRFD, 2012)

AASHTO LRFD-12 (AASHTO-LRFD, 2012) provisions regarding development length and lap splicing of bundled bars are presented in clause 5.10.3.1.5 and 5.11.2.3 which are the same as ACI 318-14.

2.5.2.3. CSA A23.3-14 (Canadian Standards Association, 2014b)

The provisions of CSA A23.3-14 (Canadian Standards Association, 2014b) are mostly similar to those of ACI 318-14. However, Clause 12.4 points out that for two-bar bundles the development length of individual bars should be increased by 10%. The CSA A23.3-14 provisions regarding splicing of bundled bars seem confusing. Although it is not explicitly mentioned in the code, increased development lengths for three- and four-bar bundles seems to be attributed to reduction in effective perimeter of bars in bundle. However, the reason behind 10% increment in the development length of two-bar bundle is still unclear. According to Clause 12.14.2.2, however, the splice length of individual bars within bundle should be that of individual bar increased by 10%, 20%, and 33% for two, three, and four-bar bundles. It should be noted that stating the term “two-bar bundle” in this Clause reveals that terms “two-, three-, and four-bar bundles” refer to the number of bars in bundle outside splice region. Otherwise, two-bar bundle would be similar to in-contact splice of individual bars. Considering this terminology, splicing of four-bar bundles (which comprises a total of five bars in touch within splice length) is permissible which is not in agreement with Clause 7.4.2.1 where the total number of bars in a bundle is restricted to four. Therefore, considering underlying assumption for development length of bundled bars described in Clause 12.4, the splice length of individual bars within bundle of two and three bars should be increased by 20% and 33% respectively. At least making some clarification regarding splice length of bundled bars in new version is recommended.

2.5.2.4. Eurocode2 (BS EN 1992-1-1:2004, 2004)

According to Clause 8.9.1 of Eurocode2 (BS EN 1992-1-1:2004, 2004) bars in bundle should be from the same type and grade. The number of bars in bundle is limited to four for vertical

bars in compression and for bars in a lapped joint. Otherwise, the number of bars in bundle is limited to three. Only lap splicing of two- and three-bar bundles is permissible according to Clause 8.9.3. For design purpose, entire bundle is replaced with a notional bar having the same area as total area of bundle. In the case where all bars in bundle are from the same size, the notional bar diameter is calculated as follows:

$$d_n = d\sqrt{n_b} \leq 55\ mm \tag{2-21}$$

where d_n and d are the notional and individual bar diameters, respectively, and n_b is the number of bars in bundle. Equivalent bar diameter may be used to calculate clear distance between bundles and clear cover, but these values may be measured from external contour of the bundle of bars. According to Clause 8.9.2, if the equivalent diameter of bundle of bars is not greater than 32 mm, the entire bundle could be cut at the same section. Otherwise, the bundled bars should be staggered as shown in Figure 2-24. In staggered anchorages, if individual bars within a bundle are staggered by more than 1.3 times of its basic required anchorage length (l_b), the anchorage length may be based on individual bar diameter. Otherwise, an equivalent diameter may be used in calculation of splice length.

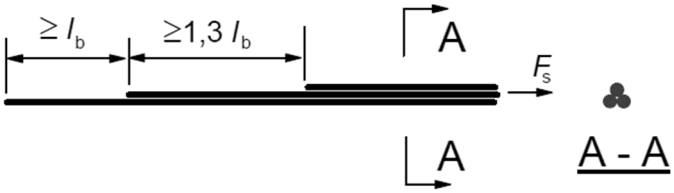

Figure 2-24: Anchorage of widely staggered bars in bundle (BS EN 1992-1-1:2004 2004)

According to Clause 8.9.3, lap splices may be staggered in most cases. Only one bar within two- or three-bar bundles may be spliced at a section, and splices may be staggered by at least 1.3 times lap splice length of the single bar. However, for two-bar bundles with notional diameter not greater than 32 *mm*, the entire bundle may be spliced at the same section. In this case, the splice length may be calculated based on notional bar diameter. As recommended by Clause 8.7.3, the lap length, whether for individual or bundled bars, may be increased by $\alpha_6 = \sqrt{\rho_1/25}$, where $1 \leq \alpha_6 \leq 1.5$ and ρ_1 is the percentage of bar lapped within $0.65l_0$ from center of lap length.

CHAPTER 3 Experimental Program

A total of 22 full-scale concrete beams reinforced with different configurations of single and bundled GFRP bars, were tested under a four-point bending setup to failure. In the following, the details of the test specimens, test method, test setup, material properties, and instrumentation are described.

3.1. Details of test specimens

Each beam measured 5200 *mm* in length with cross-sectional dimensions of 450 *mm* high and 300 *mm* wide. In all the specimens, the constant-shear and constant-moment spans were 1250 and 2500 *mm*, respectively. The center of supports was placed 100 *mm* away from the ends of beams. The length of the constant-moment span of specimens was designed to accommodate the entire splice length within the constant-moment region at least one effective beam depth away from the loading points.

The beam specimens were designated using a combination of letters and numbers. The nomenclature commences with the letter B followed by a number identifying the bar size (4, 5 and 8 for No. 4 (12.7 *mm*), No. 5 (15.9 *mm*) and No. 8 (25.4 *mm*) bars, respectively). Its second letter indicates the bundle type (S, D, and T for single bars, two-bar bundles, and three-bar bundles, respectively), while its second number (33, 50, and 100) represents the percentage of bars staggered in each section within the splice length. The digits after the letter L identify the splice length of individual bars in mm. The final digits after the letter C, in confined specimens, define the stirrup spacing within the splice zone, while the final number of 51 expresses the clear cover in the specimen with larger clear cover. In addition, B4-D-NS stands for the reference beam, which was reinforced with a total of four continuous bars detailed in bundles of two bars.

Table 3-1 provides the beam details, while Figure 3-1 illustrates the bar arrangement within the splice zone. The number of test specimens was optimized to a total of 22 specimens. Among them, 16 specimens were reinforced with bundled-bars including two-bar bundles of No.4, No.5, and No.8 along with three-bar bundles of No.4 and No.5. Two-bar bundle of No.8 was included to investigate the bond strength of bundled bars with maximal permitted bar size by CSA S806-12. Moreover, five specimens reinforced with single lap-spliced bars of No.4, No.5 and No.8 were constructed to scrutinize the effect of number of bars in a bundle on the bond strength and to propose possible incremental coefficients for the splice length of individual GFRP bars within a bundle with respect to single bar.

Based on CSA S806-12 (Canadian Standards Association, 2012), individual bars in a bundle may be cut off at different points at least $45d_b$ apart, and overlapping of individual bar splices within a bundle is prohibited. Due to the limitations in the total length of specimens, however, this provision could not be complied with in this study. Nonetheless, a space of 40 mm was left between the ends of two adjacent splices to avoid any interruption in the bond strength due to the installation of strain gages.

Table 3-1: Details of test beams

Specimens	Bar size	No. of bars in Bundle	l_s	f_c'	f_t	Splice pattern [#]
	-	-	mm	MPa	MPa	-
B4-T33-L320	No.4	3	320	40.9	3.7	T33
B4-T100-L320	No.4	3	320	40.9	3.7	T100
B4-S50-L320	No.4	1	320	40.9	3.7	S50
B4-T33-L320-51	No.4	3	320	40.9	3.7	T33
B4-D50-L320	No.4	2	320	40.3	3.96	D50
B4-D-NS	No.4	2	-	40.3	3.96	-
B4-S100-L320	No.4	1	320	40.3	3.96	S100
B5-D50-L400	No.5	2	400	40.3	3.96	D50
B4-T33-L400	No.4	3	400	39.6	4	T33
B4-D100-L320	No.4	2	320	39.6	4	D100
B4-T33-L510	No.4	3	510	39.6	4	T33
B5-T33-L510	No.5	3	510	33.7	3.42	T33
B5-D50-L510	No.5	2	510	33.7	3.42	D50
B5-D50-L640	No.5	2	640	33.7	3.42	D50
B5-S50-L510	No.5	1	510	33.7	3.42	S50
B8-D50-L640	No.8	2	640	35.3	2.86	D50
B8-S50-L510	No.8	1	510	35.3	2.86	S50
B8-D50-L510	No.8	2	510	35.3	2.86	D50
B4-S50-L320-C125	No.4	1	320	42	3.48	S50
B5-D50-L400-C250	No.5	2	400	42	3.48	D50
B4-T33-L320-C125	No.4	3	320	42	3.48	T33
B5-D50-L400-C125	No.5	2	400	42	3.48	D50

Note:
l_s is the splice length;
f_c' is the compressive strength of concrete;
f_t is the splitting tensile strength of concrete;
[#] see Figure 3-1 for more details.

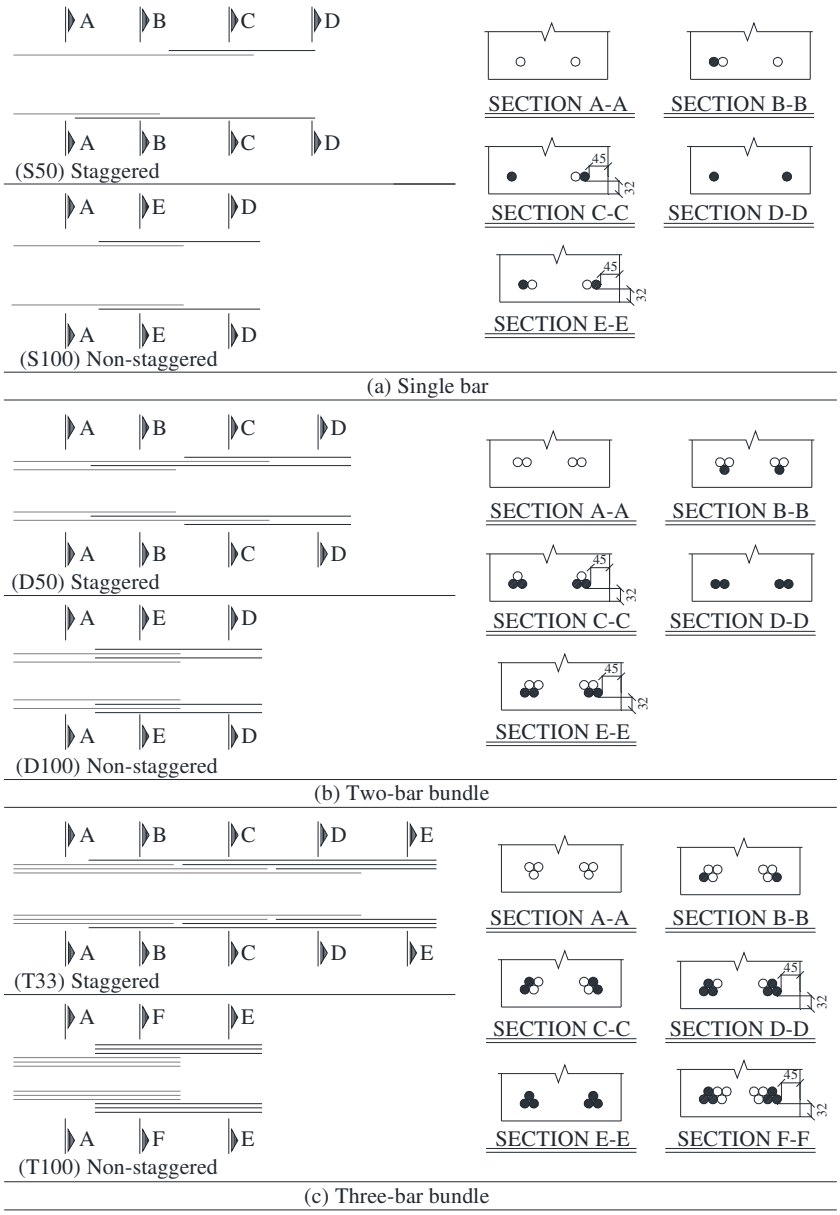

Figure 3-1 Arrangement of bars along the splice zone and location of strain gages (all dimensions are in mm)

3.2. Description of selected testing method

The beam-splice test was used in the experimental program as: (a) it was successfully used by other researchers (Tighiouart et al., 1999; Aly, 2005; Mosley et al., 2008; Harajli & Abouniaj, 2010; Esfahani et al., 2013; Pay et al., 2014), and (b) in this test method the concrete around the bar is in the same stress state as the real application. Figure 3-2 shows a

schematic illustration of the test setup, while Figure 3-3 illustrates a beam specimen under testing.

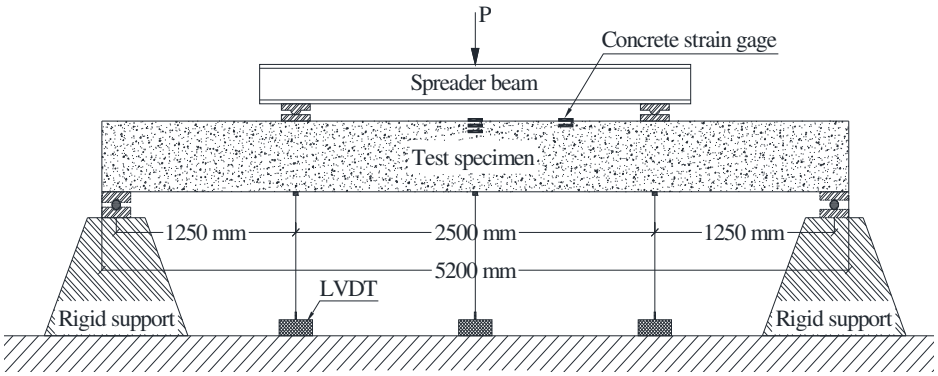

Figure 3-2: Test setup, and location of LVDTs and concrete strain gages

Figure 3-3: A beam specimen under testing

3.3. Design of specimens

In a given FRP RC section, depending on the splice length, reinforcement type, concrete properties, and reinforcement ratio, five general failure modes are expected: a) the pullout of tensile reinforcements (excessive slip), b) concrete splitting, c) FRP rupture, d) concrete crushing, and e) concrete shear. Among them, concrete crushing and shear modes are undesirable. If a specific splice length results in the FRP rupture or concrete crushing (in the case of an under-reinforced and an over-reinforced section, respectively), it can only lead to the conclusion that the provided splice length is greater than or equal to the required splice length. The provided splice length, however, can be much longer than or very close to the minimum splice length. If the bond failure occurs, it is realistic to extrapolate the minimum splice length corresponds to a given stress in FRP rebars from limited number of test results. Moreover, the pullout mode of failure, which can be due to a short splice length and high concrete cover to bar diameter ratio, is the less probable bond failure mode in practice (ACI 408 Committee, 2003). Consequently, the general aim of the design was to select splice lengths which would fail in the bond splitting failure.

The flexural design was performed so that the bond splitting failure precedes either the concrete crushing or the FRP rupture. In this regard, the selected splice lengths were designed to be shorter than the required lengths determined according to ACI 440.1R-15. The side and bottom clear covers as well as the clear bar spacing were designed to ensure having the face splitting mode of failure (the splitting of the bottom cover). As shown in Figure 3-1, the minimum bottom and side clear covers were, respectively, 32 mm and 45 mm in all beams. Moreover, the clear spacing of the bars was greater than two times the bottom cover. Thus, the bond behavior of specimens was governed by the bottom cover as it is the smallest value of the clear covers and half of the clear spacing between the spliced bars.

Shear design was performed using limit state design equations of CSA-S806-12 without considering the material resistance factors. Accordingly, the shear spans of the beams were reinforced with 10M steel stirrups spaced at approximately 125 mm on center. Two 15M

steel bars were used as compression reinforcement to provide support for stirrups during cage construction and for handling purpose after failure. Details of shear and longitudinal-compression reinforcement are shown in Figure 3-4.

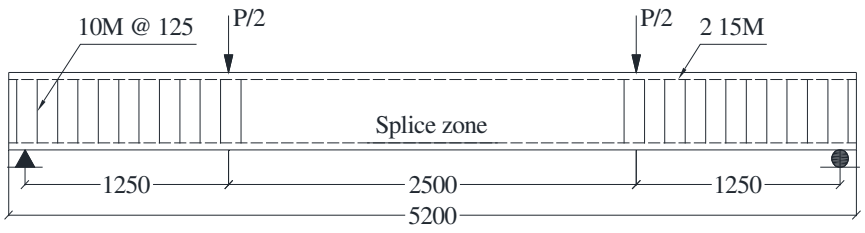

Figure 3-4: Details of the geometry and transverse reinforcement of the test beams

3.4. Materials

3.4.1. Reinforcement

Deformed 10M and 15M steel bars were used as transverse and longitudinal-compression reinforcements, respectively. Sand-coated GFRP bar in three different diameters (No. 4, No. 5, and No. 8) was used as tension reinforcement. Figure 3-5 shows the reinforcing bars used in this study. Moreover, Table 3-2 presents the mechanical properties of the GFRP and steel bars. The values associated with the GFRP bars were determined based on the average of five specimens tested in accordance with CSA S806-12 (Canadian Standards Association, 2014b).

Figure 3-5: Sand-coated GFRP reinforcing bars

Table 3-2: Mechanical properties of reinforcing bars

Bar Type	Bar Size	Bar Diameter (*mm*)	Elastic Modulus (*GPa*)	Tensile Strength (*MPa*)	Tensile Strain (%)
GFRP	No.4	12.7	51.7	1243	2.40
	No.5	15.9	51.1	1296	2.54
	No.8	25.4	51.6	1035	2.00
Steel	10M	11.3	200	f_y =460	ε_y =0.20
	15M	16	200	f_y =460	ε_y =0.20

Note: ε_y is the yield strain and f_y is the yield stress.

3.4.2. Concrete

A normal-weight ready-mixed concrete was used to cast the test specimens. The target 28-day concrete compressive strength was 35 *MPa* with a maximum aggregate size of 14 *mm*. The actual compressive and tensile strengths of the concrete in each casting were, however, determined on concrete cylinder specimens measuring 100×200 *mm* tested on approximately the same day as the beam testing. The day after casting, all the beams and cylinders were demolded and then moist-cured for seven days. The specimens were kept under the same environmental conditions until the testing day. Table 3-1 gives the compressive and tensile strengths, determined based on the average value of five cylinders tested on approximately the same day (± 2 days) at the beginning of the testing day.

3.5. Fabrication of specimens

3.5.1. Fabrication of formwork

To be cost-effective, the formwork was designed and constructed such that four specimens could be cast at the same time (Figure 3-6). Thus, the 22 specimens of this study were cast in six series from the same concrete type. The sides and base were constructed using two layers of plywood of 20 *mm* thickness. Steel angles were then employed as the perimeter frame to adjust the width of specimens and to stabilize the sides during casting. An additional layer of 20 *mm* plywood was screwed to the base at the bottom of each specimen to keep

bottom width constant along the beam length. Moreover, for each specimen, five threaded bars were provided to adjust and secure top width during placing and finishing the concrete. Before casting, great care was taken to ensure leveling of the test specimens. Prior to placing cages inside the formwork, the interior surfaces of the plywood were coated with a thin layer of release agent and all joints were sealed with silicon sealant to prevent leakage.

Figure 3-6: Details of the formwork fabricated for casting of specimens

3.5.2. Fabrication of reinforcement cages

The cages were constructed of GFRP rebars, 15M steel rebars, and 10M steel stirrups as tension, compression, and transverse reinforcement, respectively. All required steel stirrups were accurately fabricated using a steel bar bending machine at UdeS structural laboratory. As an example, Figure 3-7 shows the assembled cage of S4-T33-L320.

Figure 3-7: Assembled cage of B4-T33-L320

3.5.3. Installation of strain gages

The strain gages with gage lengths of 10 and 60 *mm* were utilized for GFRP rebars and concrete, respectively. The surface preparation of the GFRP bars for strain gage bonding included removing surface treatment using a sand grinder, smoothing with two grades of sand paper and finally cleaning with acetone. The strain gages were mounted to the GFRP rebars using a high-quality super glue. The reinforcement strain gages were then covered by a waterproof coating and two-compound epoxy to protect them from humidity and damage during casting. Figure 3-8 shows a photograph the instrumented splice region of specimen S8-D50-L640.

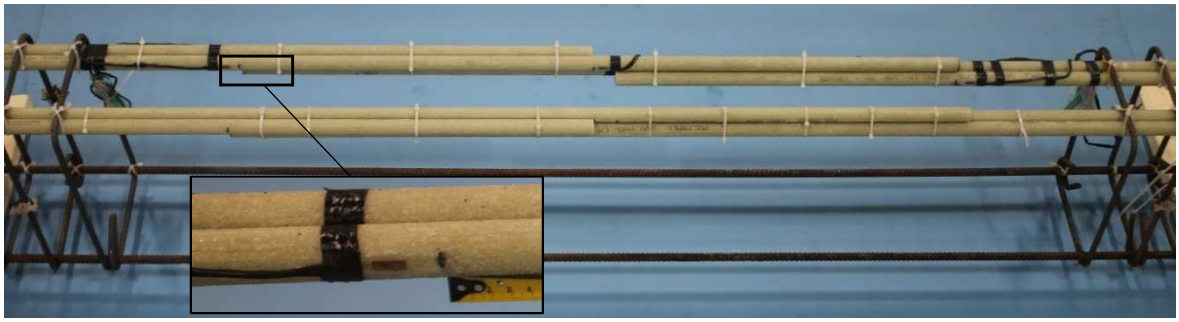

Figure 3-8: Instrumented splice zone in S8-D50-L640

3.5.4. Concrete casting and moist curing

Reinforcement cages were positioned concentrically inside the formwork before casting as shown in Figure 3-9. The GFRP bars were rested on plastic chairs to maintain clear cover of either 32 *mm* or 51 *mm*.

Figure 3-9: Cages inside formwork for first casting

The required concrete was delivered by a local ready-mix plant. To assess the workability of the delivered concrete, the slump test was performed before casting of each series as shown in Figure 3-10. For the cast series, the concrete slump was kept between 100 and 125 *mm* throughout the entire project. The beams and the representative cylinders were cast simultaneously using the same batch of concrete. They were unmolded one day after casting and moist-cured for seven days in the same condition as illustrated in Figure 3-11.

Figure 3-10: In-situ slump test

Figure 3-11: Moist curing of specimens

3.6. Test setup and instrumentation

All beams were monotonically loaded in a four-point bending setup up to failure. The load was applied with a 1000 *kN* actuator at a stroke-controlled rate of 1.2 *mm/min*. Figure 3-2 shows a schematic illustration of the test setup, while Figure 3-3 illustrates a beam specimen under testing. The displacement variations along the beams were recorded using four linear variable differential transformers (LVDTs), two of which were placed at the mid-span and the other two below the loading points. In addition, the horizontal elongations of the splice zone and constant moment span were obtained using two string potentiometers installed on the two sides of the beam (Figure 3-12). During the test, the beams were observed visually to draw the cracking pattern and record the corresponding loads. The test was paused at the onset of the first two cracks initiated close to the splice ends. For each of these two cracks: first, the initial crack width was measured manually using an electronic microscope; then, a LVDT was installed perpendicular to the crack to automatically measure the crack width up to failure. The width of other cracks within the flexural span was also visually monitored during loading. The visual inspection was stopped once it was considered unsafe to approach the beam.

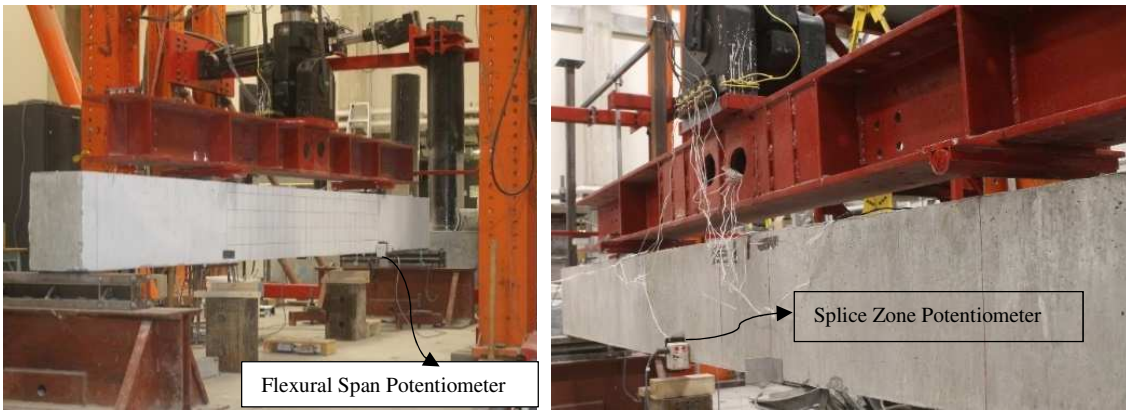

Figure 3-12: Illustration of flexural span and splice zone potentiometers

The variation of strain values in the GFRP reinforcing bar, steel stirrup and concrete was measured with a set of electrical-resistance strain gages. Figure 3-13 illustrates the position of strain gages bonded to the GFRP reinforcement and steel stirrup of specimens with splices. Due to changing of stiffness and discontinuity of the bars at the splice ends, cracks were very likely to develop at these locations. Thus, the strain gages were installed 20 *mm* away from the ends of splices to minimize the possibility of damage ensued by crack propagation during loading. In addition, a total of five strain gages were installed on the concrete surface in each beam, as shown in Figure 3-2. Two strain gages were mounted at a section corresponding to one end of the splice zone: one on the top compression surface and one on the side, 30 *mm* below the top one. The other three, were attached at the mid-span: one on the top compression surface and two on the side of the beams 30 and 60 *mm* below the top one. During the test, all the data—including loads, displacements, crack widths, and strain values—were automatically recorded by a computerized automatic data-acquisition system.

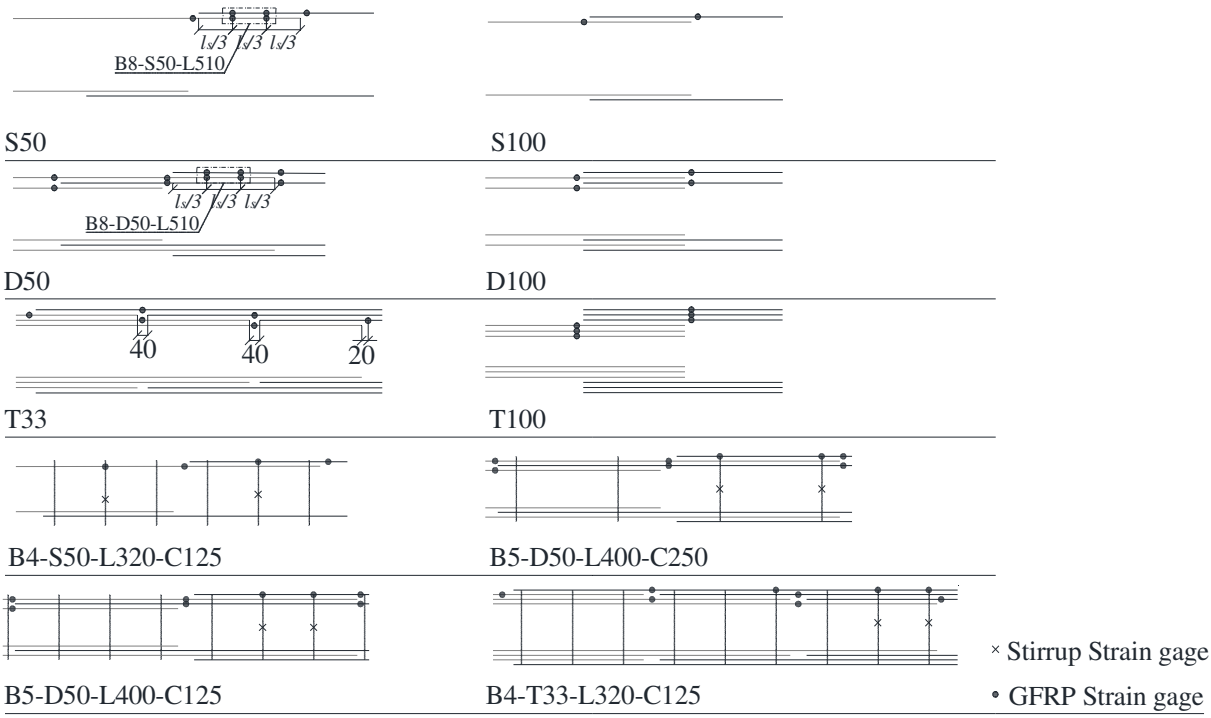

Figure 3-13: Illustration of the position of GFRP and stirrup strain gages

CHAPTER 4 Splice Strength of Staggered and Non-Staggered Bundled GFRP Rebars in Concrete

Avant-propos

Auteurs et affiliation:

Alireza Asadian: étudiant au doctorat, faculté de génie, département de génie civil, Université de Sherbrooke

Abolfazl Eslami : post-doctorat, faculté de génie, département de génie civil, Université de Sherbrooke.

Ahmed S. Farghaly : professionnel de recherche, faculté de génie, département de génie civil, Université de Sherbrooke.

Brahim Benmokrane: professeur, Faculté de génie, Département de génie civil, Université de Sherbrooke.

Date d'acceptation : 4 octobre 2018

État de l'acceptation : acceptée

Revue: ACI Structural Journal

Titre: Splice strength of staggered and non-staggered bundled GFRP rebars in concrete

4.1. Abstract

While bundling of reinforcing bars in concrete is inevitable in field applications, the behavior of lap-spliced glass-fiber-reinforced polymer (GFRP) bars in bundles has not yet been fully investigated. Therefore, this study aimed at elaborating on the splice strength of bundled GFRP bars in concrete under tension. Twelve full-scale beams with different staggering patterns, splice lengths, and GFRP-bar sizes were tested under a monotonically increasing load using a four-point bending setup. The test results indicated that staggering had a pronounced effect on the bond strength of the three-bar bundle, although it was insignificant for splices of single- and two-bar bundles. Moreover, the bond strength was found to be dependent on the number of bars within a bundle as the splice strength was reduced by increasing the number of bundled bars. The reliability of the current provisions in CSA S806-12 and the applicability of the provisions in ACI 318-14 relating to GFRP bars were assessed, and design recommendations were made based on the experimental findings. The recommendations herein may support the work of the North American technical committees engaged in the development of standards and design provisions for development and lap splice lengths of bundled reinforcement in concrete members reinforced with GFRP bars.

Keywords: Concrete, lap splicing; bond strength; GFRP reinforcing bar; bundled bars; staggering effect; bundle size.

4.2. Introduction

Glass-fiber-reinforced-polymer (GFRP) reinforcing bars are considered as a distinct alternative to steel bars where corrosion in reinforced-concrete (RC) structures is the main concern. Apart from the primary feature of corrosion resistance, GFRPs offer large strength-to-weight ratios, and lower life-cycle maintenance costs than steel. Their bond strength to concrete is, however, expected to be different than that of steel reinforcement due to diverse mechanical and physical characteristics, such as lower modulus of elasticity and various surface treatments. Given the same reinforcement size and splice length, the splice strength of sand-coated GFRP bars—the type used in this study—was around 27% lower than that of steel bars (Zemour et al., 2018).

When design criteria require heavy reinforcement, reinforcing bars should be arranged in bundles of two or three instead of using single bars. This arrangement can prevent reinforcement congestion and reduce the overall cross-sectional dimensions. Bundling also facilitates the placing of reinforcing bars and consolidation of concrete, which, in turn, leads to lower labor costs and construction time. In addition, bundling increases the clear spacing between bars, thereby providing a higher level of confinement compared to equally-spaced single bars. On the other hand, based on the current design guidelines,(Canadian Standards Association, 2012; ACI Committee 318, 2014) the splicing of bundled bars requires special considerations and splices need to be staggered in real field applications. This would increase the complexity of detailing and impede reinforcement placement, thereby impeding the construction process. Moreover, the cement paste may not easily penetrate into the bundles, thus reducing the contact area between individual bars and the concrete.

Despite its advantages, the use of bundled GFRP bars in RC members has been limited due to the scarcity of design provisions in most of the international design codes such as ACI 440.1R-15 (ACI Committee 440, 2015), CSA S06-14 (Canadian Standards Association, 2014a) and JSCE-97 (Japan Society of Civil Engineers, 1997). This dearth of design provisions is mainly attributed to the lack of experimental data on the lap splicing of bundled FRP bars.

The splice strength of GFRP bars to concrete has been investigated in several studies (Tighiouart et al., 1999; Aly et al., 2006b; Mosley et al., 2008; Harajli & Abouniaj, 2010; Choi et al., 2012; Esfahani et al., 2013; Pay et al., 2014; Zemour et al., 2018). The influencing parameters on the bond strength of GFRP bars in tension includes, but are not limited to, splice length, bar diameter, confinement, surface treatment, and concrete type and compressive strength (Tighiouart et al., 1999; Aly et al., 2006b; Mosley et al., 2008; Harajli & Abouniaj, 2010; Choi et al., 2012; Esfahani et al., 2013; Pay et al., 2014; Zemour et al., 2018). However, all experimental studies in the literature considered FRP bars spliced in the same section. Staggering reinforcing bars may affect the bond behavior of reinforcing bars in several ways. Staggering could alter the bond–stress distribution along the lap length (Cairns, 2013). It may also increase bar spacing in splices of single bars and consequently augment the confinement provided by the concrete. Moreover, with the same quantity of reinforcing bars (the same splice length), staggering increases the total length of the splice zone. Therefore, in sections with a similar clear cover, staggering bundled bars would increase the effective concrete cover. Last but not least, after splice failure, continuous bars within the lap-splice zone may continue carrying stress if only a portion of bars are spliced in the same section (Cairns, 2013). Thus, the staggered lap splices may exhibit less brittle performance (Cairns, 2013).

Despite several research endeavors pertaining to the bond behavior of lap splices of single bars (Tighiouart et al., 1999; Aly et al., 2006b; Mosley et al., 2008; Harajli & Abouniaj, 2010; Choi et al., 2012; Esfahani et al., 2013; Pay et al., 2014; Zemour et al., 2018), only one study —conducted by Aly et al. (2006a)— investigated the bond behavior of spliced bundled FRP bars. Their study comprised nine full-scale beam specimens reinforced with bundled bars spliced in the same section. The experimental program was aimed at evaluating the influence of the number of bars in a bundle and that of the splice length on the bond strength of sand-coated CFRP bars. Based on their results, the development length of individual bars within a bundle shall be equal to that of a single bar, increased by 60% for a two-bar bundle, and 100% for a three-bar bundle (Aly et al., 2006a). Their conclusion raised questions regarding the reliability of the current provisions stipulated in CSA S806-12 (Canadian Standards Association, 2012) and the applicability of the steel-reinforcing-bar

provisions specified in ACI 318-14 (ACI Committee 318, 2014) to FRP bars. Nonetheless, the splice arrangement adopted by Aly et al. (2006a) did not comply with code provisions, as all the bars were spliced in the same section. Moreover, as only No. 3 CFRP bars were tested, it is not clear whether or not the conclusions can be appropriate for GFRP bars and other bar sizes. It should also be noted that, to the best of the authors' knowledge, no other experimental studies on the bond strength of bundled FRP bars have yet been reported. Moreover, the literature contains no studies on the effect of staggering on the splice strength of GFRP bars. Therefore, this study was conducted to fill the current gap of knowledge and to provide more information about the splice strength of staggered and non-staggered bundled GFRP bars.

4.3. Research Significance

There is very limited knowledge on the behavior of spliced bundled GFRP bars in tension, which has led to the scarcity of related design provisions. Thus, the current study was conducted to evaluate the strength of spliced bundled GFRP bars and the influencing parameters, such as staggering, number of bars in a bundle, and bar size. In addition, the reliability of the provisions proposed by CSA S806-12 (Canadian Standards Association, 2012) along with the applicability of those recommended in ACI 318-14 (ACI Committee 318, 2014) to GFRP bars was assessed by comparison with the experimental findings. Moreover, the recommendations made for the splice strength of bundled GFRP bars could be included in future versions of design codes for GFRP-reinforced concrete structures.

4.4. Experimental Program

4.4.1. Design of the Test Specimens

The experimental program consisted of 12 full-scale concrete beams reinforced with different configurations of spliced bundled, single, or continuous GFRP bars, which were loaded using a four-point bending setup. The beams had a total length of 5200 *mm* [204.7 *in.*] with a clear span of 5000 *mm* [196.9 *in.*], a shear span of 1250 *mm* [49.2 *in.*], and a constant-moment span of 2500 *mm* [98.4 *in.*]. The constant-moment region was designed to

accommodate the entire splice zone. The gross cross-sectional area of all beams was 300×450 *mm* [11.81×17.72 *in*]. Figure 4-1 illustrates the geometry and transverse reinforcement details of the specimens.

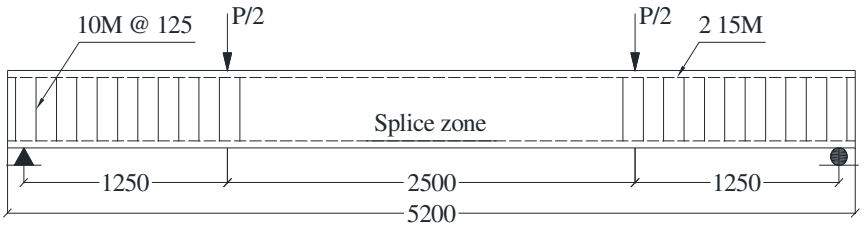

Figure 4-1: Details of the geometry and transverse reinforcement of the test beams [Note: 1 mm=0.0394 in.]

All the beams reinforced with the spliced bars were designed so that bond splitting failure precedes either flexural or shear failure. To prevent premature shear failure, the beams were designed in accordance with CSA S806-12 (Canadian Standards Association, 2012). Consequently, the shear spans were reinforced with 10M steel stirrups spaced at 125 *mm* [4.92 *in.*] on center. In order to evaluate the minimal bound of the bond strength of GFRP bars, no confinement was provided within the flexural span. It is worth noting, however, that the lap splicing of bundled bars with no transverse reinforcement is not in accordance with the design codes (Canadian Standards Association, 2012; ACI Committee 318, 2014) and may not be a common practice in field applications. Two 15M steel bars were used as compression reinforcement to provide support for stirrups during caging and to facilitate specimen handling after testing. The side and bottom clear covers as well as the clear bar spacing were designed so that the expected mode of failure in all specimens would be face splitting. As shown in Figure 4-2, the minimum bottom and side clear covers were, respectively, 32 *mm* [1.25 *in.*] and 45 *mm* [1.75 *in.*] in all beams. Moreover, the clear spacing of the bars was greater than two times the bottom cover. Thus, the bond behavior of specimens is governed by the bottom cover as it is the smallest value of the clear covers and half of the clear spacing between the spliced bars.

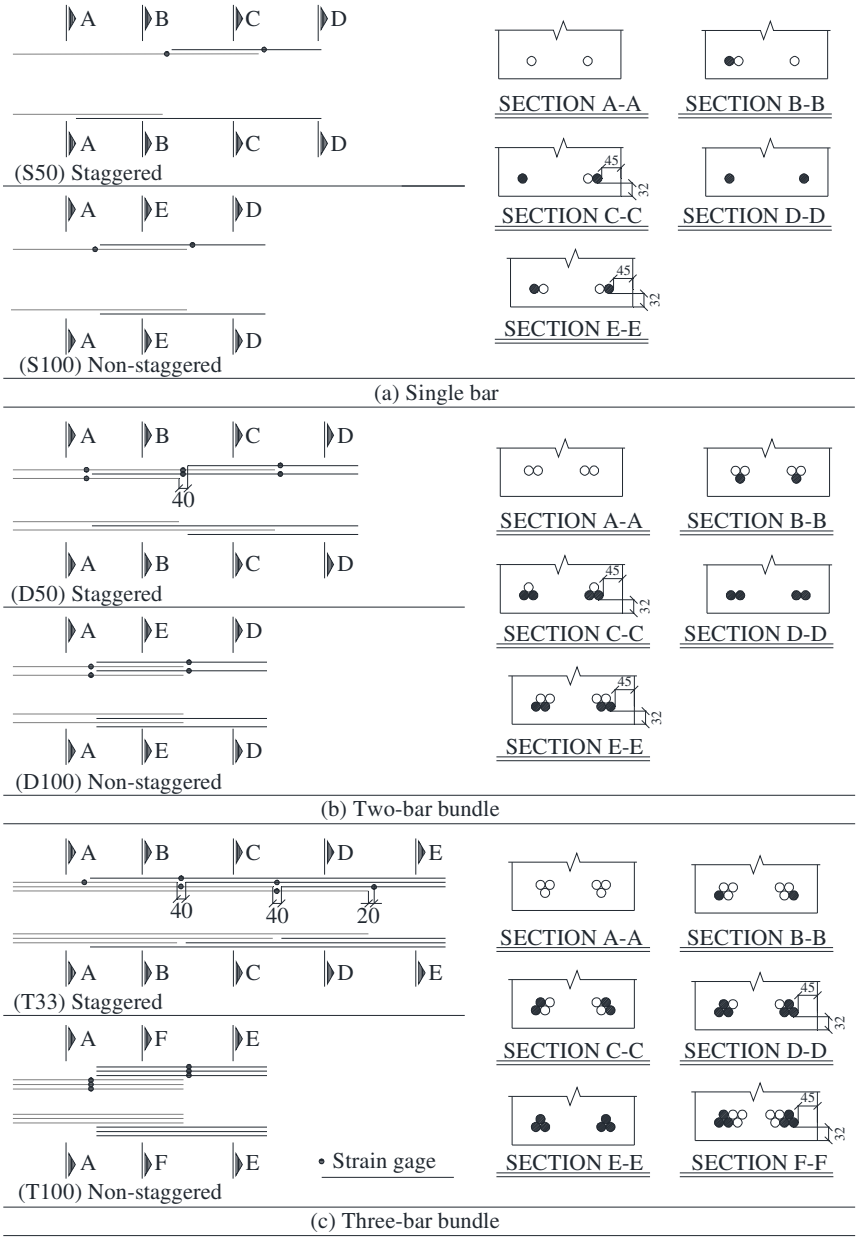

Figure 4-2 Arrangement of bars along the splice zone and location of strain gages [Note: all dimensions are in mm; 1 mm=0.0394 in.]

4.4.2. Description of the Test Specimens

The test specimens were designed to represent a full range of bundling patterns and bar sizes. Table 4-1 provides the beam details, while Figure 4-2 illustrates the bar arrangement within the splice zone. Based on CSA S806-12 (Canadian Standards Association, 2012), individual bars in a bundle should be cut off at different points at least 45db apart, and overlapping of

individual bar splices within a bundle is prohibited. Due to the limitations in the total length of specimens, however, this provision could not be complied with in this study. Nonetheless, a space of 40 *mm* [1.57 *in.*] was left between the ends of two adjacent splices to avoid any interruption in the bond strength due to the installation of strain gages.

Table 4-1: Details of test beams

Series	Specimen	Bar Size	Total Number of Bars	Number of Bars in Bundle	Splice Length	f_c'	f_t	Splice Pattern[#]
					mm	*MPa*	*MPa*	
Series I	B4-S100-L320	No.4	2	1	320	40.3	3.96	S100
	B4-D100-L320	No.4	4	2	320	39.6	4.00	D100
	B4-T100-L320	No.4	6	3	320	40.9	3.70	T100
	B4-S50-L320	No.4	2	1	320	40.9	3.70	S50
	B4-D50-L320	No.4	4	2	320	40.3	3.96	D50
	B4-T33-L320	No.4	6	3	320	40.9	3.70	T33
	B4-D-NS	No.4	4	2	-	40.3	3.96	-
Series II	B5-S50-L510	No.5	2	1	510	33.7	3.42	S50
	B5-D50-L510	No.5	4	2	510	33.7	3.42	D50
	B5-T33-L510	No.5	6	3	510	33.7	3.42	T33
Series III	B8-S50-L510	No.8	2	1	510	35.3	2.86	S50
	B8-D50-L510	No.8	4	2	510	35.3	2.86	D50

Note:
[#] see Figure 4-2 for more details.
1 *mm* = 0.0394 *in.*; 1 *MPa* = 0.145 *ksi*

The beams were divided into three series based on the bar sizes. Each series was to investigate the effect of the number of bars in a bundle on the bond strength. The first series included a reference beam reinforced with a total of four continuous bars arranged in the form of bundles of two bars along with two sets of three beams to study the influence of staggering. The second series was composed of three beams reinforced with staggered No. 5 (15.9 *mm*) bars. The third series included two beams reinforced with staggered No. 8 (25.4 *mm*) bars, which is the maximum size allowed for bundling by CSA S806-12.

The beam specimens were designated according to a mnemonic system made of letters and numbers. The nomenclature starts with the letter B, followed by a number identifying the bar size (4, 5, and 8 for No. 4 (12.7 *mm*), No. 5 (15.9 *mm*), and No. 8 (25.4 *mm*) bars, respectively). The second letter indicates the bundle type (S, D, or T for single bars, two-bar bundles, and three-bar bundles, respectively), while the second number (33, 50, or 100) represents the percentage of bars staggered in each section within the splice length. The final

digits after the letter L identify the splice length of individual bars in mm. In addition, B4-D-NS stands for the reference beam, which was reinforced with a total of four continuous bars detailed in bundles of two bars.

4.4.3. Material Properties

Deformed 10M (11.3 *mm*) and 15M (16 *mm*) steel bars were used as compression and transverse reinforcement, respectively. As indicated in Figure 4-3, three different sizes of sand-coated GFRP bars—No. 4 (12.7 *mm*), No. 5 (15.9 *mm*), and No. 8 (25.4 *mm*)—were used as tension reinforcement. All GFRP bars of identical diameter were from the same production lot. Table 4-2 summarizes the mechanical properties of the reinforcing bars. The values associated with the GFRP bars were recorded as the average properties of five specimens tested in accordance with CSA S806 (2012) (Canadian Standards Association, 2012).

Figure 4-3: Sand-coated GFRP bars

Table 4-2: Mechanical properties of the reinforcing bars

Bar Type	Bar Size	Bar Diameter (*mm*)	Elastic Modulus (*GPa*)	Tensile Strength (*MPa*)	Tensile Strain (%)
GFRP	No.4	12.7	51.7	1243	2.40
	No.5	15.9	51.1	1296	2.54
	No.8	25.4	51.6	1035	2.00
Steel	10M	11.3	200	f_y = 420	ε_y = 0.2
	15M	16	200	f_y = 420	ε_y = 0.2

ε_y = yield strain and f_y = yield stress
1 *mm* = 0.0394 *in.*; 1 *MPa* = 0.145 *ksi*

The beams were cast using a normal-weight ready-mixed concrete with a target 28-day compressive strength of 35 *MPa* [5076 *psi*] and a maximum aggregate size of 14 mm [0.55 *in.*]. Control cylinders measuring 100×200 *mm* [3.94×7.87 *in.*] were cast simultaneously with the corresponding beams from the same batch of concrete. The beams and cylinders were demolded one day after casting and then moist cured for 7 days. Afterwards, they were kept under the same environmental conditions until the testing day. Table 4-1 lists the compressive and tensile strengths obtained by testing five cylinders on the testing day.

4.4.4. Test Setup and Instrumentation

All beams were monotonically loaded in a four-point bending setup up to failure. The load was applied with a 1000 *kN* [224.8 *kip*] actuator at a stroke-controlled rate of 1.2 *mm/min* [0.05 *in./min*]. Figure 4-4 shows a schematic illustration of the test setup, while Figure 4-5 illustrates a beam specimen under testing. The displacement variations along the beams were recorded using four linear variable differential transformers (LVDTs), two of which were placed at the middle and the other two below the loading points. During the test, the beams were observed visually to draw the cracking pattern and record the corresponding loads.

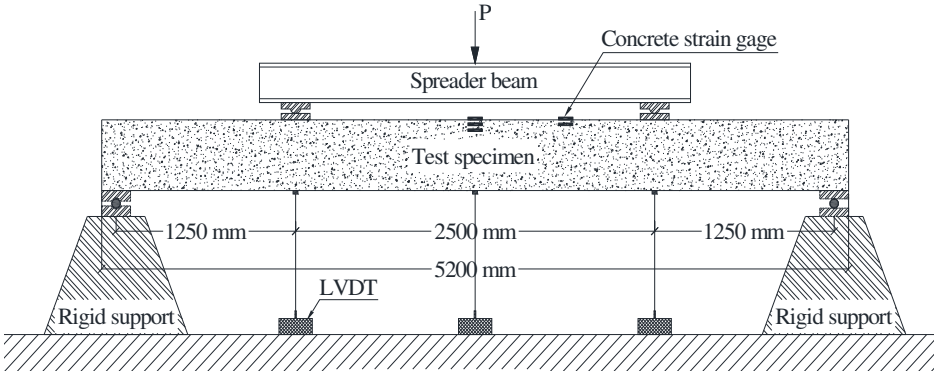

Figure 4-4: Test setup, and location of LVDTs and concrete strain gages [1 *mm* = 0.0394 *in.*]

Figure 4-5: A beam specimen under testing

The test was paused at the onset of the first two cracks initiated close to the splice ends. For each of these two cracks: first, the initial crack width was measured manually using an electronic microscope; then, a LVDT was installed perpendicular to the crack to automatically measure the crack width up to failure. The width of other cracks within the flexural span was also visually monitored during loading. The visual inspection was stopped once it was considered unsafe to approach the beam.

During the test, the strain values in the reinforcing bars and concrete were measured with a set of electrical-resistance strain gages. Figure 4-2 illustrates the position of strain gages bonded to reinforcement in specimens with splices. Due to changing of stiffness and discontinuity of the bars at the splice ends, cracks were very likely to develop at these locations. Thus, the strain gages were installed 20 *mm* [0.79 *in.*] away from the ends of splices to minimize the possibility of damage ensued by crack propagation during loading.

In addition, a total of five strain gages were installed on the concrete surface in each beam, as shown in Figure 4-4. Two strain gages were mounted at a section corresponding to one end of the splice zone: one on the top compression surface and one on the side, 30 *mm* [1.18 *in.*] below the top one. The other three, were attached at the mid-span: one on the top compression surface and two on the side of the beams 30 and 60 *mm* [1.18 and 2.36 *in.*] below the top one. During the test, all the data—including loads, displacements, crack widths, and strain values—were automatically recorded by a computerized automatic data-acquisition system.

4.5. Test Results and Observations

4.5.1. Modes of Failure

During the experimental tests, flexural cracks initially appeared inside the constant-moment region, generally outside the splice zone. In addition, the first flexural crack within the splice zone commonly occurred at the splice ends. As the load approached the failure point, the number of flexural cracks in the constant-moment region increased. At higher loads, hairline splitting cracks were initiated from the flexural crack in the vicinity of the splice end, and gradually propagated within the splice zone on the bottom and sides of the beams. The staggered bundled beams failed upon splitting failure of an individual pair of spliced bars within the bundle.

Due to the similarity of the failure modes of the beams with staggered splices, the representative failure modes of the beams in Series II are shown in Figure 4-6. Based on the test observations, the single-bar splices exhibited slightly different splitting crack patterns at failure than the bundled-bar splices. In the latter case, hairline splitting cracks appeared on the sides of the beam before failure, while side splitting cracks coincided with failure in the former. In addition, the horizontal splitting cracks in the beams with bundled-bar splices were developed further from the extreme tension surface compared to the beams with single-bar splices, as indicated in Figure 4-6. This might stem from the fact that pairs of bars in individual splices within a bundle were not located at the same depth within a section. Therefore, the bursting forces could not evolve in the same horizontal plane, in contrast to a

pair of bars spliced individually. As anticipated in the initial design, the failure of spliced beams was accompanied by precipitous splitting of the concrete cover within the splice zone. The splitting was explosive with no sign of bond splitting cracks on the sides of beams up to the failure in the non-staggered bundled beams (B4-D100-L320 and B4-T100-L320). Testing of the reference beam (B4-D-NS) continued up to a load of 230.2 *kN* [51.75 *kip*], at which point loading was stopped for safety-related reasons.

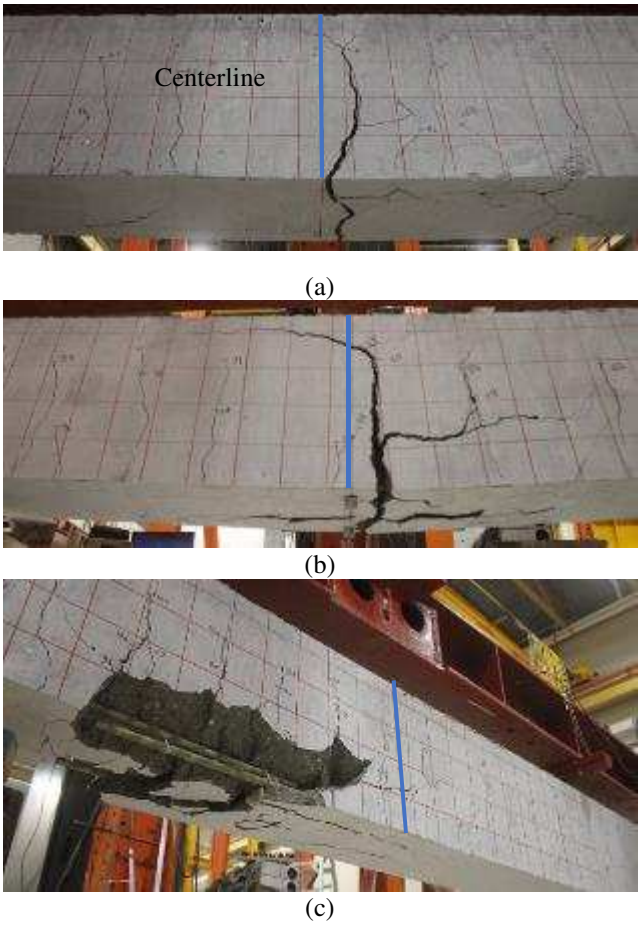

Figure 4-6: Failure modes of (a) B5-S50-L510, (b) B5-D50-L510, and (c) B5-T33-L510

4.5.2. Load–Deflection Behavior

The distribution of total applied load versus mid-span deflection is plotted in Figure 4-7 for all the test beams. The load–deflection responses displayed a bilinear behavior, exhibiting a significant reduction in the flexural stiffness after cracking. All the beams had similar uncracked stiffness. The post-cracking stiffness, however, increased for the beams with

higher reinforcement ratios. This can indicate that the post-cracking flexural stiffness was controlled by the axial stiffness of the longitudinal reinforcement.

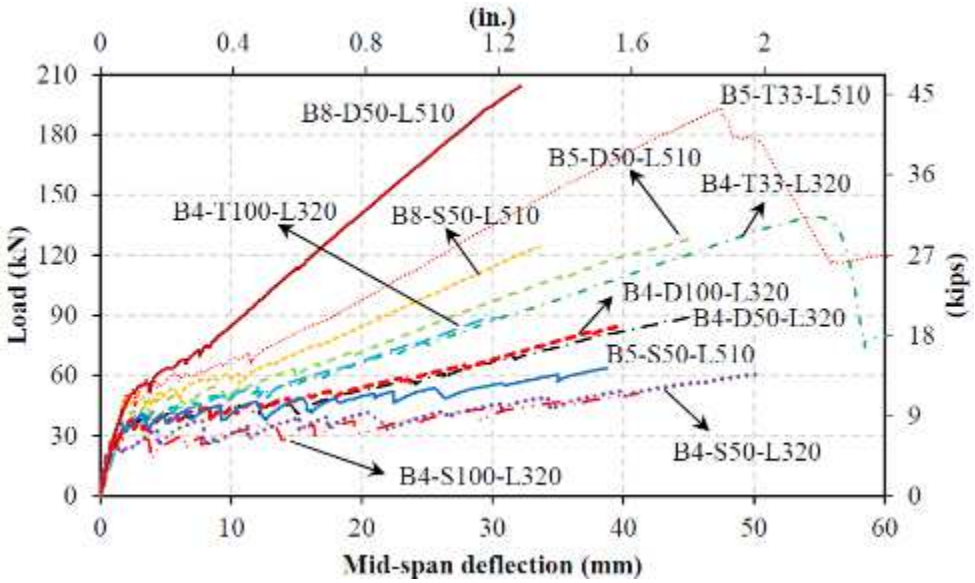

Figure 4-7: Load–deflection responses of all specimens

As shown in Figure 4-7, the cracking loads of the non-staggered beams (i.e., B4-S100-L320, B4-D100-L320, and B4-T100-L320) were similar to their staggered counterparts (i.e., B4-S50-L320, B4-D50-L320, and B4-T33-L320, respectively). Staggering also had negligible effect on the beam stiffness. It was, however, found to be effective in enhancing the splice strength as the beams with staggered splices could withstand higher loads than their non-staggered counterparts. Considering the post-failure behavior, it was noticed that the loading capacity of the specimens with staggered three-bar bundles (B4-T33-L320 and B5-T33-L510) dropped to around 65% of the maximum load, unlike the other specimens, whose strength was completely lost at the onset of failure. With 33% of bars being spliced at a section, the post-failure resistance of the beams with staggered splices of three-bar bundles might be attributed to the stress transfer from the spliced bars to the neighboring continuous bars after reaching their bond strengths (peak load).

4.5.3. Crack Width

As mentioned earlier, the development of the crack width during loading was measured with two LVDTs. The greater of the two measurements was considered as the maximum crack

width and plotted in Figure 4-8. Table 4-3 lists the maximum crack widths at failure for all the test specimens. Based on the experimental observations, regardless of the staggering pattern, bar size, and number of bars in a bundle, the widest cracks commonly occurred at the splice ends. In other words, the cracks formed in the flexural span but outside the splice zone and those within the splice length were narrower than those at the splice ends. This was anticipated given the bar slippage in splices.

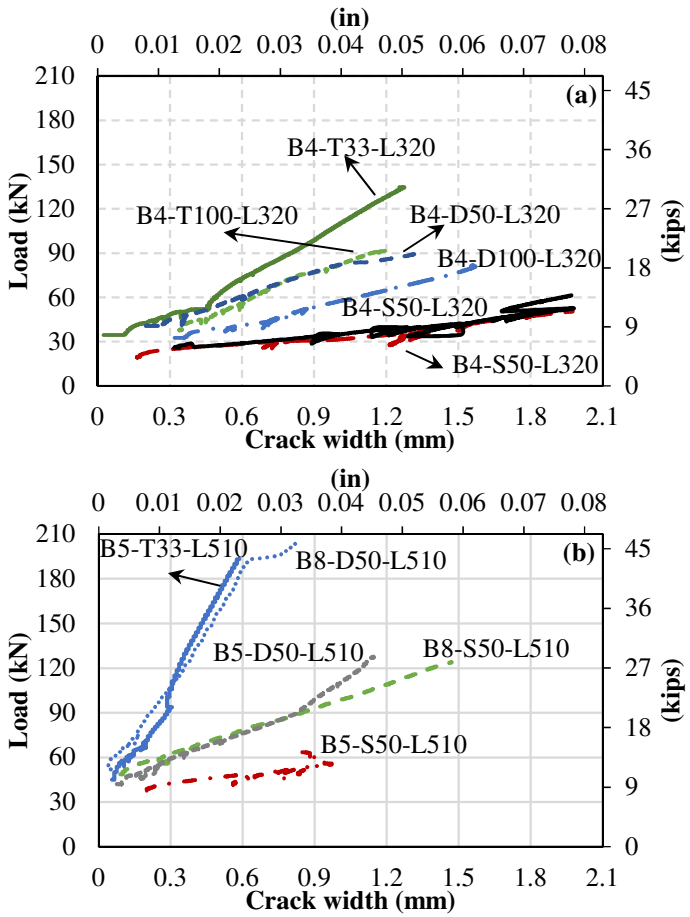

Figure 4-8: Distribution of applied load versus maximum crack width of all specimens

Table 4-3: Test results

	Recorded			Normalized		
	P_u	ε_{test}	f_{test}	$\varepsilon_{test,n}$	$f_{test,n}$	$w_{cr,max}$
Beam	*kN*	$\mu\varepsilon$	*MPa*	$\mu\varepsilon$	*MPa*	*mm*
B4-S100-L320	50.7	7624	394	7609	393	1.98
B4-D100-L320	84.6	6161	319	6176	319	1.57
B4-T100-L320	91.6	4610	238	4584	237	1.20
B4-S50-L320	60.6	8048	416	8003	414	1.98
B4-D50-L320	89.8	6575	340	6563	339	1.33
B4-T33-L320	134.6	6478	335	6442	333	1.28
B4-D-NS	230.2$^+$	-	-	-	-	-$^+$
B5-S50-L510	63.6	6780	346	7077	362	0.98
B5-D50-L510	128.7	6081	311	6347	324	1.16
B5-T33-L510	193.2	5699	291	5948	304	0.59
B8-S50-L510	124.0	4205	217	4338	224	1.47
B8-D50-L510	204.4	3509	181	3620	187	0.84

P_u= maximum applied load; ε_{test}= reinforcement strain at failure; f_{test}= reinforcement stress at failure; $\varepsilon_{test,n}$= normalized reinforcement strain at failure; $f_{test,n}$= reinforcement stress at failure; $w_{cr,max}$= maximum crack width at failure.
$^+$ the test stopped before failure
1 *kN*= 0.225 *kips*; 1 MPa = 0.145 *ksi*

It should also be noted that, due to the uncertainties related to cracking patterns, the initial locations of cracks as well as the position of the widest crack in different specimens cannot be identical. In most staggered specimens, the widest crack was located where the two splice ends coincided. For instance, the widest cracks in the case of staggered single and two-bar bundle splices were normally located at the mid-span (Figure 4-6 (a) and (b)). Providing a gap between the ends of the staggered splices may reduce the maximum crack width. This observation was not, however, consistent in all the staggered specimens, as in the staggered splices of three-bar bundles, the maximum crack width was normally observed at the end of the splice zone (Figure 4-6 (c)). Thus, more experimental investigations are recommended to fully grasp the variation in crack width within the splice zone of bundled GFRP bars.

To evaluate the effect of staggering on the maximum crack width of the beams with bundled reinforcement, the distribution of applied load versus the maximum crack width of the companion beams has been compared in Figure 4-8 (a). Moreover, the maximum values of load and crack widths at failure are reported in Table 4-3. As shown, the beams with non-

staggered bundled reinforcement exhibited wider flexural cracks at the splice end compared to their companion staggered ones. Consequently, the non-staggered bundled GFRP bars experienced more slip than the staggered bars. This may provide an idea of the role played by staggering in reducing the maximum crack width. The beam with staggered single bars (B4-S100-L320) exhibited crack widths similar to its non-staggered counterpart (B4-S50-L320). As mentioned before, providing a gap between the ends of the staggered lap splices might have further reduced the maximum crack widths.

It should be also noted that, the crack widths presented in Figure 4-8 and Table 4-3 correspond to the maximum widths observed at the ends of splices in beams designed to experience premature bond failure. Therefore, the results can not represent the average crack widths of GFRP-reinforced beams in practice as they might be narrower.

4.6. Discussion of Results

4.6.1. Bond Mechanism

Generally, stress is transferred between the reinforcement and concrete by three main mechanisms: (a) chemical adhesion of bar–concrete interface; (b) friction forces caused by the roughness of the interface and bar–concrete slip; and (c) mechanical interaction arising from the texture of the reinforcing-bar surface (ACI 408 Committee, 2003). The stress transfer between the reinforcing bar and concrete consists of two components acting on their interface: (a) longitudinal, and (b) radial stresses. The former acts along the bar length, which prevents the bar from pulling out of the concrete, while the latter acts perpendicular to the bar length causing longitudinal splitting cracks.

Tepfers (Tepfers, 1973, 1982) introduced a concrete-ring model in which the radial force was modeled as the internal water pressure acting on a partially cracked thick-wall pipe. The inner diameter of the hypothetical pipe is assumed to be equal to the bar diameter, and its thickness is taken as the smaller of the clear cover or half of the clear spacing between adjacent bars. The radial force is balanced by tensile stress in the pipe thickness. When the radial force exceeds the concrete tensile strength, internal cracks are initiated parallel to the

bar and propagate outward to the surface of the member, causing splitting failure on the critical plane (Tepfers, 1979, 1982).

The circumferential area of an individual splice in direct contact with concrete is reduced in the case of lap splices of two- and three-bar bundles. The bond behavior of individual splices within a bundle might be different than that of single-bar splices for the following reasons:

(a) As the contact area between the reinforcement and concrete in the case of spliced bars within a bundle is decreased, it is reasonable to assume that the contribution of chemical adhesion to the bond strength would be lost at a lower stress level. Therefore, the friction and mechanical interaction mechanisms take effect at a lower stress level. This might trigger the early initiation of the splitting cracks, which can alter the bond stress–slip relationship and result in a lower bond strength.

(b) The smaller contact area would also cause concentration of radial forces on the surrounding concrete. In other words, at the same tensile stress level, an identical internal pressure acts only on a portion of the hypothetical thick-wall pipe in the case of the bundled splices. It might change the bond mechanism by altering the initiation of the splitting crack and its outward propagation pattern. Therefore, the critical splitting plane and the number of splitting cracks would be different between bundled and single-bar splices.

(c) Pairs of bars in individual splices within a staggered bundle are inevitably located at different depths within a section (see Figure 4-2). Therefore, the bursting forces may not be created in the same horizontal plane in contrast to the single-bar splices.

(d) The reduction in the bond strength of bundled GFRP rebars, as well as the splitting failure mode, might be partly affected by the change in the effective concrete cover of the individual bars in a bundle, resulting in lower confinement provided by the surrounding concrete for the bundled bars.

4.6.2. Assessment of the Bond Strength

As mentioned earlier, the strain in reinforcing bars was measured with a set of strain gauges installed at the splice ends (see Figure 4-2). The mean value of the measured strains was

considered as the failure strain of the reinforcement (ε_{test}). This failure strain (ε_{test}) was then multiplied by the modulus of elasticity (E) of the corresponding rebar to determine the failure stress (f_{test}). The corresponding force at failure was calculated as $F_{test} = nf_{test}A_b$, where n and A_b are the number of bars and the nominal cross-sectional area of an individual bar in a bundle, respectively.

It should also be mentioned that a limited number of strain gauges (6 out of a total of 50) were damaged during either casting (4) or testing (2). The damaged gauges were excluded from the average values. Moreover, the accuracy of the strain-gauge measurements was confirmed by the moment–curvature analysis. These confirmed the reliability of the test results.

As per ACI 408R-03 (ACI 408 Committee, 2003) and Darwin et al. (2005), the bond strength of reinforcing bars is proportional to the fourth root of the compressive strength of concrete. Thus, for comparison purposes and to avoid the effect of variations in the concrete compressive strength on the calculated bond strengths, all stresses and forces were normalized by the fourth root of the compressive strengths divided by 40 *MPa* [5802 *psi*] ($\sqrt[4]{(f_c'/40)}$ in SI units). Table 4-3 presents the recorded and normalized experimental results for all the test beams.

4.6.3. Strain State in Reinforcement

Figure 4-9 plots the distribution of strain values against the total applied load for all the beams with splices in Series I. The load–strain curves of all beams were similar before flexural cracking. Thereafter, some discrepancies were observed, depending on the position of the strain gage within the splice zone. The differences in the strain measurement at different sections within the splice zone were expected as strain could be affected by the gage position relative to the neighboring cracks and tension stiffening.

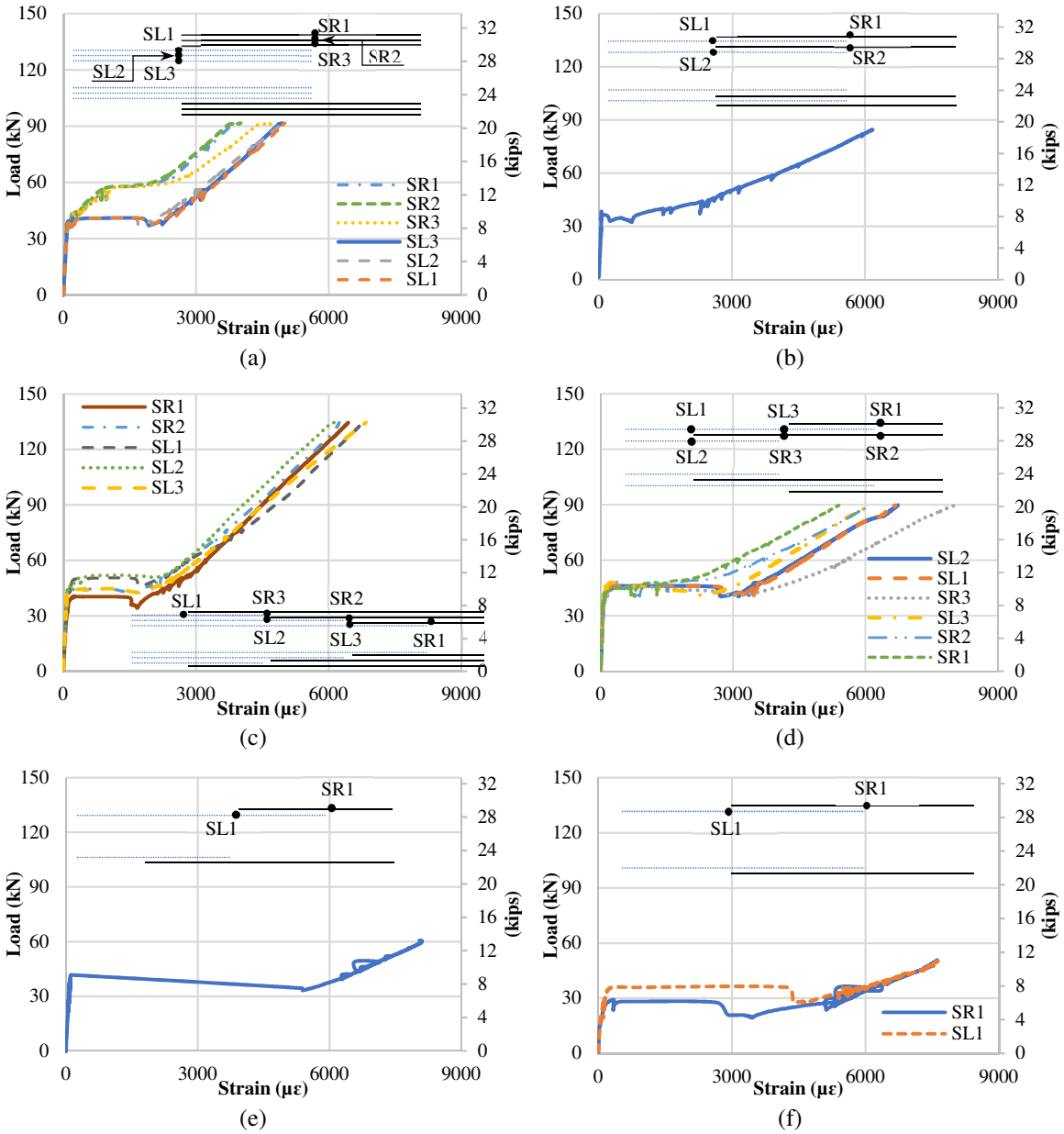

Figure 4-9: Distribution of stresses among bars in a bundle: (a) B4-T100-L320; (b) B4-D100-L320; (c) B4-T33-L320; (d) B4-D5-L320; (e) B4-S50-L320; (f) B4-S100-L320

A noteworthy observation was obtaining different strains by the strain gages installed at the same cross section. As shown in Figure 4-9 (a), in the case of B4-T100-L320, one bar within a bundle (SR3) developed higher strain than its adjacent bars (SR1 and SR2). This might indicate that bars SR1 and SR2 experienced additional slippage within the splice zone. It is evident from this observation that all bars in a bundle could not act as a single unit as relative displacement between them occurred. More experimental studies are, however, required to

confirm the behavior of spliced bundled GFRP bars when all the bars are spliced in the same section, more specifically, using longer splices and greater covers. It should also be noted that, during the loading of B4-D100-L320, only one gage out of four remained intact, as indicated in Figure 4-9 (b).

A similar trend was also noted for the beams with staggered splices of bundled bars. As shown in Figure 4-9 (c), bars SL3 and SR2 in B4-T33-L320 developed different strains. Similarly, strain gages L2S and R2S in B4-D50-L320 attained markedly different strains, as indicated in Figure 4-9 (d). Moreover, the strains obtained for B5-T33-L510, B5-D50-L510, and B8-D50-L510 were likewise consistent. It should be noted that the clear spacing, concrete cover, and reinforcing-bars depth varied within the splice zone of bundled bars. This might exert different degrees of confinement on the reinforcing bars within a bundle and cause diverse performances.

Another noteworthy observation for beams with staggered two-bar bundles was that, at the sections corresponding to the ends of the splice zone, the continuous bars (SL1 and SR2 in Figure 4-9 (d)) always developed similar or higher strains than the neighboring spliced bars (SL2 and SR1 in Figure 4-9 (d), respectively). The strains measurements in B5-D50-L510 and B8-D50-L510 also confirmed this observation. This trend was, however, expected as the spliced bar would experience more slippage than the neighboring continuous bar.

4.7. Effect of Test Parameters

4.7.1. Staggering

The influence of staggering on the bond behavior of single and bundled bars can be described by comparing the failure stresses and loads of the beams in Series I, as indicated in Figure 4-10. The ratios of the failure stress (Figure 4-10 (a)) and load (Figure 4-10 (b)) of the non-staggered beams to those of their companion staggered ones, referred to as R, are also given in this figure. Overall, staggering the reinforcing bars in a bundle could increase the splice strength of bundled bars. The amount of enhancement is highly dependent on the number of bars in the bundle. For single and two-bar bundle splices, the bond strength of non-staggered

beams (B4-S100-L320 and B4-D100-L320) was roughly 6% less than their companion staggered beams (B4-S50-L320 and B4-D50-L320, respectively). Staggering could also improve the loading capacity by around 19% and 6% in the beams reinforced with the single and two-bar bundle splices, respectively. For three-bar bundles, the difference reached a peak. The normalized bond strength and loading capacity of B4-T100-L320 (no staggering) were, respectively, about 29% and 32% less than its staggered counterpart (B4-T33-L320). The reduction in the splice strength of non-staggered bundled splices compared to the staggered ones might be attributed to the reduced effective concrete cover to the effective bar diameter ratio of the non-staggered splices. Generally, with the same quantity of reinforcing bars (same splice length), staggering increases the total length of splice zone. Therefore, in sections with a similar clear cover, staggering bundled bars would increase the effective concrete cover. The bond strength of non-staggered bundles might be enhanced by providing greater concrete cover. The effect of confinement provided by concrete cover on the bond strength of GFRP bars has not yet been well quantified. Therefore, more experimental investigations are recommended to fully grasp this effect. Considering the obtained results and until more experimental results become available, splicing of all GFRP bars in three-bar bundle splices at the same section is not recommended in practice.

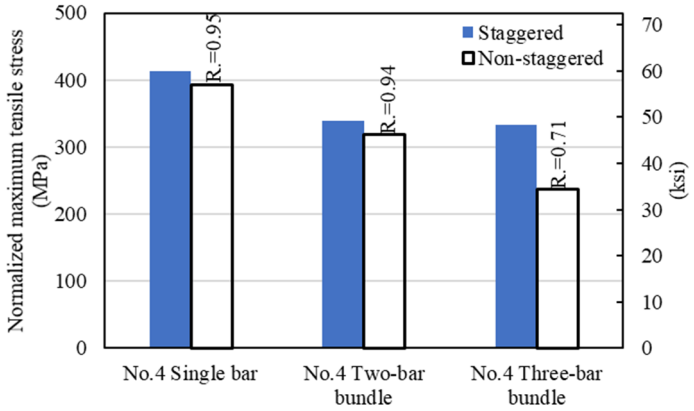

Figure 4-10: Influence of staggering on (a) tensile stress at failure; and (b) failure load

4.7.2. Number of Bars

The number of bars in a bundle can remarkably affect the bond strength of splices. Figure 4-11 compares the tensile stress of single-bar ($f_{b,single}$) splices at failure to that of an individual bar of the same size in splices of two- and three-bar bundles ($f_{b,bundled}$). This figure also gives the ratio these stresses ($f_{b,bundled}/f_{b,single}$). Comparison of the results indicates that the maximum tensile stress resisted by a reinforcing bar decreases when the number of bars in a bundle increase. This confirms the assumption that the greater the number of bars in a bundle, the greater the amount of reduction due to the bundling.

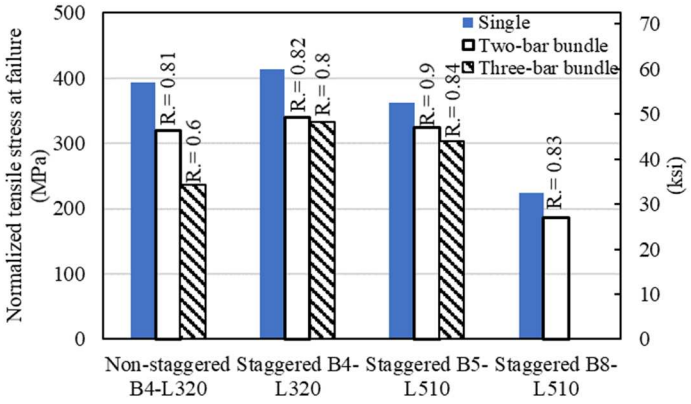

Figure 4-11: Comparison of developed stress in splices of single bars and two-bar and three-bar bundles

The decrease in the bond strength was, however, dependent on the staggering pattern, number of bars bundled, and ratio of splice length to bar diameter (l_s/d_b). Figure 4-12 compares the values of $f_{b,bundled}/f_{b,single}$ for different ratios of splice length to bar diameter for beams with staggered splices. As evident from the data trend in Figure 4-12, the bond strength of bundled bars generally increases for the higher ratios of splice length to bar diameter. Furthermore, it also indicates that the bond strength of individual bars in three-bar bundles was lower than that in the two-bar bundles. This brings out the reduction in the bond strength as a result of decreased effective perimeter of bars in contact with concrete. Generally, the ratios of $f_{b,bundled}/f_{b,single}$ ranged from 82% to 90% with an average of 85% for the two-bar bundles, and from 80% to 84% with an average of 82% for the three-bar bundles. As mentioned before, the minimum concrete cover on splices of single bars was similar to that of the companion individual splices within the staggered splices of bundled bars. However, the clear spacing, concrete cover, and depth of reinforcing bars varied within the splice zone of staggered bundled bars, which may exert different levels of confinement on the individual splices within a bundle compared to the companion single-bar splices. Nonetheless, it can hardly be the main reason for the reduced bond strength of individual splices within a staggered bundle with respect to that of the companion single-bar splices.

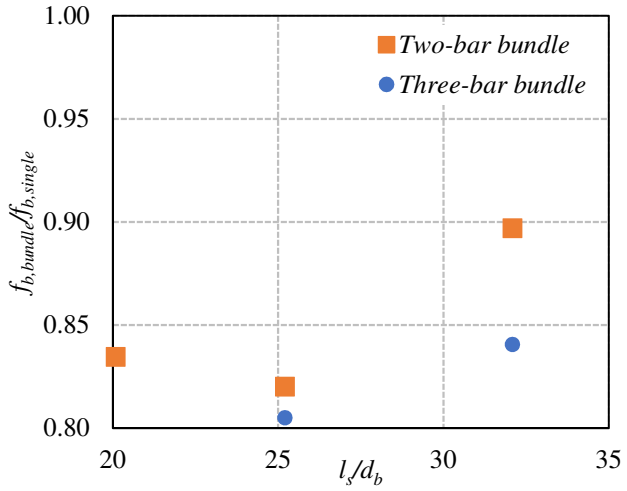

Figure 4-12: Influence of the number of bars in a bundle

4.7.3. Bar Size

The effect of bar size on bond behavior can be investigated by comparing the results of the beams with the same splice length, staggering pattern, and number of bars in a bundle. Figure 4-13 compares the normalized tensile stress and force at failure for No. 5 and No. 8 single bars and two-bar bundles. The normalized tensile force at failure was determined by multiplying the normalized tensile stress at failure by the nominal cross-sectional area of the reinforcing bar. As observed, the normalized tensile stress at failure was reduced, while the tensile force at failure was improved by increasing the bar diameter. Nonetheless, more experimental results are required to fully understand and quantify the influence of bar size on the bond behavior of GFRP bars.

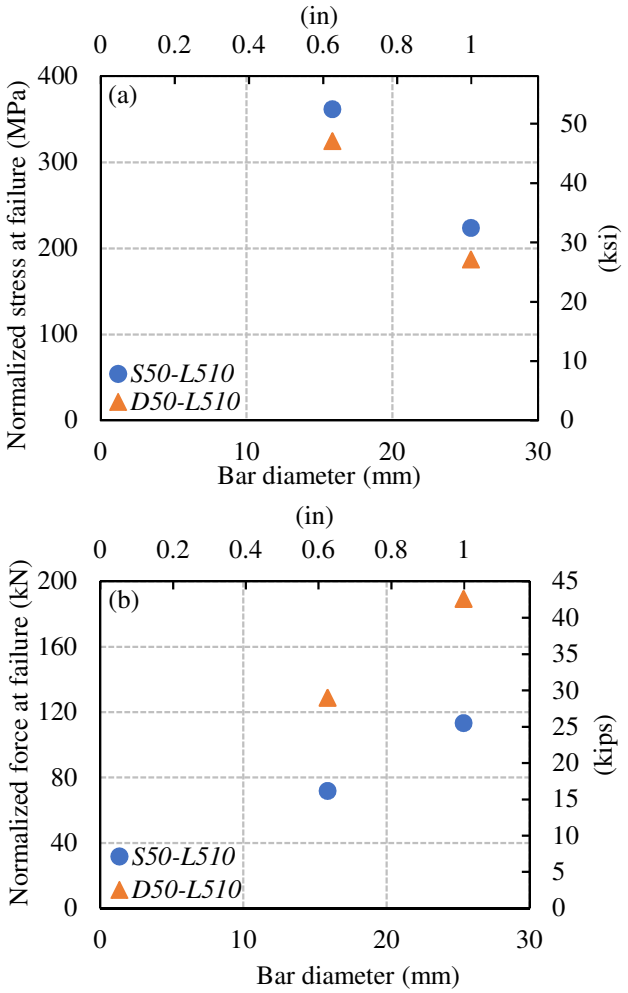

Figure 4-13: Influence of bar size on bond behavior

4.8. Design Provisions and Comparisons

ACI 440.1R-15 contains no design provisions for the lap splicing of bundled FRP bars. Consequently, this section first described the provisions stipulated in CSA S806-12 and ACI 318-14 for lap splicing of bundled GFRP and steel bars, respectively. The experimental results of the tested beams were then used to assess the accuracy of the design provisions in CSA S806-12 and the applicability of those of ACI 318-14 to bundled GFRP bars. In this regard, the incremental factors recommended in these codes were compared with the experimental findings of this study. In addition, the splice lengths used in the tested beams ($l_{s,test}$) were compared with those required to develop the experimental stresses (f_{test}) based on the code provisions ($l_{s,code}$).

4.8.1. CSA S806-12

According to CSA S806-12, the development length of each bar in a bundle shall be provided by the manufacturer. The number of bars in a single bundle is also restricted to three, while bundling is proscribed for GFRP bars larger than 25 *mm* in diameter [No. 8]. In addition, individual bars in a bundle should be cut off at different points at least $45d_b$ apart, where d_b is the diameter of individual bar and overlapping of individual bar splices in a bundle is prohibited. Furthermore, the splice length of bundled bars should be calculated based on the splice length of individual bars (1.3 times the development length) increased by 20% and 30% for two- and three-bar bundles, respectively.

Although according to CSA S806-12, the development length of each bar in a bundle shall be provided by the manufacturer, this code determines the development length of a single FRP bar as:

$$l_d = 1.15 \frac{k_1 k_2 k_3 k_4 k_5}{d_{CS}} \frac{f_F}{\sqrt{f_c^{'}}} A_b \quad \text{SI units} \tag{4-1}$$

where d_{CS} is the smaller of the distance from the closest concrete surface to the center of the bar being developed and two-thirds of the center-to-center bar spacing being developed. Moreover, k_1 is the casting position factor; k_2 is the concrete-density factor; k_3 is the bar-size factor; k_4 is a factor indicating the fiber type; and k_5 is a factor standing for the bar surface. In addition, f_F indicates the design stress in the FRP tension reinforcement at ultimate limit state. The value of d_{CS} and $f_c^{'}$ shall not be greater than $2.5d_b$ and 25 *MPa* [3626 *psi*], respectively.

4.8.2. ACI 318-14 and ACI 440.1R-15

Since ACI 440.1R-15 contains no recommendations regarding the splice length of bundled bars, the applicability of ACI 318-14 provisions to GFRP bars was assessed based on the experimental results of the current study. ACI 318-14 stipulates that the development length of bundled bars shall be at least equal to that of individual bars increased by 20% for bundles of three bars and 33% for bundles of four. This provision was aimed at considering the

reduction in the exposed perimeter of bars in a bundle compared to that of a single bar as reported in the commentaries in ACI 318-14. Considering these regulations, the lap-splice length of bundled bars shall be at least equal to that of individual bars increased by 20% for two-bar bundles and 33% for three-bar bundles (which comprise, respectively, a total of three and four bars in contact within the splice zone). According to ACI 440.1R-15, the requisite development length of an FRP bar in concrete can be determined by:

$$l_d = \frac{\alpha \dfrac{f_{fr}}{0.083\sqrt{f_c'}} - 340}{13.6 + \dfrac{C}{d_b}} d_b \quad \text{SI units} \tag{4-2}$$

where α is the casting position factor, f_{fr} is the required bar stress, and C is the smaller of the concrete cover to the center of the bar and half of the center-to-center spacing of the bars being developed. Moreover, the cover-to-diameter ratio (C/d_b) shall not be taken greater than 3.5. Furthermore, ACI 440.1R-15 (ACI Committee 440, 2015) recommends that the splice length of FRP bars should be at least 30% longer than the development length for all splices, regardless of splice percentage.

4.8.3. Incremental Factors for Bundled Bars

As mentioned above, CSA S806-12 and ACI 318-14 recommend 30% and 33% increases, respectively, in the splice length of individual bars in three-bar bundle splices. This incremental factor is 20% for splices of two-bar bundles in both codes. Considering the reduction of maximum perimeter of bars within a bundle as the rationale behind these increments, both CSA S806-12 and ACI 318-14 assume roughly 25% and 17% reduction in the effective perimeter of three-bar and two-bar bundles, respectively.

As discussed above, the experimental results indicate the average $f_{b,bundled}/f_{b,single}$ ratios of 85% for staggered two-bar bundles and 82% for staggered three-bar bundles. As these average experimental ratios are higher than those proposed in the design codes, it can be concluded that the reduction factors assumed in the codes are conservative. In contrast, the

non-staggered three-bar bundle revealed severe reductions in splice strength (40% as shown in Figure 4-11) in comparison with the values considered in the codes (around 25%). It can therefore be concluded that using the code provisions for non-staggered three-bar bundles might lead to a non-conservative splice length.

For non-staggered two-bar bundles, however, the reduction in splice strength as a result of bundling was close to the value in the codes (19% compared to 17% assumed by the codes). As mentioned earlier, the effective concrete cover was reduced in the non-staggered bundled splices, which can be considered the principal reason for the reduced bond strength. Therefore, for non-staggered bundled splices, an alternative design approach of using reduced equivalent concrete cover or using the concept of equivalent bar diameter instead of the reduction in the exposed area of individual splices in a bundle might result in a safer design splice/development length. A comprehensive experimental study is required to verify these design alternatives for non-staggered bundled splices, but this is beyond the scope of the current study. It should be mentioned that neither CSA S806-12 nor ACI 318-14 allowed splicing of bundled bars at the same section.

4.8.4. Splice Length and the Proposed Modification

The ratios of the required splice lengths based on the code provisions to those tested in this study ($l_{s,code}/l_{s,test}$) for all the tested beams are presented in Figure 4-14. As shown, the accuracy of the code provisions seems to be a function of the splice length-to-bar-diameter ratio (l_s/d_b) and bar diameter (d_b). In addition, Figure 4-15 illustrates the distribution of $l_{s,code}/l_{s,test}$ versus the ratio of the splice length-to-bar-diameter ratio (l_s/d_b) and bar diameter (d_b) in the beams with staggered splices. Based on these graphs, the accuracy of CSA S806-12 is a function of the splice length to bar diameter ratio, while the accuracy of ACI 440.1R-15 is reduced by increasing the bar diameter. The dependency on the bar size in ACI 440.1R provisions for splice strength of single bars has also been observed by other researchers (Pay et al., 2014; Zemour et al., 2018).

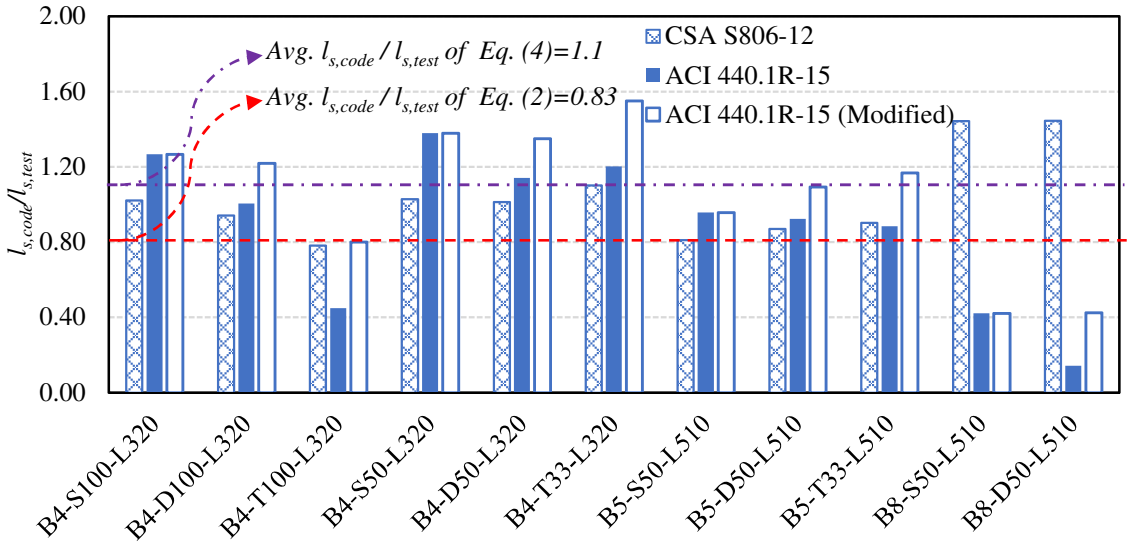

Figure 4-14: Assessment of splice length in CSA S806-12 and ACI 440.1R-15

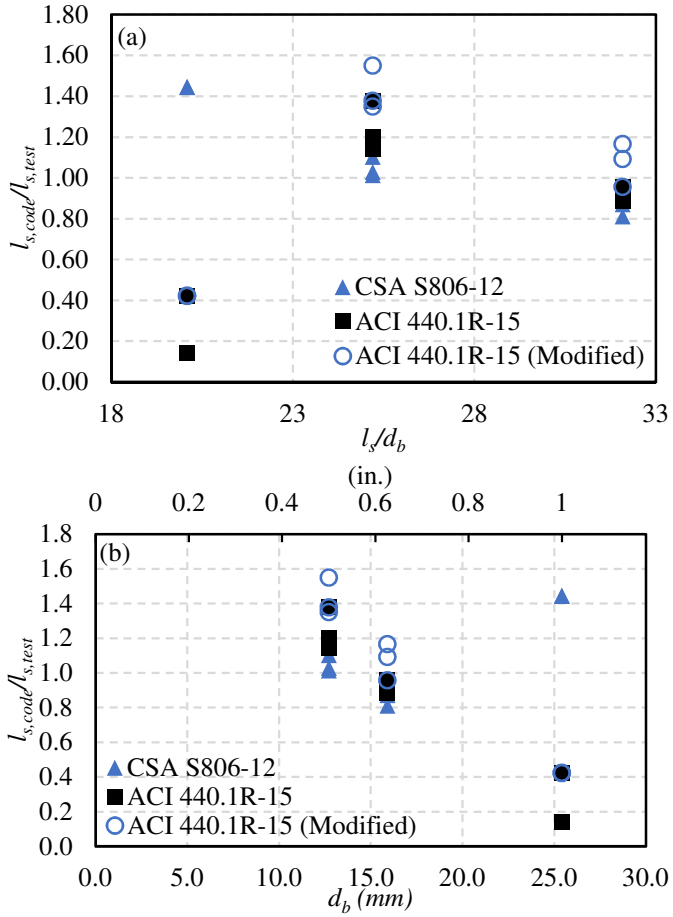

Figure 4-15: Variation of $l_{s,code}/l_{s,test}$ versus (a) the splice length-to-bar-diameter ratio, and (b) bar diameter according to CSA S806-12 and ACI 440.1R-15

Based on the provisions specified in the design codes, the splice length of an individual bar in a bundle should be increased linearly proportional to the reduction of the effective bar perimeter. The validity of this assumption is, however, arguable. Experimental studies on the effect of splice length on the bond strength of a single GFRP bar have indicated that the bond strength might not be linearly proportional to splice length in the case of unconfined beams (Mosley et al., 2008; Pay et al., 2014). Therefore, to compensate for the reduction in the bond strength of GFRP bars in an unconfined beam, the splice length should be increased by an amount larger than the amount of reduction in the bond strength. In other words, the splice length should be increased by amounts greater than 20% and 33% for two- and three-bar bundles, respectively. More experimental investigations are required to evaluate the effect of splice length on the bond strength of bundled GFRP bars. To avoid this complication, the splice length of an individual bar in a bundle could be designed based on a design stress (f_F and f_{fr} in Eq.(4-1) and Eq.(4-2), respectively) increased by 20% and 33% for two- and three-bar bundles, respectively. Accordingly, Eqs. (4-1) and (4-2) could be modified as Eqs.(4-3) and (4-4), respectively.

$$l_d = 1.15 \frac{k_1 k_2 k_3 k_4 k_5 k_6}{d_{CS}} \frac{f_F}{\sqrt{f_c'}} A_b \quad \text{SI units} \tag{4-3}$$

$$l_d = \frac{\alpha\beta \dfrac{f_{fr}}{0.083\sqrt{f_c'}} - 340}{13.6 + \dfrac{C}{d_b}} d_b \quad \text{SI units} \tag{4-4}$$

where k_6 and β are the bundling factor, and should be taken as follows:

k_6: 1.2 and 1.3 for two- and three-bar bundle splices, respectively;

β: 1.2 and 1.33 for two- and three-bar bundle splices, respectively.

It is worth mentioning that, according to CSA S806-12, the design stress and splice length are linearly proportional (see Eq. (4-1)). Therefore, considering this recommendation would have no effect on the resultant splice length. ACI 440.1R-15 was, however, assessed considering the modified expression (Eq. (4-4)) suggested herein, and the corresponding ratios of $l_{s,code}/l_{s,test}$ were illustrated in Figure 4-14. Overall, the average $l_{s,code}/l_{s,test}$

ratio of bundled bars improved from 0.83 as per ACI 440.1R-15 (Eq. (4-2)) to 1.10 using the modified expression (Eq. (4-4)). Therefore, predicting a splice length based on an increased stress could result in more reasonable splice lengths for bundled GFRP bars than the current design method of increasing splice length. Note that, although the ratios improved for the beams reinforced with No. 8 GFRP bars, ACI 440.1R-15 provisions still seem non-conservative. It is worth mentioning that no confinement was provided within the splice length of the bundled bars, which is not permissible based on code provisions. Transverse reinforcement confines concrete, which delays the initiation of the splitting cracks. It also helps control splitting-crack width and propagation, thereby increasing the bond strength between the reinforcing bars and concrete. Therefore, the bond strengths achieved experimentally are the least possible in practice.

4.9. Summary and Conclusions

Twelve full-scale beams were tested to investigate the effect of different variables on the bond behavior of spliced bundled GFRP bars. Based on the experimental results and observations, the following conclusions and design recommendations can be made:

1) Staggering had negligible effect on beam stiffness. It, however, could increase the splice strength, particularly in the case of three-bar bundles. It also reduced the maximum crack width.
2) Based on the strain measurements, all bars in a bundle may not act as a single unit as there was a relative displacement between them.
3) The splice strength decreased as the number of bars in a bundle increased. On average, the ratios of the bond strength of bundled bars to those of their companion single bars were 85% and 82% for two- and three-bar bundles, respectively.
4) Increasing the bar diameter reduced the normalized tensile stress at failure, while it increased the total tensile force at failure.
5) The factors assumed by the design codes for reduction in the bond strength of single bars as a part of a bundle were found to be conservative.
6) Based on the design codes, an increased development/splice length is required for individual bars that are part of a bundle. It was, however, found that the design of the

splice length of an individual bar in a bundle based on a design stress increased by 20% and 33% for two- and three-bar bundles, respectively, would provide more reasonable results.

As mentioned earlier, the staggered specimens did not completely comply with the design code and guidelines recommendations as: (a) the minimum staggering space of $45d_b$ was not complied with in this study due to the limitations in specimen size; and (b) no confinement was provided within the splice length. Although these configurations might lead to conservative results, considering the code recommendations might influence the ratio of the bond strength of single to bundled bars. Thus, further research needs to be conducted to better evaluate the bond behavior of bundled FRP bars and concrete. In addition, it is recommended to conduct more experimental investigations on the splice strength of non-staggered splices due to the simplicity they can add to both detailing and caging of reinforcement in real field applications.

4.10. Acknowledgments

This research was conducted with funding from the Tier-1 Canada Research Chair in Advanced Composite Materials for Civil Structures, the Natural Sciences and Engineering Research Council of Canada (NSERC), the NSERC Industrial Research Chair in FRP Reinforcement for Concrete Infrastructure, the Fonds de recherche du Québec en nature et technologies (FRQ-NT), and the Quebec Ministry of Transportation. The authors would like to thank the technical staff of the Canadian Foundation for Innovation (CFI) structural & materials lab in the Department of Civil Engineering at the University of Sherbrooke.

CHAPTER 5 Lap-splice Length of Bundled GFRP Bars in Unconfined Concrete

Avant-propos

Auteurs et affiliation:

Alireza Asadian: étudiant au doctorat, faculté de génie, département de génie civil, Université de Sherbrooke

Abolfazl Eslami : post-doctorat, faculté de génie, département de génie civil, Université de Sherbrooke.

Ahmed S. Farghaly : professionnel de recherche, faculté de génie, département de génie civil, Université de Sherbrooke.

Brahim Benmokrane: professeur, Faculté de génie, Département de génie civil, Université de Sherbrooke.

Date de soumission : 13 février 2019

État de l'acceptation : acceptée

Revue: ACI Structural Journal

Titre: Lap-Splice length of bundled GFRP bars in unconfined concrete

5.1. Abstract

This paper reports on the tensile lap splicing of bundled glass-fiber-reinforced-polymer (GFRP) bars and their bond behavior in unconfined concrete. The experimental program was comprised of 11 full-scale beam-splice tests and aimed at providing more insights into the design parameters that might affect the splice strength of bundled GFRP bars. The studied parameters included the splice length, bar diameter, and number of bars within a bundle. The results indicated that the bond strength of lap-spliced bundled GFRP bars was not linearly proportional to the splice length. Moreover, the splice strength was found to be inversely proportional to the bar diameter. In addition, the bond strength of individual bars in a bundle was lower than that of single bars. Their general behavior in terms of splice length effect, failure mode, bar-size effect, and stress distribution, however, appeared to be similar. Finally, a design recommendation is proposed based on the experimental results and observations that might provide a significant improvement in the safety level for lap-spliced bundled GFRP bars.

Keywords: Bond strength, concrete, bundled GFRP bars, beams, splice length, moment–curvature analysis, design recommendation

5.2. Introduction

Glass-fiber-reinforced-polymer (GFRP) bars are being used as the internal reinforcement in reinforced-concrete (RC) structural elements to overcome steel-corrosion issues and reduce the lifecycle maintenance cost of RC structures (ACI Committee 440, 2015). GFRP bars and steel bars have different mechanical properties. While steel reinforcing bars are ductile with plastic deformations after yielding, GFRPs are brittle with linear elastic behavior up to failure. Furthermore, the elastic modulus of steel is almost four times higher than that of GFRP.

Different mechanical properties are the basis for the different flexural-design philosophies for FRP- and steel-reinforced concrete members (ACI Committee 440, 2015). Designing for tension-controlled failure is commonly practiced for steel-reinforced-concrete flexural members to ensure ductile structural behavior. On the other hand, compression-controlled failure is highly desirable in designing FRP-reinforced concrete members to ensure the member displays some inelastic behavior before failure (Nanni, 1993; ACI Committee 440, 2015).

If an FRP-RC section is controlled by compression failure of concrete, the reinforcement stress at the ultimate-limit-state (ULS) would be lower than its guaranteed tensile strength. In such circumstances, the full tensile strength of FRP bars would not need to be developed in design. Moreover, the serviceability-limit-state (SLS) requirements often govern the design of FRP-RC sections, which, in turn, increases the reinforcement ratio. Due to these reasons, FRP design codes normally permit the design of the development or splice length of FRP bars based on the developed reinforcement stress at ULS instead of their guaranteed tensile strength (Japan Society of Civil Engineers, 1997; Canadian Standards Association, 2012, 2014a; ACI Committee 440, 2015). Therefore, the reinforcement stress at ULS and the practical design of the development length may vary entirely from one section geometry and loading condition to another. This brings out the importance of development length on the bond behavior of FRP bars.

When an RC section requires heavy reinforcement, bundling offers several advantages over other alternatives. In comparison with equally spaced single bars, bundling reduces the reinforcement congestion, facilitating the placement of reinforcing bars and consolidation of the concrete. Compared to placing the reinforcement in layers, bundling increases the effective depth of the longitudinal reinforcement and thus provides moment-capacity efficiency. Moreover, bundling offers a practical alternative for large-size bars, which might not be available on the market at the time of construction.

5.3. Literature Review

In the past couple of decades, the bond behavior of spliced GFRP bars and concrete has been extensively investigated with the beam–splice test method (Tighiouart et al., 1999; Aly et al., 2006b; Mosley et al., 2008; Harajli & Abouniaj, 2010; Choi et al., 2012; Esfahani et al., 2013; Pay et al., 2014; Zemour et al., 2018). Many parameters have been found to influence the strength of GFRP splices. They include the splice length, bar diameter, confinement provided by the surrounding concrete and transverse reinforcement, surface treatment, concrete type, casting position, and concrete compressive strength (Tighiouart et al., 1999; Aly et al., 2006b; Mosley et al., 2008; Harajli & Abouniaj, 2010; Choi et al., 2012; Esfahani et al., 2013; Pay et al., 2014; Zemour et al., 2018). It has also been indicated that, for the same bar diameter and splice length, the GFRP bars had lower splice strength than steel bars (Mosley et al., 2008; Pay et al., 2014; Zemour et al., 2018). The difference in the splice strength was attributed to the difference in their mechanical properties and surface treatments. Therefore, it is expected that the effect of bundling on the splice strength of GFRP bars will be different than that of steel bars.

Research on single-bar splices also found that bond strength might not be linearly proportional to splice length (Mosley et al., 2008; Choi et al., 2012; Pay et al., 2014; Zemour et al., 2018). This relation, however, is believed to be dependent on splice length (Pay et al., 2014; Zemour et al., 2018). The results obtained by Mosley et al. (2008) indicate that the bond strength of GFRP bars in unconfined concrete would be proportional to the square root of the splice length for short splices. Pay et al. (2014), however, reported that the square-

root relationship might provide nonconservative predictions for longer splices in unconfined concrete. Similar nonlinearly proportional relationships between bond strength and splice length can also be observed from the data reported by other researchers (Tighiouart et al., 1999; Aly et al., 2006b; Harajli & Abouniaj, 2010; Choi et al., 2012; Zemour et al., 2018).

Despite the vast number of experimental studies on the bond behavior of spliced single FRP bars, the number of beam–splice tests on the bond behavior of bundled FRP bars is rather limited. Aly et al. (2006a) tested nine full-scale beams reinforced with 9.5 mm [0.37 in.] Carbon (CFRP) bars, all spliced in the same section. Their beams were confined with 8 mm [0.31 in.] steel transverse reinforcement spaced at 150 mm [5.91 in.] on centers over the splice length. The relationship between the maximum bar stress at the splice end and splice length was linear. Accordingly, a procedure was proposed to determine the critical splice length of FRP bars. Based on their results, the critical splice lengths required for developing the full tensile strength of single bars and two- and three-bar bundles of 9.5 mm [0.37 in.] CFRP bars were determined to be around $75d_b$, $90d_{be}$, and $95d_{be}$, respectively, where d_b is the diameter of a single bar and d_{be} is the equivalent diameter of bundled bars (Aly et al., 2006a). Furthermore, they indicated that the splice length of individual bars within a bundle is equal to that of a single bar, increased by 60% for a two-bar bundle, and 100% for a three-bar bundle. It should be noted that the splice arrangement used by Aly et al. (2006a) did not comply with code recommendations(Canadian Standards Association, 2012), as all bars were spliced in the same section.

Few research studies have been conducted on the splices of bundled steel bars. Bashandy (2009) performed 16 beam–splice tests in which all the bars in a bundle were spliced at the same section within the splice length. The results indicated that the cracking pattern, failure load, and splice strength of two-, three-, and four-bar bundles were similar to those of a bar having a similar cross-sectional area, level of confinement, and splice length. It was also found that the stress distribution along the splice length at failure followed a similar trend for the bundled bars and equivalent companion bars (Bashandy, 2009). Bashandy (2009) also concluded that splicing all bars in a bundle in the same section could be a safe practice. It was also noted that calculating the splice length of bundled bars based on the diameter of

a bar having the same cross-sectional area as the bundle could provide an accurate estimation (Bashandy, 2009). Later, Cairns (2013) tested 10 large-scale beams to investigate the performance of two- and three-bar bundles and assessed the accuracy of ACI 318-08 provisions for calculating the splice length of bundled bars. Cairns observed that the bond strength of individual bars within a bundle was similar to an equally spaced single bar. In addition, it was noted that the strength of lap splices did not correlate to the exposed area of bars in a bundle. Instead, it was controlled by resistance to the splitting force induced by the bond action (Cairns, 2013). Moreover, it was pointed out that the concept underlying the ACI 318-08 provision for increasing the splice length due to a reduction in the exposed perimeter might not be justified (Cairns, 2013).

The paucity of experimental data has led to the lack of knowledge and scarcity of design provisions in most international design codes and guidelines such as ACI 440.1R-15 (ACI Committee 440, 2015), CSA S06-14 (Canadian Standards Association, 2014a) and JSCE-97 (Japan Society of Civil Engineers, 1997). Only CSA S806-12 (Canadian Standards Association, 2012) stipulates some recommendations for bundled GFRP bars, which are mostly similar to those for steel bars proposed in North American codes (ACI Committee 318, 2014; Canadian Standards Association, 2014b), despite the differences in their mechanical properties and bond behavior.

CSA S806-12 (Canadian Standards Association, 2012) provisions indicate that the splice length of individual bars within a bundle should be increased by 20% and 30%, respectively, for two- and three-bar bundle splices, regardless of the splice length. Given the dependency of the bond strength of GFRP bars on splice length, this assumption might not be valid and necessitate further investigation. Consequently, the current study was undertaken to provide more insight into how splice length can affect the splice strength of bundled GFRP bars in unconfined concrete. In addition, bar size, which is considered a crucial factor affecting splice strength, was also examined. The bond behavior of spliced single bars was also compared to that of bundled bars, and a recommendation was made for design purposes.

5.4. Research Significance

The paucity of experimental data has led to the lack of knowledge and scarcity of design provisions in most design codes and guidelines such as ACI 440.1R-15 (ACI Committee 440, 2015), CSA S06-14 (Canadian Standards Association, 2014a) and JSCE-97 (Japan Society of Civil Engineers, 1997). Thus, the current study was conducted to provide more insight into the effect of splice length and bar diameter on the splice strength of bundled GFRP bars in unconfined concrete. The bond behavior of spliced single bars was also compared to that of bundled bars, and a recommendation was made for design purposes. In addition, the results of moment–curvature analysis in terms of the neutral-axis depth as well as reinforcement and concrete strains were compared to the experimental measurements and observations. Moreover, the findings of this study may support the work of the North American technical committees engaged in developing standards and design provisions for GFRP-RC flexural members.

5.5. Experimental Program

5.5.1. Specifications of the Test Specimens

The experimental program was compromised of 11 full-scale beam specimens reinforced with different diameters of GFRP bars and with different splice lengths. The beams were tested under four-point bending load. Figure 5-1 provides the details of the geometry of the test specimens. All beams had a rectangular cross section of 300×450 *mm* [11.81×17.71 *in.*]. The total length and effective span of each beam was 5200 [204.72 *in.*] and 5000 mm [196.85 *in.*], respectively. To accommodate the entire splice length, the constant-moment region was designed to be 2500 *mm* [98.43 *in.*], leading to a shear span of 1250 *mm* [49.21 *in.*].

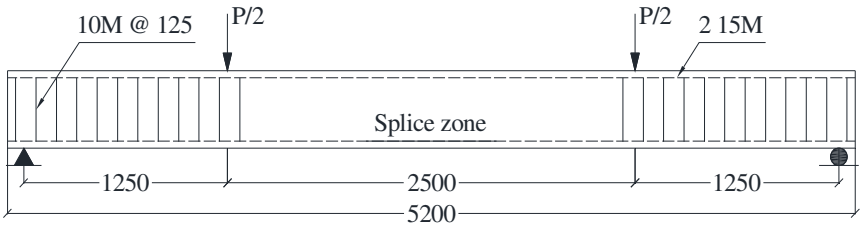

Figure 5-1: Details of the geometry and transverse reinforcement of the test beams (Note: all dimensions are in mm; 1 mm=0.0394 in.)

The design of the beams with lap splices aimed at achieving a bond-splitting failure prior to either flexural or shear failure. The shear design of the beams was carried out according to CSA S806-12 (Canadian Standards Association, 2012). Accordingly, the shear span of each beam was reinforced with 10M steel stirrups at 125 *mm* [4.92 *in.*] spacing. To exclude the confining effect of stirrups from other parameters and assess the minimum bound of the splice strength of bundled GFRP bars, no stirrups were provided within the flexural span. In field applications, however, the lap splicing of bundled bars without any transverse reinforcement may not be typical. Sand-coated GFRP bars in three different diameters (No. 4, No. 5, and No. 8) were used as tension reinforcement, as shown in Figure 5-2. In addition, to provide support for the stirrups during caging and to facilitate specimen handling after testing, two 15M steel bars were used as compression reinforcement. Figure 5-3 shows a completed reinforcement cage. The side concrete cover of the spliced bars and the clear bar spacing were designed in such a way that the failure of all specimens be governed by the bottom concrete cover splitting. To fulfill this objective, the bottom clear cover was taken as 32 *mm* [1.26 *in.*] for all the test specimens. In addition, side clear cover was 45 *mm* [1.75 *in.*] and the clear spacing of the spliced bars was greater than two times the bottom cover. Therefore, the bond behavior of specimens was expected to be governed by the bottom cover as the smallest value of the clear covers and half of the clear spacing between the spliced bars.

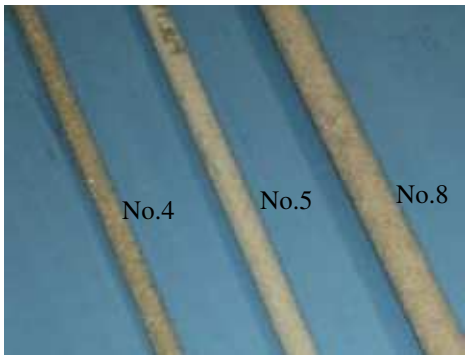

Figure 5-2: Sand-coated GFRP reinforcing bars

Figure 5-3: A completed reinforcement cage

The test specimens were designed to represent a full range of bundling patterns and bar diameters, as indicated in Table 5-1. Figure 5-4 illustrates the bar arrangements within the splice zone. According to CSA S806-12 (Canadian Standards Association, 2012), each bar within a bundle should be cut off at different points at least $45d_b$ apart; the overlapping of bar splices within a bundle is not permitted. The spliced bars in this study, however, were not compliant with this limitation due to the total length of the test specimens. Nonetheless, a space of 40 *mm* [1.57 *in.*] was left between two consecutive splices to avoid any interruption in bond strength due to the installation of strain gauges.

The specimens were designated with a system of letters and numbers. The nomenclature starts with the letter B, followed by a number identifying the bar size (4, 5, or 8 for No. 4, No. 5, or No. 8 bars, respectively). The second letter refers to the bundle type (S, D, and T for single bars, two-bar bundles, and three-bar bundles, respectively), while the second number (33 or 50) represents the percentage of bars staggered in each section within the splice length. The final digits after the letter L indicate the splice length of individual bars in mm.

Table 5-1: Details of test beams

Beam	Bar size	l_s *mm*	Splice Pattern#	f_c' *MPa*	f_t *MPa*
B4-T33-L320	No.4	320	T33	40.9	3.70
B4-T33-L400	No.4	400	T33	39.6	4.00
B4-T33-L510	No.4	510	T33	39.6	4.00
B5-D50-L400	No.4	400	D50	40.3	3.96
B5-D50-L510	No.5	510	D50	33.7	3.42
B5-D50-L640	No.5	640	D50	33.7	3.42
B5-T33-L510	No.5	510	T33	33.7	3.42
B5-S50-L510	No.5	510	S50	33.7	3.42
B8-S50-L510	No.8	510	S50	35.3	2.86
B8-D50-L510	No.8	510	D50	35.3	2.86
B8-D50-L640	No.8	640	D50	35.3	2.86

Note:
see Figure 5-4 for details
1 *mm*=0.0394 *in.*, 1 *MPa*=0.145 *ksi*

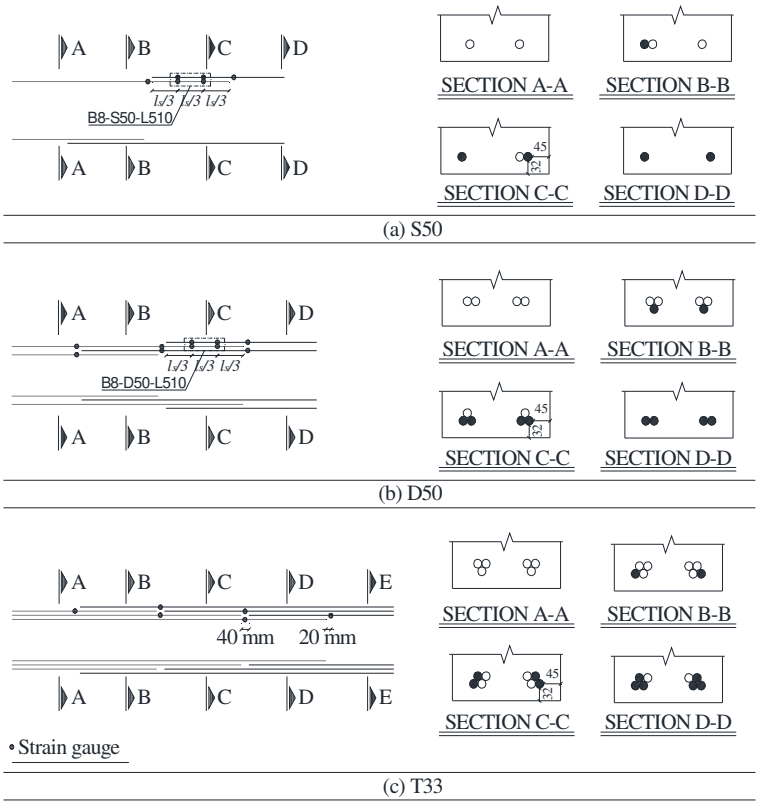

Figure 5-4: Schematic illustration of the bar arrangement along the splice length and location of strain gauges in different staggered patterns: (a) S50, (b) D50, and (c) T33 (Note: all dimensions are in mm; the reinforcement in black is pairs of bars from the right side of the splice zone; 1 *mm* = 0.0394 *in.*)

5.5.2. Material Properties

Deformed 10M and 15M steel bars were used as transverse and compression reinforcement, respectively. Sand-coated GFRP bars in three different sizes (No. 4, No. 5, and No. 8) were used as tension reinforcement (Figure 5-2). Table 5-2 presents the mechanical properties of the GFRP and steel bars. The values associated with the GFRP bars were determined based on the average of five specimens tested in accordance with CSA S806-12(Canadian Standards Association, 2014b).

Table 5-2: Mechanical properties of reinforcing bars

Bar Type	Bar Size	Bar Diameter (*mm*)	Elastic Modulus (*GPa*)	Tensile Strength (*MPa*)	Tensile Strain (%)
GFRP	No.4	12.7	51.7	1243	2.40
	No.5	15.9	51.1	1296	2.54
	No.8	25.4	51.6	1035	2.00
Steel	10M	11.3	200	f_y =460	ε_y =0.20
	15M	16	200	f_y =460	ε_y =0.20

Note:
ε_y is the yield strain and f_y is the yield stress.
1 *mm*=0.0394 *in.*, 1 *MPa*=0.145 *ksi*

A normal-weight ready-mixed concrete was used to cast the test specimens. The target 28-day concrete compressive strength was 35 *MPa* [5.08 *ksi*] with a maximum aggregate size of 14 *mm* [0.55 *in.*]. The actual compressive and tensile strengths of the concrete in each casting were, however, determined on concrete cylinder specimens (100×200 *mm* [3.94×7.87 *in.*]) tested on the same day as the beam testing. The day after casting, all the beams and cylinders were demolded and then moist-cured for seven days. Subsequently, the specimens were kept under the same environmental conditions until the testing day. Table 5-1 gives the compressive and splitting tensile strengths, determined based on the average value of five cylinders tested on the same day at the beginning of the testing day. It should be noted that the differences in the compressive and splitting tensile strengths reported in Table 5-1 can be due to the fact that the beams were cast from different batches delivered to the laboratory.

5.5.3. Test Setup, Instrumentation, and Loading

The beams were tested under four-point bending load, as shown in Figure 5-5. The load was applied through a 1000 *kN* [225 *kip*] MTS actuator at a stroke-controlled rate of 1.2 *mm/min*. Figure 5-5 provides a schematic illustration of the test setup. The displacement was monitored with four linear variable differential transformers (LVDTs); two were placed at the mid-span and two below the loading points. During the test, the beam cracking patterns were marked visually, and their corresponding loads recorded. The test was paused once the first two cracks initiated close to the splice ends. For each crack, the initial crack width was measured using an electronic microscope, thereafter a LVDT was installed perpendicular to the crack to record the crack width development up to failure. Other cracks within the flexural span was visually inspected during loading. The visual monitoring was stopped once it was considered unsafe to approach the beam.

The strain variation in the reinforcing bars and concrete were obtained with a series of electrical resistance strain gauges. Figure 5-4 illustrates the position of the strain gauges bonded to the spliced bars. Bar discontinuity at the splice ends can alter beam stiffness, leading to crack formation at these locations. Thus, to avoid the possibility of strain-gauge damage induced by crack propagation during testing, the strain gauges were installed 20 *mm* [0.79 *in.*] away from the splice ends (Figures 4-3 and 4-4). In addition, the distribution of strain values on the concrete surface was measured with a total of five strain gauges attached to each beam (Figure 5-5). Two of the five gauges were attached to the section corresponding to one end of the splice zone; one on the top compression surface and one on the side of the beams, 30 *mm* [1.18 *in.*] below the top compression surface. The remaining three gauges were attached at the mid-span: one on the top compression surface and two on the side of the beams; 30 and 60 *mm* [1.18 and 2.36 *in.*] below the top compression surface. During the test, an automatic data-acquisition system was implemented to record all the data collected, including loads, displacements, crack widths, and strain values.

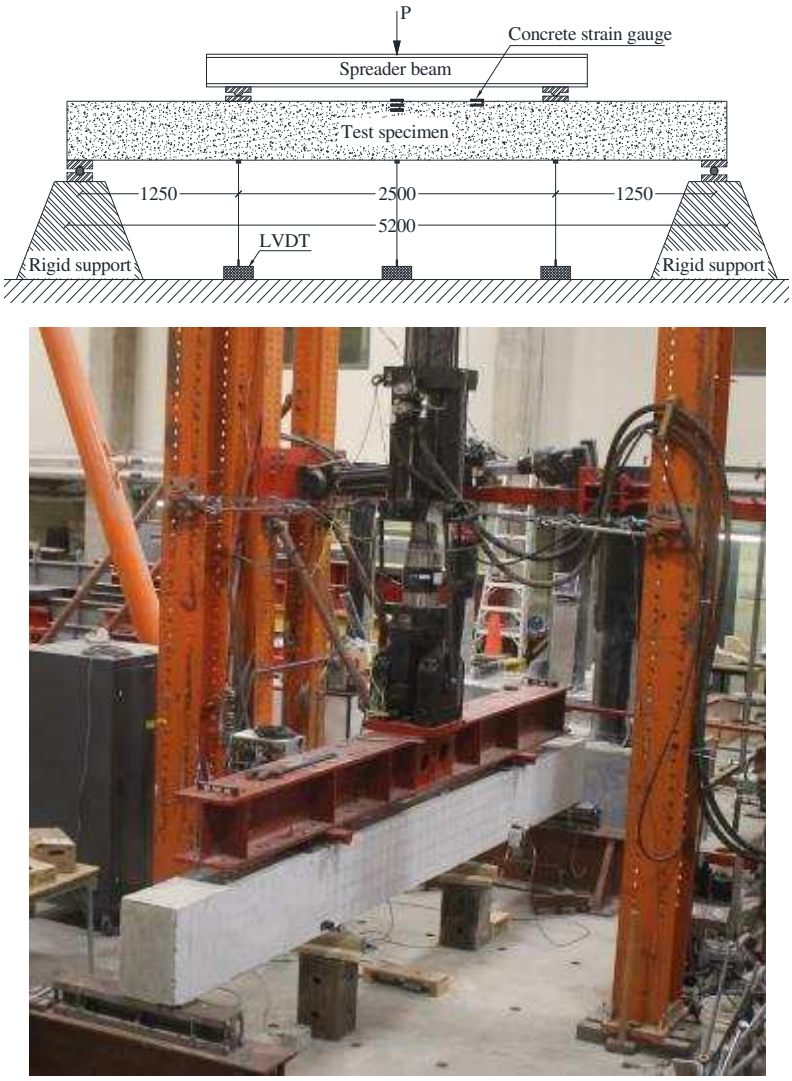

Figure 5-5: Details of test setup, and location of LVDTs and concrete strain gauges (All dimensions are in mm; 1 *mm*=0.0394 *in.*)

5.6. General Behavior

5.6.1. Load–Deflection Curves

Figure 5-6 shows the total load versus mid-span deflection for all beams. All the load–deflection curves followed a similar trend. The behavior was linear elastic up to cracking, after which the curves rose linearly up to the failure point with a noticeable reduction in stiffness.

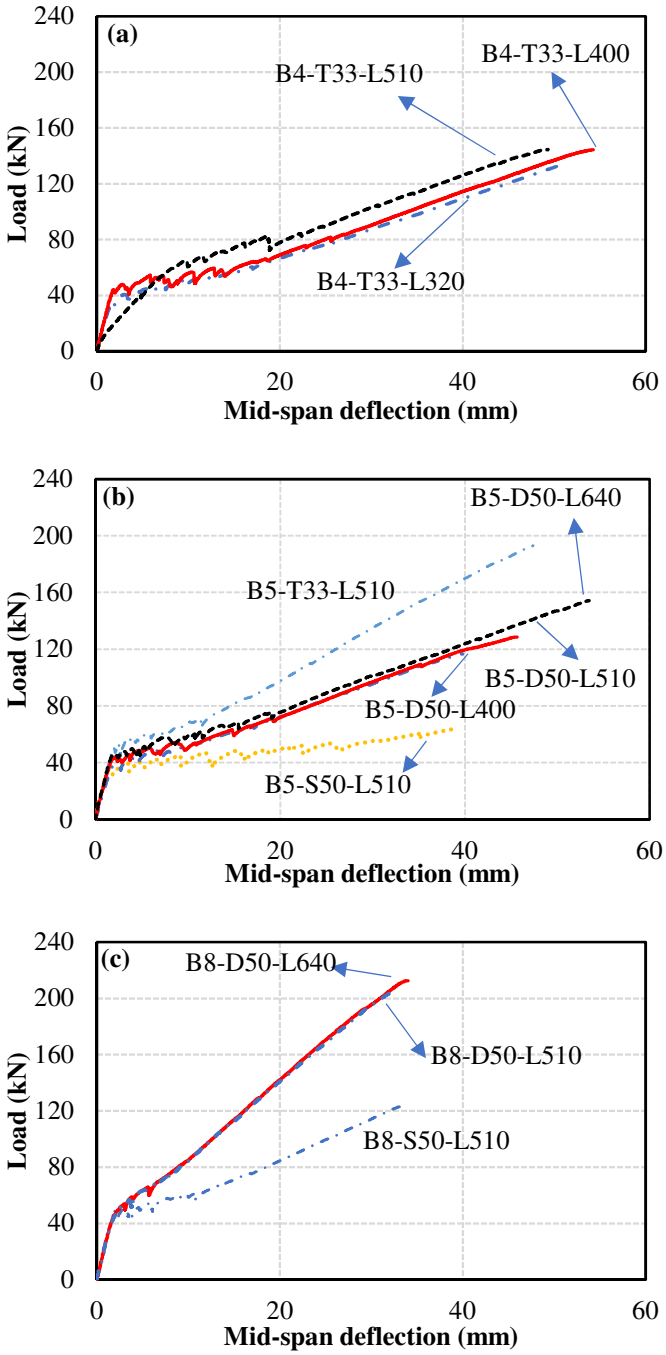

Figure 5-6: Load–deflection responses of (a) No. 4, (b) No. 5, and (c) No. 8 (Note: 1 *mm*=0.0394 *in.*; 1 *kN*=0.2248 *kip*)

As shown in Figure 5-6, regardless of the splice length, the companion beams with the same bar size showed similar pre-cracking stiffness. Table 5-3 gives the cracking loads (P_{cr}) of all beams. Overall, increasing the splice length could slightly increase the cracking load. Likewise, the post-cracking stiffness of the companion beams reinforced with different

splice lengths were barely different (Figure 5-6). It is worth noting that some small discrepancies in P_{cr} and post-cracking stiffness with the companion beams might be attributed to the slight difference in concrete compressive strength. Figure 5-6 shows the clear effect of the splice length in increasing the failure load (except for B4-T33-L50). In B4-T33-L510, pre-existing cracks were observed prior to loading, which might be resulted from handling and transportation and led to a substantial reduction in the beam's initial stiffness and no improvement in failure load as a result of increasing its splice length compared to B4-T33-L400. Therefore, the failure mode and general behavior of B4-T33-L510 are discussed herein, but its results were discarded in calculating bond behavior.

Table 5-3: Experimental and analytical results

Beam	Experimental			M-φ	Normalized	
	P_{cr} *kN*	P_u *kN*	f_{test} *MPa*	$f_{M-\varphi}$ *MPa*	$f_{test,n}$ *MPa*	$F_{test,n}$ *kN*
B4-T33-L320	34	134.6	335	320	333	127
B4-T33-L400	44	144.4	367	334	368	143
B4-T33-L510	-	144.5	356	-	357	136
B5-D50-L400	37	116.6	263	268	263	104
B5-D50-L510	44	128.7	311	298	324	129
B5-D50-L640	46	154.4	359	343	375	149
B5-T33-L510	51	193.2	291	289	304	181
B5-S50-L510	38	63.6	346	311	362	72
B8-S50-L510	50	124.0	217	226	224	113
B8-D50-L510	50	204.4	181	213	187	189
B8-D50-L640	49	212.5	198	223	204	207

Note:
1 *mm*=0.0394 *in.*, 1 *kN*=0.2248 *kip*, 1 *MPa*=0.145 *ksi*

5.6.2. Failure Modes

The initial flexural cracks developed within the constant-moment region and, in most cases, outside the splice zone. The number and depth of flexural cracks within the constant-moment region increased as the load increased. At higher load levels, hairline splitting cracks appeared on the bottom and sides of the beams. As anticipated in the initial design, the failure of all beams was accompanied with the sudden splitting of the concrete cover in the spliced region.

Figure 5-7 shows the observed failure modes of representative specimens with single, two-bar bundle, and three-bar bundle splices. As shown in Figure 5-7, the splitting pattern of specimens reinforced with the bundled bars of the same size but with different splice lengths were similar. A close inspection of the beams after failure revealed that the splitting pattern of beams reinforced with No. 8 bars differed from that reinforced with No. 5 and No. 4 bars. In the former, a horizontal splitting crack developed in the clear spacing between the bars just before failure; the splitting cracks appeared only on the bottom and sides of the beams with No. 5 and No. 4 bars. Regardless of the reinforcement size, the depth of horizontal splitting cracks appearing on the beam sides were comparable, as shown in Figure 5-7.

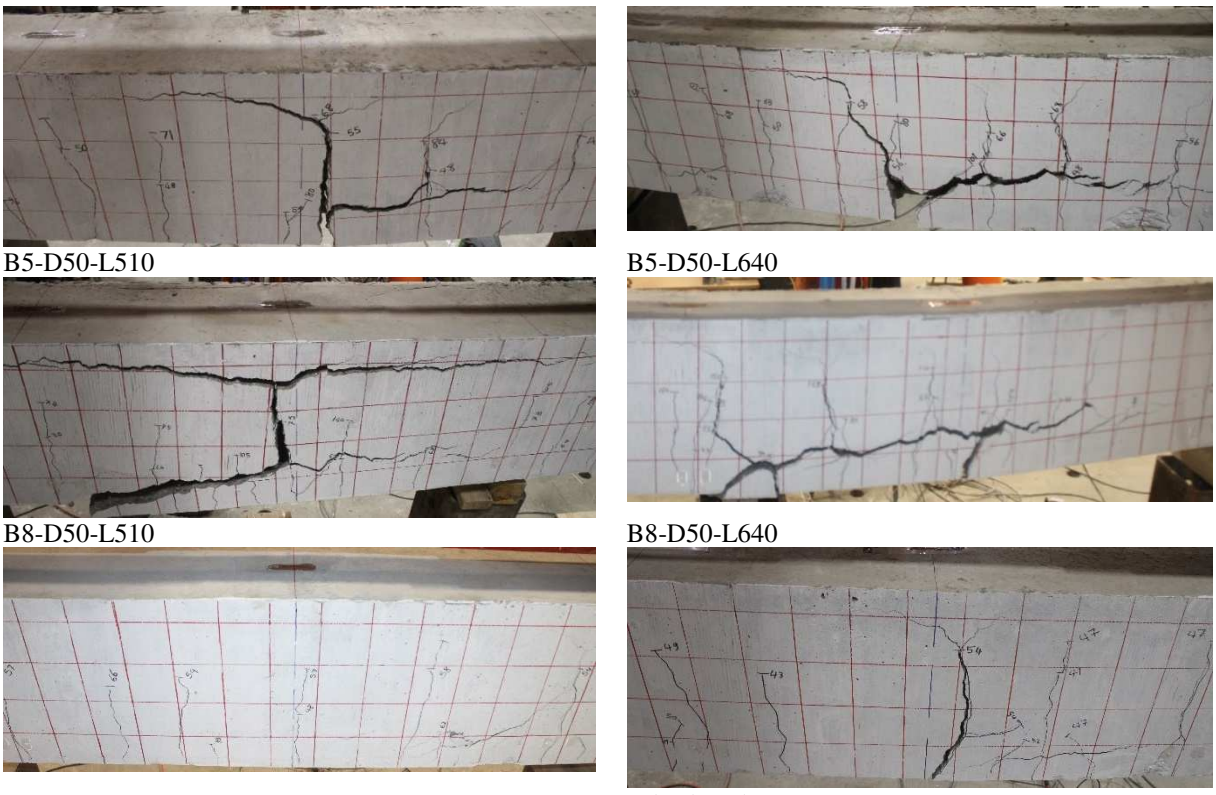

B5-D50-L510 B5-D50-L640

B8-D50-L510 B8-D50-L640

B4-T33-L400 B5-S50-L510

Figure 5-7: Observed failure modes

5.6.3. Crack Width

Based on observations, the widest cracks always extended at the splice ends. In other words, the cracks formed outside the splice zone and those within splice length were narrower. This was confirmed by visual inspections during testing. Figure 5-8 provides a comparison of the

distributions of maximum crack width versus the applied load of the companion beams to evaluate the effect of splice length and bar size on the maximum crack width of bundled beams. In general, increasing the bar size could substantially reduce the maximum crack width observed at the same load level. This is mainly ascribed to the increasing axial rigidity of longitudinal reinforcement in beams with larger bar-size. Moreover, the beams reinforced with longer splices exhibited slightly narrower cracks compared to those with shorter splices. Given the same reinforcement ratio and surface treatment, the wider cracks in shorter splices might be related to less slippage sustained by the longer splices. It should also be noted that the initial locations of crack as well as the position of the widest crack in different specimens were not similar. This is due to the uncertainties associated with cracking of RC members. In addition, the widest crack widths reported herein, are related to the greater of the two LVDTs measurements. It is also worth mentioning that the actual crack width in GFRP-RC beams with spliced bars might be narrower in practice, as the values presented herein indicate the maximum widths observed at the ends of splices designed with insufficient splice length. Moreover, providing a gap between the ends of the staggered splices may decrease the maximum crack widths. However, as no companion specimen with a gap between the staggered splices was tested herein, more experimental researches are recommended to confirm this.

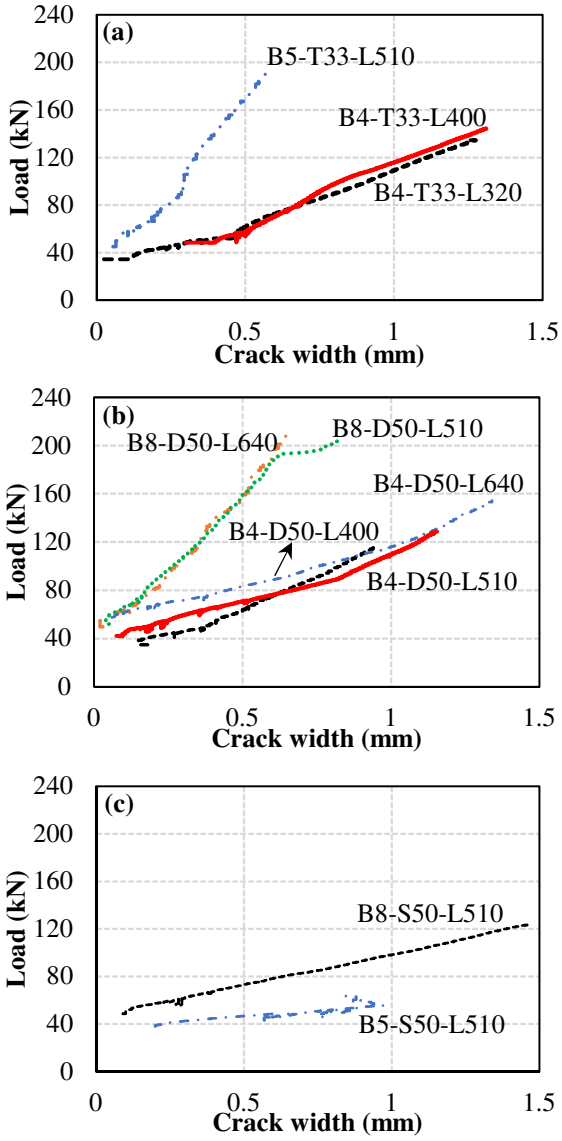

Figure 5-8: Distribution of maximum crack width versus applied load: (a) No. 4 and No. 5 three-bar bundles, (b) No. 5 and No. 8 two-bar bundles, and (c) No. 5 and No. 8 single bars (Note: 1 *mm*=0.0394 *in.*; 1 *kN*=0.2248 *kip*)

5.7. Test Results and Discussion

5.7.1. Evaluation of the Bond Strength

The bond strength was considered as the stress withstood by the spliced bar at peak load. This stress, herein referred to as the failure stress of reinforcement (f_{test}), was obtained by multiplying the elastic modulus (E) of the GFRP bars by the mean value of the strains

measured at peak load at the splice ends, (ε_{test}). Subsequently, the corresponding peak force was calculated as $F_{test} = nf_{test}A_b$, where n is the number of bars bundled together and A_b is the nominal cross-sectional area of each individual bar. It should also be mentioned that a few strain gauges damaged during the test were excluded from the calculations.

It is believed that the bond strength of reinforcing bars would be proportional to the fourth root of the compressive strength of concrete (ACI 408 Committee, 2003; Darwin et al., 2005). Thus, for comparison purposes and to avoid the effect of variations in concrete strength on the calculated bond strengths, all stresses and forces were normalized to the fourth root of the concrete compressive strengths divided by 40 *MPa* [5.80 *ksi*] ($\sqrt[4]{(f_c'/40)}$ in SI units). Table 5-3 presents the recorded and normalized experimental results for all the test specimens.

5.7.2. Strain State in the Reinforcing Bars and Concrete

Representing the general behavior of all specimens, Figure 5-9 shows the data obtained from the strain gauges versus the total applied load for the specimens reinforced with No. 5 two-bar bundles. The strain measurements in the other specimens were likewise consistent, so they are not discussed herein for the sake of brevity. Figure 5-9 (d) provides a schematic sketch of strain-gauge position and numbering. As observed in Figure 5-9 (a-c) the magnitudes of developed strain in the reinforcing bars and concrete before the initiation of the flexural cracks were not considerable. Thereafter, sudden increases in strain were noticed, especially in the reinforcing bars. In addition, the post-cracking strain values diverged depending on the position of the strain gauge in the splice zone and cross section. The strains in the reinforcing bars revealed that increasing splice length could slightly reduce the discrepancy in strains recorded in the splice length. It should be noted that strain measurements might be influenced by tension-stiffening effect and the position of strain gauges with respect to the nearby flexural cracks. Moreover, concrete cover and the effective depth of reinforcing bars varied in the splice zone of the bundled bars (refer to Figure 5-4 for the detail of the reinforcement in different sections in the splice zone). This variation

might exert various degrees of confinement on the reinforcing bars in a bundle, causing different performance of the spliced bars.

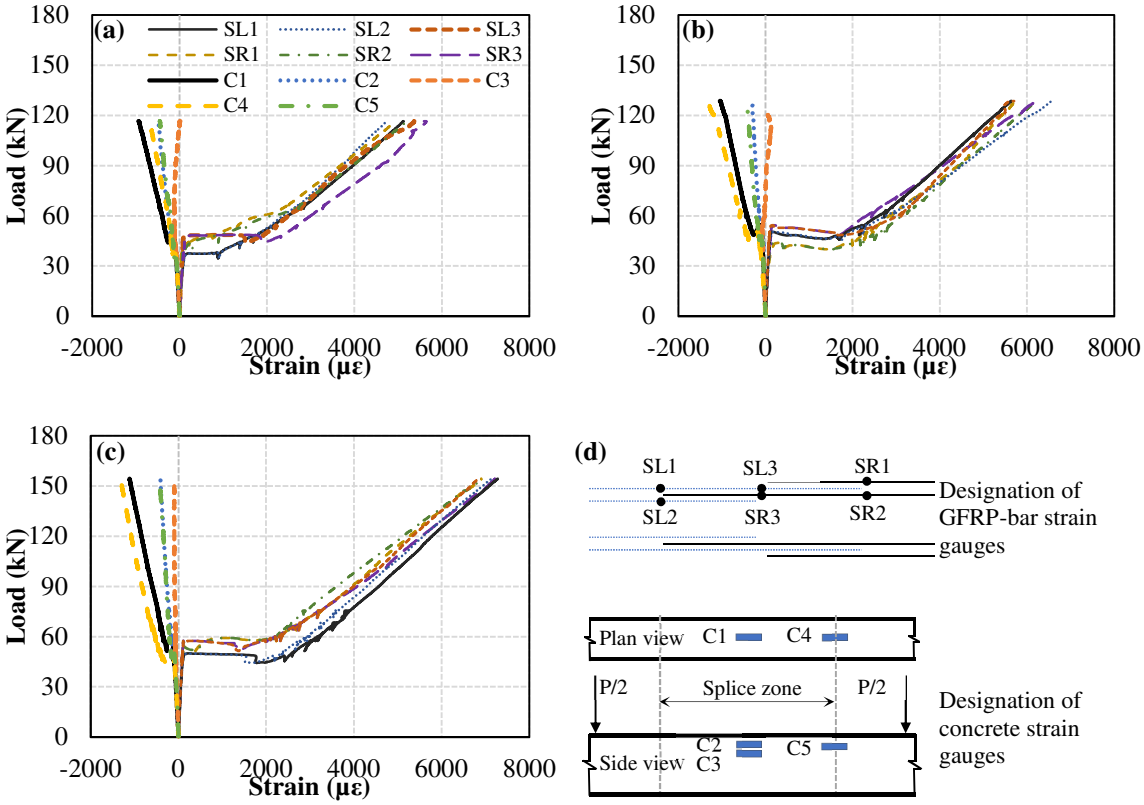

Figure 5-9: Reinforcing-bar and concrete strain versus applied load: (a) B5-D50-L400, (b) B5-D50-L510, (c) B5-D50-L640, (d) position of strain gauges (1 kN=0.2248 kip)

5.7.3. Comparison of Experimental and Analytical Stresses

In order to evaluate the accuracy of the analytical methods in estimating the strain values of beams reinforced with spliced bars, the experimentally measured strain values were compared with those calculated analytically. In the analytical approach, the cracking load was determined from the elastic flexural theory and considered as the load at which the stress in the extreme tension fiber equals to the modulus of rupture (f_r), where $f_r = 0.6\sqrt{f_c'}$ (SI units). The elastic load–deflection stiffness was assumed up to the cracking load. A constant strain was assumed for the transition from the uncracked to the cracked stage. After cracking, the strain in the reinforcing bars at different loads ($P > P_{cr}$) was calculated using moment–curvature analysis. In the analysis, the parabolic stress–strain relationship given by

Hognestad (1951) for concrete was utilized. It was also assumed that all bars were stressed equally at the end of the splice length. Figure 5-10 plots the applied load versus the analytical and experimental strains for B5-D50-L510.

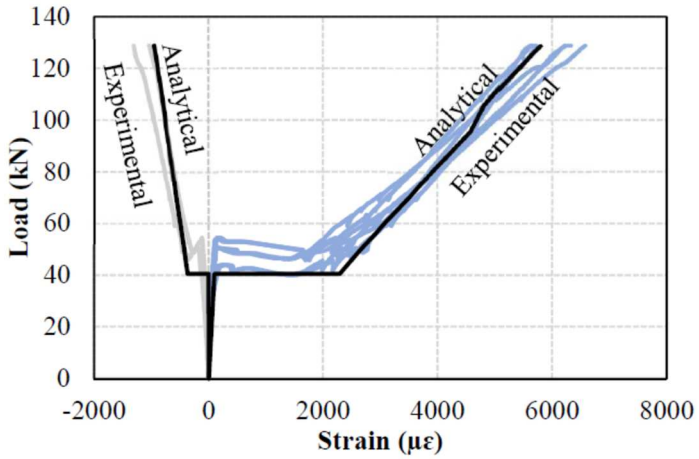

Figure 5-10: Comparison of the analytical and experimental strain values in concrete and FRP bars for B5-D50-L510 (Note: 1 *kN*=0.2248 *kip*)

Comparing the elastic portions of the curves, it can be concluded that the elastic stiffness and cracking load obtained with the theoretical approach was very close to the experimentally measured values. It is worth noting that the relationship from which the modulus of rupture, f_r, was calculated also influenced prediction accuracy as discussed by El-Nemr et al. (2018).

As shown in Figure 5-10, the moment–curvature analysis yielded fairly accurate strain predictions for both concrete and reinforcing bars. The analytical predictions were accurate for all the beams. Table 5-3 gives the stresses calculated at failure based on the moment–curvature analysis. Generally, the ratio of stresses calculated at failure to the mean experimental values ranged from 0.92 to 1.18 with an average of 1.00 and a standard deviation of 0.09. It can be concluded that calculating the reinforcement stress at splice ends at failure based on the moment–curvature analysis can provide accurate results for spliced GFRP-RC beams. This method is recommended by ACI 408R-03(ACI 408 Committee, 2003) for spliced steel-reinforced concrete beams.

Figure 5-11 shows the experimental and analytical strains distribution over the critical cross section at failure for B5-D50-L510. The experimental strain values had a linear trend, which

was estimated analytically with reliable accuracy. Moreover, the extent of flexural cracks observed experimentally at failure was comparable to the neutral-axis depth determined from the moment–curvature analysis. Therefore, predicting the neutral-axis depth, reinforcement strains, and concrete strains based on the moment–curvature analysis can provide satisfactory results. This conclusion was also confirmed in previous studies conducted on beams reinforced with spliced single FRP bars (Aly et al., 2006b; Mosley et al., 2008; Choi et al., 2012; Pay et al., 2014).

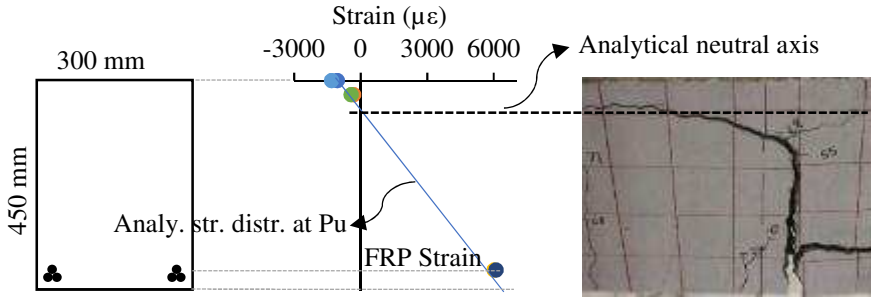

Figure 5-11: Typical strain distribution within the section for B5-D50-L510

5.7.4. Influence of Splice Length

Splice lengths ranging from 320 to 640 *mm* [12.60 to 25.20 *in.*] were implemented to assess the influence of splice length on the bond strength of bundled GFRP bars. Figure 5-12 shows the variation in bar stress ($f_{test,n}$), bar force ($F_{test,n}$) and failure load versus the splice length. Both $f_{test,n}$ and $F_{test,n}$ are increased as the splice length increased. As mentioned earlier, B4-T33-L420 was not included in the analysis and comparison because of its pre-existing cracks before loading, which reduced the splice strength.

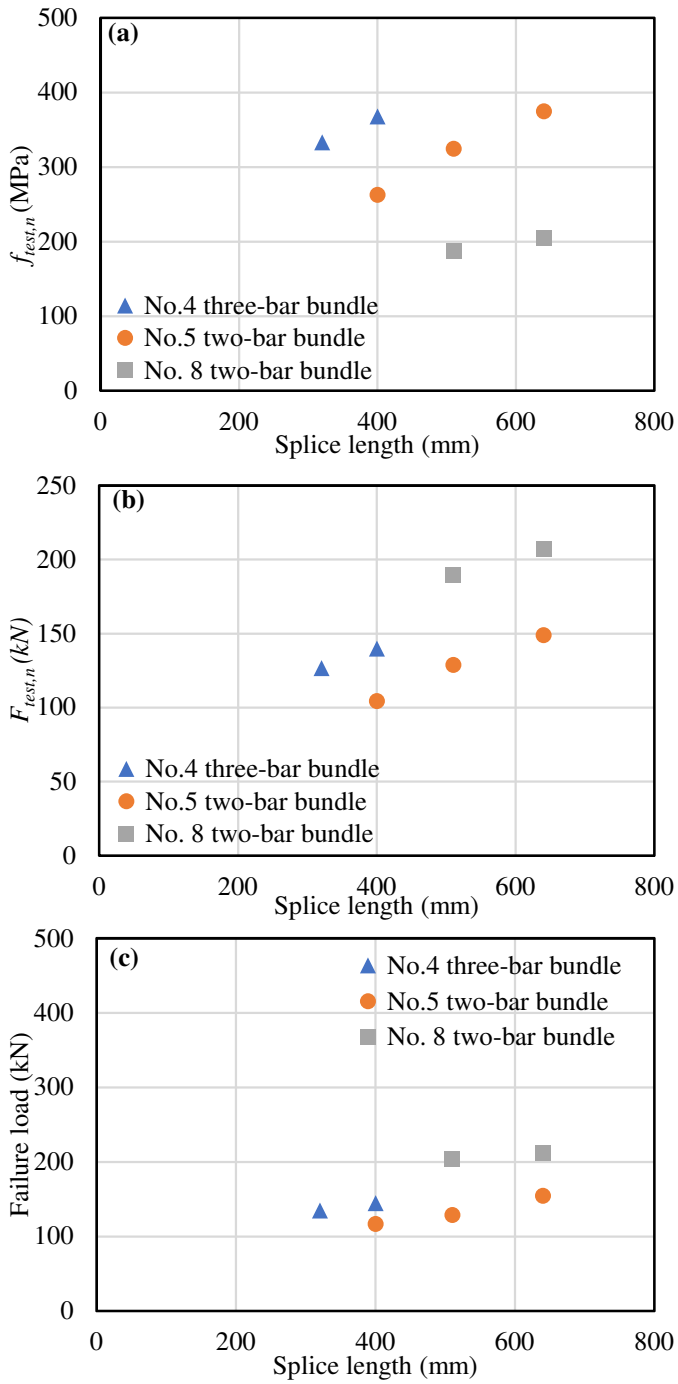

Figure 5-12: Influence of splice length on: (a) tensile stress at failure; (b) tensile force at failure; (c) failure load (Note: 1 mm=0.0394 in., 1 kN=0.2248 kip, 1 MPa=0.145 ksi)

As evidenced by the trend of data in Figure 5-12 (a) for No. 5 two-bar bundles, the effectiveness of increasing the splice decreased as the splice length increased. Increasing the splice length by 28% from 400 to 510 *mm* [15.75 to 20.08 *in.*] resulted in 23% increase in splice strength. A similar increase in the splice length from 510 to 640 *mm* [20.08 to

25.20 *in.*] (25%) improved the splice strength by around 16%. In addition, the strength enhancement due to increasing the splice length differed for each bar size. As observed, increasing the splice length of No. 5 two-bar bundles by 25% (from 510 to 640 *mm* [20.08 to 25.20 *in.*]) resulted in a 16% improvement in bond strength, whereas the same increase in the splice length of No. 8 two-bar bundles enhanced the bond strength by approximately 9%. Moreover, increasing the splice length of No. 4 three-bar bundles by 25% (from 320 to 400 *mm* [12.60 to 15.75 *in.*]) resulted in a 10% increase in splice strength. Overall, splice strength did not seem to be linearly proportional to splice length. In other words, doubling the splice length would not result in a splice with two times higher strength. Other researchers (Mosley et al., 2008; Choi et al., 2012; Pay et al., 2014; Zemour et al., 2018) reported similar trends for splices of single FRP bars.

5.7.5. Influence of Bar Diameter

In order to investigate the effect of bar diameter on $f_{test,n}$ and $F_{test,n}$ for the single and bundled splices, Figure 5-13 presents three groups of two companion beams with the same splice length and number of bundled bars, but with different bar diameters. In general, for a given splice length and the same level of confinement provided by surrounding concrete, increasing the bar diameter reduced $f_{test,n}$ while augmenting $F_{test,n}$. It can also be deduced that the force causing the splitting failure is an increasing function of the area of spliced GFRP bars, similar to lap splices of single steel reinforcing bars (Orangun et al., 1977; Darwin et al., 1992; David Darwin et al., 1996; ACI 408 Committee, 2003).

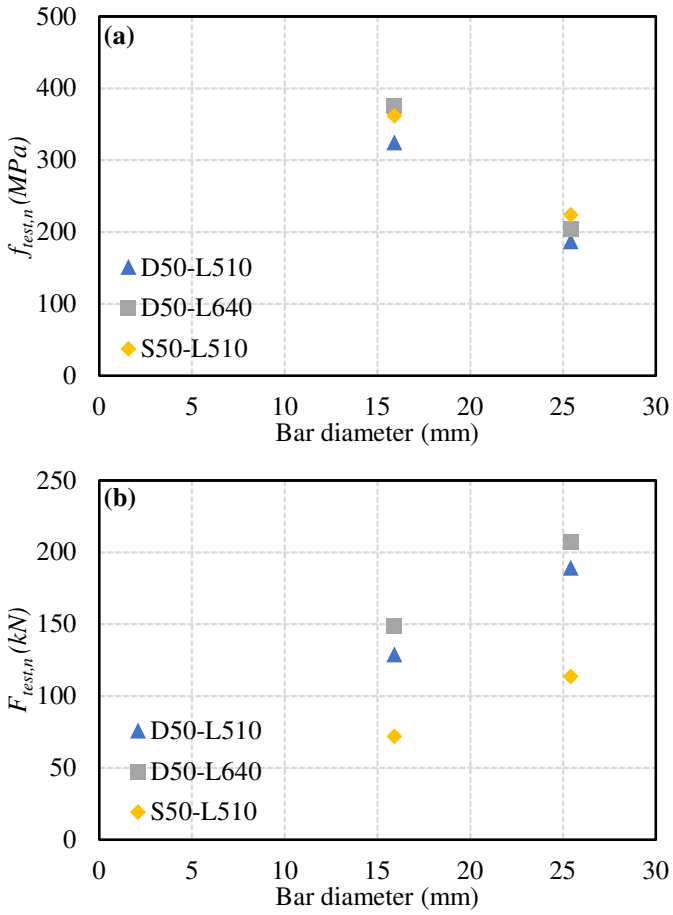

Figure 5-13: Influence of bar size: (a) tensile stress at failure; (b) tensile force at failure (Note: 1 *mm*=0.0394 *in.*, 1 *kN*=0.2248 *kip*, 1 *MPa*=0.145 *ksi*)

Increasing the bar diameter from 15.9 to 25.4 *mm* [No.5 to No.8], which is equivalent to a 60% increase in the exposed perimeter of bars in contact with concrete and a 155% increase in the axial rigidity (AE) of reinforcing bars, resulted in a 48% increase in the total force $F_{test,n}$ at failure. These results indicate that the increase in the $F_{test,n}$ (48%) was less than the increase in the exposed perimeter (60%) and the bar area (155%). The latter implies that a longer splice length is required for a bar with larger diameter to fully develop a given bar stress.

The increase in the $F_{test,n}$ might be attributed to the increase in the contact area of reinforcing bar and concrete and/or the axial rigidity of reinforcing bars. The exact contribution of each parameter is, however, hard to quantified. Pay et al. (2014) showed that reinforcement axial rigidity is one of the main factors influencing splice strength. More experimental

investigations are recommended to evaluate the contribution of axial rigidity on the bond strength of GFRP bars.

Moreover, comparing the results of single-bar and two-bar splices, it can be observed that increasing the bar diameter from 15.9 to 25.4 *mm* [No.5 to No.8] led to a 38% and 42% reduction in $f_{test,n}$ for the single-bar and two-bar bundle splices, respectively. Therefore, it can be concluded that increasing the bar diameter affected the bond strength of the spliced single bars and two-bar bundles similarly.

5.7.6. Influence of the Number of Bars in a Bundle

For a given splice length and bar diameter, increasing the number of bars within a bundle increased the bar circumferential area not in direct contact with concrete. Therefore, it is expected that the bond strength of an individual bar in a bundle might be lower than that of a single bar. Table 5-4 lists the ratio of tensile stress of single-bar splices at failure ($f_{b,single}$) to that of an individual bar of the same size in splices of two- and three-bar bundles ($f_{b,bundle}$). Based on these results, the maximum tensile stress resisted by a reinforcing bar would decrease as the number of bars in a bundle increased. For a given splice length of 510 *mm* [20.08 *in.*], the $f_{b,bundle}/f_{b,single}$ of two-bar bundles ranged from 83% to 90%, depending on bar diameter, while it was around 84% for No. 5 three-bar bundles. Note that the $f_{b,bundle}/f_{b,single}$ values for three-bar bundles might be influenced by the percentage of bars staggered in the same section, since only 50% of bars in the staggered single specimens was spliced in the same section compared to about 33% in the specimens with staggered three-bar bundles.

Table 5-4: Influence of bundle size on bond strength

Bundle Size	Bar Size	$f_{b,bundle}/f_{b,single}$
Two-bar bundle	No. 5	0.90
	No. 8	0.83
Three-bar bundle	No. 5	0.84

To evaluate the effect of the number of bars in a bundle on the distribution of the sustained stresses along the splice length, the average normalized tensile stresses along the splice

length of B8-S50-L510 are compared to those of B8-D50-L510 at 80% and 100% of their maximum stresses (Figure 5-14). It is evident that, No. 8 bars in splices of two-bar bundles and single bars had similar stress distributions along their splice lengths. Furthermore, the stress distribution along the splice length just prior to failure was very close to linear, while it was nonlinear at lower stress levels. Similar trends were reported by other researchers (Aly et al., 2006b; Tekle et al., 2017; Zemour et al., 2018) for splices of single FRP bars. It should be noted again that the strain values might be influenced by the position of gauges with respect to their adjacent cracks.

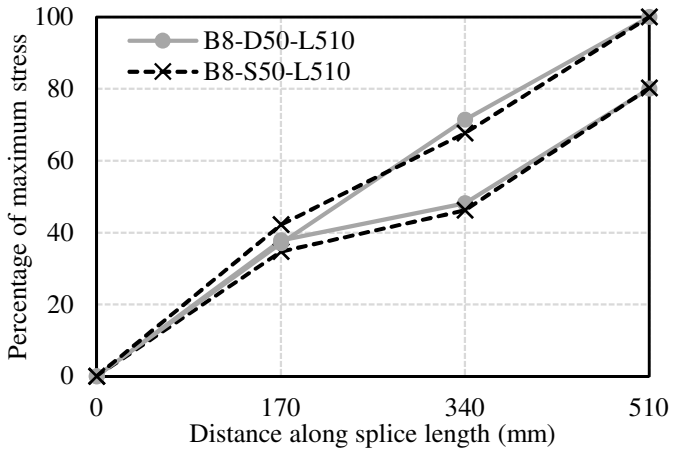

Figure 5-14: Distribution of tensile stress along splice length of B8-D50-L510 at 80 and 100% of their maximum stresses (Note: 1 *mm*=0.0394 *in.*)

5.8. Splice-length Prediction and Design Recommendations

5.8.1. Prediction of Splice Length

Among major design guidelines and codes, only CSA S806-12 (Canadian Standards Association, 2012) stipulates provisions for the splice length of individual bars within a bundle. According to CSA S806-12, this length can be calculated as the splice length required for a single bar increased by 20% and 30% for two- and three-bar bundles, respectively. Since no testing has been conducted for FRP bars in bundles in which the bar arrangement complies with code requirements, splice length modification factor might be implemented to compensate the percentage of the circumferential area of a single bar in a bundle that is not in direct contact with concrete.

In this study, the splice length modification factor for individual bars in a bundle can be estimated by comparing the results of beams reinforced with single splices (B5-S50-L510 and B8-S50-L510) with their companion beams reinforced with two-bar bundles (B5-D50-L510, B5-D50-L640, B8-D50-L510, and B8-D50-L640). The splice length of the beams reinforced with splices of two-bar bundles was increased by 25% (510 to 640 *mm*) [20.08 to 25.20 *in.*] to explore whether the two-bar bundle splice of 640 *mm* [25.20 *in.*] would withstand a stress level comparable to the single-bar splice of 510 *mm* [20.08 *in.*].

Figure 5-15 compares the splice strength of two-bar bundles of No. 5 and No. 8 bars with different splice lengths with their companion single-bar splice. B5-D50-L640 achieved $f_{test,n} = 375MPa$ [54.39 *ksi*], which is almost 4% higher than that of B5-S50-L510 (362 MPa [52.50 *ksi*]). Therefore, it can be concluded that the splice length modification factor of 1.25 would be appropriate for two-bar bundles of No. 5 bars. The reinforcing bars in B8-D50-L640, however, developed $f_{test,n} = 204MPa$ [29.59 *ksi*], which is almost 9% lower than the splice strength of B8-S50-L510 (224 MPa [32.49 *ksi*]). Consequently, splice length modification factor greater than 1.25 would be required for two-bar bundles of No. 8 bars. In either case, No. 5 or No. 8, increasing the splice length required for a single bar by 20% recommended by CSA S806-12 would not be conservative for two-bar bundles of GFRP bars. More experimental tests need to be conducted, however, to confirm this finding.

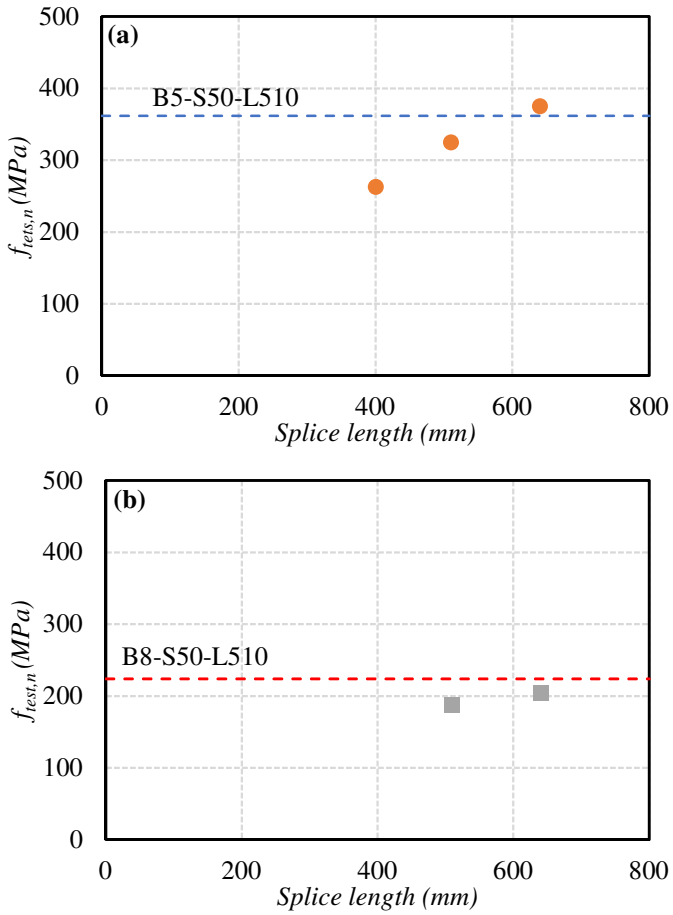

Figure 5-15: Splice strength of two-bar bundle splice and companion single-bar splice: (a): No. 5 and (b) No. 8 (Note: 1 mm=0.0394 in., 1 MPa=0.145 ksi)

5.8.2. Design Recommendations

The experimental results of the current study were used to suggest recommendations for design purposes, although these recommendations need to be validated with more experimental tests.

Although the bond strength of individual bars in a bundle was lower than that of single bars, their general behavior in terms of splice-length effect, bar-size effect, and stress distribution was similar. When designing, the reduction in bond strength of bundled GFRP bars caused by the smaller circumferential area in direct contact with concrete must be compensated by providing a longer splice length. Based on the above discussion, the additional splice length should be greater than the reduction in bond strength, due to the nonlinear relationship

between splice strength and splice length. Therefore, using the current splice-length increasing factors of 1.2 and 1.3 for two- and three-bar bundles, respectively, which are implicitly based on the assumption of a linear relationship between design stress and splice length, would not be conservative.

A plausible approach for design purposes can be introducing an increasing factor to the design-stress to compensate more effectively for a nonlinear splice length–strength relationship. In other words, in lieu of the current splice length modification factors, design-stress increasing factors of 1.2 and 1.33 can be used for two- and three-bar bundles, respectively, until more experimental results become available. Doing so would provide higher levels of safety for individual bars in a bundle, if the fact that the splice strength is not linearly proportional to the bar splice length is acknowledged in design. Therefore, having the design equation which recognizes a nonlinear relationship between the design stress and splice length of single splices is a primary prerequisite of this recommendation. It should be mentioned that the current equation recommended in CSA S806-12 (Canadian Standards Association, 2012) does not acknowledge this fact, i.e., the splice length is linearly proportional to the design stress, unlike in ACI 440.1R-15 (ACI Committee 440, 2015). More experimental investigation is required to evaluate appropriate design-stress modification factors.

5.9. Summary and Conclusion

This study presented an experimental investigation of the bond behavior of splices of bundled sand-coated GFRP bars. Based on the analysis of the results, the following concluding remarks could be drawn:

1. Increasing the splice length had a negligible effect on the flexural stiffness of the beams. In addition, the beams reinforced with longer splices exhibited slightly narrower cracks compared to those with shorter splices. Increasing the bar diameter could increase the post-cracking stiffness of beams.
2. The elastic flexural theory could provide accurate predictions of pre-cracking stiffness and cracking load. Moreover, determining the neutral-axis depth as well as the

reinforcement and concrete strains based on the moment–curvature analysis demonstrated satisfactory results compared to the experimental measurements and observations.

3. Increasing the splice length could increase both the reinforcement stress and force at failure. The effect of splice length, however, decreased with increasing splice length and bar diameter. This clearly confirms that using the design practice with the concept of a proportional relationship between bond force and splice length would lessen the level of safety by increasing splice length.
4. For a given splice length and similar level of confinement by surrounding concrete, the total force required for splitting failure ($F_{test,n}$) was found to be an increasing function of the area of bundled GFRP bars. The increase in the $F_{test,n}$ was less than the increase in the bar area. This connotes that a larger-diameter bar requires a longer splice length to fully develop a given bar stress.
5. Although the bond strength of individual bars in a bundle was lower than that of single bars, their general behavior was similar, particularly in terms of splice length, bar diameter, and stress distribution.
6. Based on the outcomes of the experimental tests, it was recommended that the incremental factors could be applied to design stresses in order to compensate more effectively for the nonlinear splice length–strength relationship. Until more experimental results become available, design-stress amplification factors of 1.2 and 1.33 can be used for two- and three-bar bundles, respectively. Note that, having the design equation which recognizes a nonlinear relationship between the design stress and splice length of single splices is a primary prerequisite of this recommendation.

5.10. Recommendations for Future Research

Despite the contribution made by this study, further research needs to be conducted to better understand the bond behavior of bundled FRP bars and concrete. FRP bars are being produced with different types of fibers (i.e., carbon, glass, aramid, and basalt) and surface deformations (e.g., braided, helically wrapped, ribbed, and indented surfaces). Thus, future work should be directed toward understanding the effect of surface treatment and material properties on the bond behavior of bundled GFRP bars. The effect of concrete type and

strength also needs to be evaluated. In addition, future work should investigate the effects of confinement on the splice strength of bundled GFRP bars. It should also validate the applicability of the design recommendations made herein to confined lap splices and to the GFRP bars with other surface deformations and bar diameters. Moreover, a comprehensive research study is required to develop a new design equation for the splice strength of GFRP bars in concrete.

5.11. Acknowledgements

This research was conducted with funding from the Tier-1 Canada Research Chair in Advanced Composite Materials for Civil Structures, the Natural Sciences and Engineering Research Council of Canada (NSERC), the NSERC Industrial Research Chair in FRP Reinforcement for Concrete Infrastructure, the Fonds de recherche du Québec en nature et technologies (FRQ-NT), and the Quebec Ministry of Transportation. The authors would like to thank the technical staff of the Canadian Foundation for Innovation (CFI) structural & materials lab in the Department of Civil Engineering at the University of Sherbrooke.

CHAPTER 6 Effects of Confinement on Splice Strength of Bundled GFRP Bars in Concrete Beams

6.1. Introduction

Glass-fiber-reinforced-polymer (GFRP) bars have become a distinct alternative to steel bars to overcome the problem of steel corrosion in reinforced-concrete (RC) structures. In addition, FRP bars have other inherent advantages such as high electromagnetic transparency and light weight, which make them a superior reinforcement in certain buildings such as magnetic-resonance-imaging (MRI) units in hospitals.

Constraints in the reinforcement bar length due to transportation force the overlapping of reinforcing bars in practice. Moreover, heavy reinforcement arrangements necessitate the bundling of rebars within a section. To provide RC structural integrity, the section in which rebars are spliced must provide strength equal to or greater than that outside the spliced zone. This is possible by providing adequate lap-splice length to sustain the design stress of reinforcement developed at the critical section (i.e., end of the spliced zone). Estimating the adequate length requires a profound understanding of the bond mechanism between a reinforcing bar and concrete as well as the major parameters affecting this mechanism.

Several parameters were found to be influential in the magnitude of the FRP-to-concrete bond. They include concrete cover and rebar spacing, lap-splice and development length, concrete compressive strength, concrete type, the amount of transverse reinforcement provided within the splice/development length, bar casting position, and bar diameter (Tighiouart et al., 1999; Aly et al., 2006b; Wambeke & Shield, 2006; Mosley et al., 2008; Harajli & Abouniaj, 2010; Choi et al., 2012; Esfahani et al., 2013; Pay et al., 2014; Zemour et al., 2018). The effectiveness of providing confinement over the splice length of an FRP bar is, however, a contentious issue. For example, a statistical study conducted by Wambeke and Shield (2006) showed that confinement provided by transverse reinforcement had no incremental effect on the average bond strength. The explanation was that FRP bars generally have very low relative rib area compared to steel materials. Nonetheless, these authors recommended conducting more experimental investigations to explore the effect of confinement. In contrast, other researchers (Aly, 2005; Harajli & Abouniaj, 2010; Esfahani

et al., 2013) have criticized this finding and found that transverse reinforcement effectively improved the bond strength of GFRP bars.

The experimental results obtained by Aly, (2005) confirmed that confinement provided by transverse reinforcement and clear cover could augment the bond strength of GFRP bars. Transverse reinforcement was more effective in this regard than increasing the clear cover. The confinement provided by transverse reinforcement improved the average bond strength by 60% while increasing the concrete cover from d_b to $4d_b$, where d_b is the bar diameter, enhanced the bond strength by 27%.

Harajli and Abouniaj (2010), reported that providing confinement along the splice length of FRP bars significantly increased the splice strength but was, dependent on the surface deformation of the GFRP bars. Based on their results, the confined beams reinforced with the ribbed and thread-wrapped GFRP bars exhibited improvements of around 31% and 13% , respectively, in maximum bond force compared to their unconfined counterparts. Moreover, they found that increasing the concrete cover (c) from 1.25 to $2d_b$, where d_b is the bar diameter, slightly improved the bond strength of the ribbed GFRP bars, while it had no effect on the bond strength of the thread wrapped bars. On the contrary, the same increase in the concrete cover for the steel rebars resulted in a 30% improvement in the bond strength. Consequently, they stated that the influence of c/d_b on the splice strength of steel rebars is more pronounced than that of GFRP rebars.

In their experimental study, Esfahani et al. (2013), concluded that the effect of transverse reinforcement on the bond strength of GFRP bars varied depending on bar surface treatment. Based on their results, while transverse reinforcement could increase the bond strength of ribbed bars remarkably, it had no noticeable effect on that of sand-coated bars. The failure modes of the specimens reinforced with the sand-coated bars shifted, however, from splitting in the specimens without transverse reinforcement to pullout in those with transverse reinforcement along the splice length.

The current design guidelines for concrete structures reinforced with FRP bars have contradictory provisions regarding the effect of confinement on bond strength. Unlike CSA

S806-12 (Canadian Standards Association, 2012) and ACI 440.1R-15 (ACI Committee 440, 2015), JSCE-97 (Japan Society of Civil Engineers, 1997) and CSA S6-14 (Canadian Standards Association, 2014a) considers the contribution of transverse reinforcement in calculating development/splice length of FRP rebars. In both JSCE-97 and CSA S6-14, the increase in bond strength due to transverse reinforcement is directly proportional to the modulus of elasticity of the confining material (steel or FRP). Moreover, the splice and development length of bundled FRP bars is either not covered in the guidelines (CSA S6-14, JSCE-97, and ACI 440.1R-15), or follows suggestions similar to steel reinforcement (CSA S806-12).

It is worth noting that, the current study is part of an ongoing comprehensive research program at the University of Sherbrooke in which the effect of various parameters including longitudinal bar arrangement (e.g. bundled, single and reinforcement in layers), transverse reinforcement material (e.g., GFRP, CFRP and steel), concrete type (e.g., normal and self-consolidating concrete), and casting position on the splice strength of GFRP bars are being investigated. The major parameters investigated herein were the effect of confinement provided by steel transverse reinforcement and clear concrete cover.

6.2. Research Significance

The primary objective of the current experimental study was to assess the influence of confinement provided by transverse reinforcement and concrete cover on the splice strength of bundled GFRP bars. Comparisons were made in terms of failure mode, crack pattern and width, ultimate load, general load-deflection behavior and splice strength. Moreover, a relationship was suggested to account for the contribution of transverse reinforcement to the overall bond strength of tension lap splices of bundled GFRP bars. The findings may improve the knowledge of the behavior of spliced bundled GFRP bars in confined and unconfined concrete members and increase the reliability of splicing bundled GFRP bars in practice. It will also support the work of the technical committees, including ACI 440, CSA S806, and CSA S6, engaged in developing standards and design provisions for GFRP-RC flexural members.

6.3. Experimental Program

6.3.1. Specifications of Test Specimens

The test comprised 8 full-scale concrete beam specimens measuring 5200×300×450 *mm*. The beams had a clear testing span of 5000 *mm*, a shear span of 1250 *mm*, and a constant-moment span of 2500 *mm*. Figure 6-1 shows the geometry and reinforcement details of the test specimens.

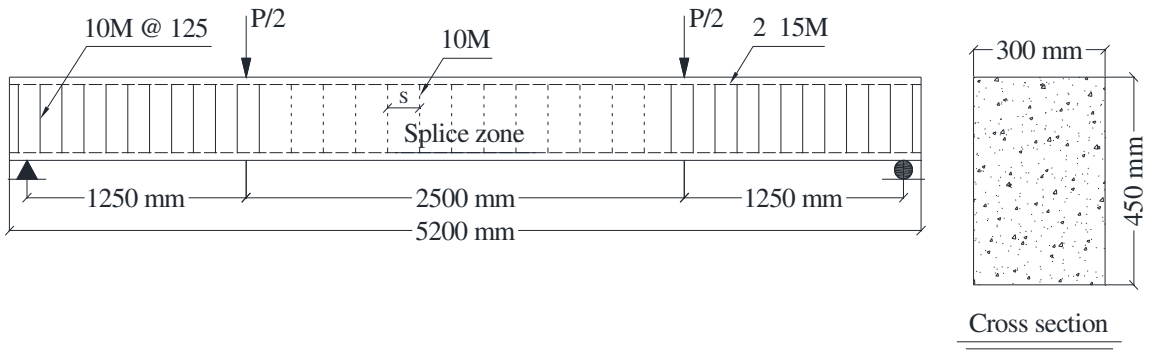

Figure 6-1: Details of the geometry and transverse reinforcement of the test specimens (Note: stirrup spacing within splice zone (s) is provided in Table 6-1)

The beam shear design was according to CSA S806-12 (Canadian Standards Association, 2012) using ribbed 10M steel stirrups spaced at 125 *mm* on centers. To investigate the effect of confinement on bond behavior, the constant-moment span of four specimens were also reinforced with ribbed 10M steel stirrups spaced at different intervals (125 and 250 mm). In order to provide support for stirrups during caging and also to facilitate specimen handling after testing, two ribbed 15M steel rebars were used as compression reinforcement. The beam specimens were designed to investigate the effect of confinement provided by transverse reinforcement and concrete cover on the bond behavior of spliced bundled GFRP bars. Table 6-1 lists the beam details, while Figure 6-2 shows the bar arrangement within the splice zone. In all specimens, the splice length was set at 25 times the bar diameter (d_b).

Table 6-1: Details of test beams

Specimen	Bar Size	Splice Pattern	l_s	s*	$\frac{l_s}{d_b}$	f_c'	f_t
			mm	*mm*	-	*MPa*	*MPa*
B4-S50-L320	No.4	S50	320	-	25	41	3.70
B4-S50-L320-C125	No.4	S50	320	125	25	42	3.48
B5-D50-L400	No.5	D50	400	-	25	40	3.96
B5-D50-L400-C250	No.5	D50	400	250	25	42	3.48
B5-D50-L400-C125	No.5	D50	400	125	25	42	3.48
B4-T33-L320	No.4	T33	320	-	25	41	3.70
B4-T33-L320-C125	No.4	T33	320	125	25	42	3.48
B4-T33-L320-51	No.4	T33	320	-	25	41	3.70

Note: * s: Stirrup spacing within the splice zone

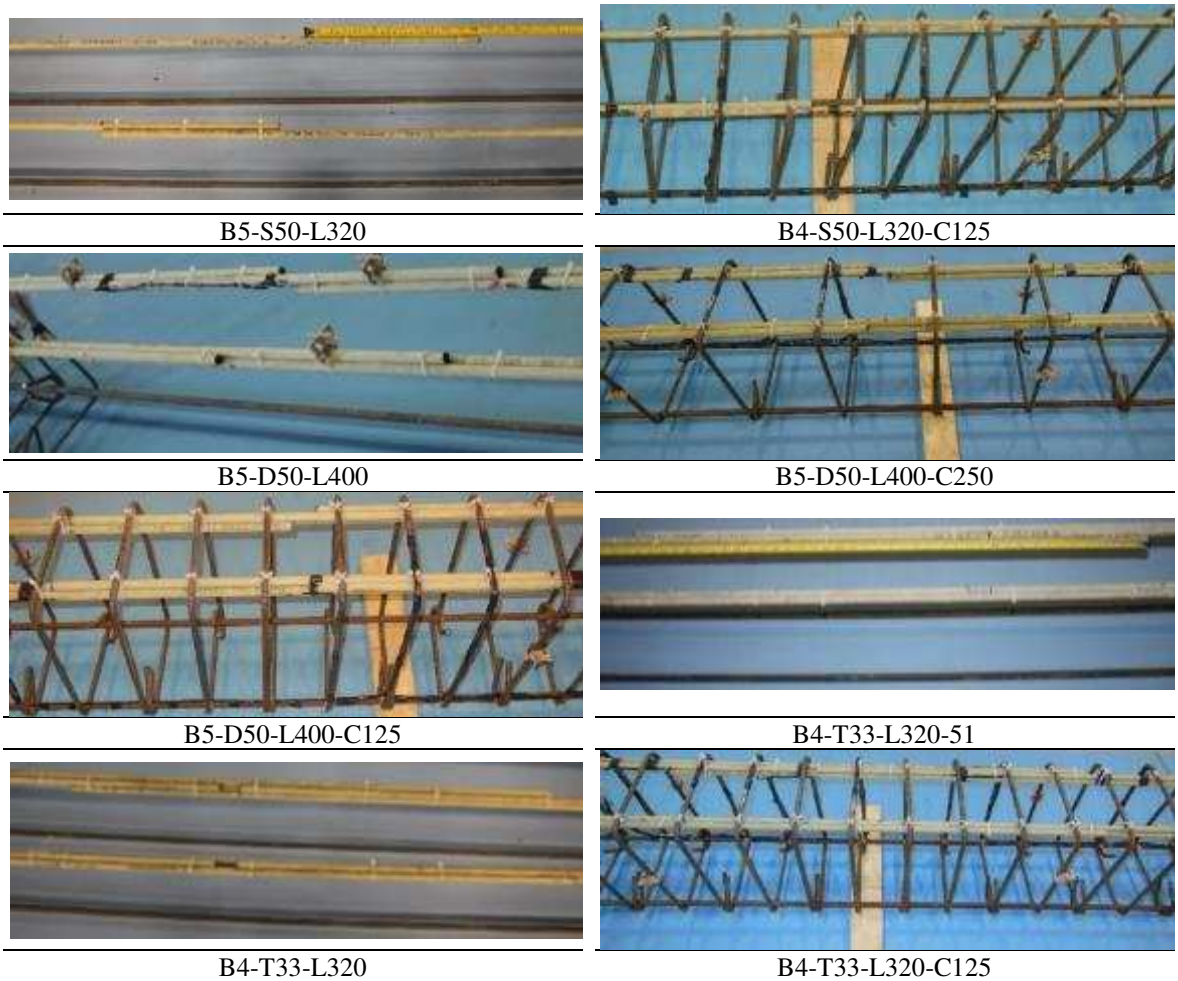

B5-S50-L320 | B4-S50-L320-C125

B5-D50-L400 | B5-D50-L400-C250

B5-D50-L400-C125 | B4-T33-L320-51

B4-T33-L320 | B4-T33-L320-C125

Figure 6-2: Splice zone of all specimens

The side and bottom clear cover as well as the clear bar spacing was designed so that the expected mode of failure would be splitting of the bottom cover (face-splitting failure) in all specimens. In this regard, all the beams were detailed so that half of the clear spacing of the adjacent bars and the side cover were greater than the bottom cover. Out of the total, the bottom and side clear cover of 7 beams were 32 and 45 mm, respectively. One beam was designed with a bottom clear cover of 51 mm and a side cover of 64 mm to examine the effect of confinement provided by the concrete cover.

As mentioned earlier, CSA S806-12 (Canadian Standards Association, 2012) is the only guideline providing recommendations for spliced bundled GFRP bars. According to this guideline, individual bars within a bundle may be cut off at different points at least 45 times the bar diameter (d_b) apart and individual bar splices within a bundle may not be overlapped. Due to the limitations in total specimen length, we could not comply with the former provision in this study. Nonetheless a space of 40 mm was left between the extremities of two adjacent splices to avoid any bond interruption due to the installation of strain gages.

The beam specimens were designated with a combination of letters and numbers. The nomenclature commences with the letter B followed by a number identifying the bar size (4 or 5 for No. 4 (12.7 *mm*) or No. 5 (15.9 *mm*) bars, respectively). The second letter indicates the bundle type (S, D, or T for single bars, two-bar bundles, or three-bar bundles, respectively). The second number (33 or 50) represents the percentage of bars staggered in each section along the splice length. The digits after the letter L represent the splice length of individual bars in millimetres. The final digits after the letter C for confined specimens, define the stirrup spacing within the splice zone, while the final number 51 gives the clear cover in the specimen with larger clear cover.

6.3.2. Material Properties

Ribbed 10M (11.3 *mm*) and 15M (16 *mm*) steel bars were used as compression and transverse reinforcement, respectively. Two different sizes of No. 4 (12.7 *mm*) and No. 5 (15.9 *mm*) sand-coated GFRP bars were used as tension reinforcement in this study. Figure 6-3 provides an illustration of the GFRP bars. Moreover, Table 6-2 summarizes the

mechanical properties of the reinforcing bars. The values associated with the steel bars are nominal, provided by the supplier. The mechanical properties of the GFRP bars were measured as the average properties of five specimens tested in accordance with CSA S806-12 (Canadian Standards Association, 2012).

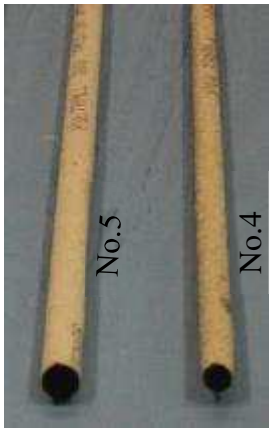

Figure 6-3: Sand-coated GFRP bars

Table 6-2: Mechanical properties of the steel and GFRP rebars

Bar type	Bar Size	Bar Diameter (*mm*)	Elastic Modulus (*GPa*)	Tensile Strength (*MPa*)	Tensile Strain (%)
GFRP	No.4	12.7	51.7	1243	2.40
	No.5	15.9	51.1	1296	2.54
Steel	10M	11.3	200	f_y =420	ε_y =0.20
	15M	16	200	f_y =420	ε_y =0.20

Note: ε_y is the yield strain and f_y is the yield stress

The specimens were cast with a normal-weight ready-mixed concrete with a target 28-day compressive strength of 35 *MPa* and a maximum coarse-aggregate size of 14 *mm* provided by a local supplier. Companion cylinders measuring 100×200 *mm* cylinders were cast with the corresponding beams from the same batch of concrete. Specimens were moist-cured for 7 days and were then kept under the ambient conditions until the testing day. Table 6-1 lists the compressive and splitting tensile strength obtained by testing five cylinders on the same day of testing as the corresponding beam specimen.

6.3.3. Test Setup, Instrumentation, and Loading

A four-point loading apparatus was used to test all the beams. The load was applied monotonically with a 1000 *kN* actuator with a displacement-controlled regime of 1.2 *mm/min*. Figs 4 and 5 show the test setup and instrumentation of the specimens. The displacements at the middle and loading points were measured with a set of linear variable differential transformers (LVDTs), as shown in Figure 6-4 (a). In addition, the horizontal elongations of the splice zone and constant moment span were obtained with two string potentiometers installed on two sides of the beam, as illustrated in Figure 6-4 (b). During the test, the formation of cracks and their corresponding loads were observed and marked visually. Furthermore, the widths of the first two cracks that were close to the ends of the splice zone were recorded with two LVDTs.

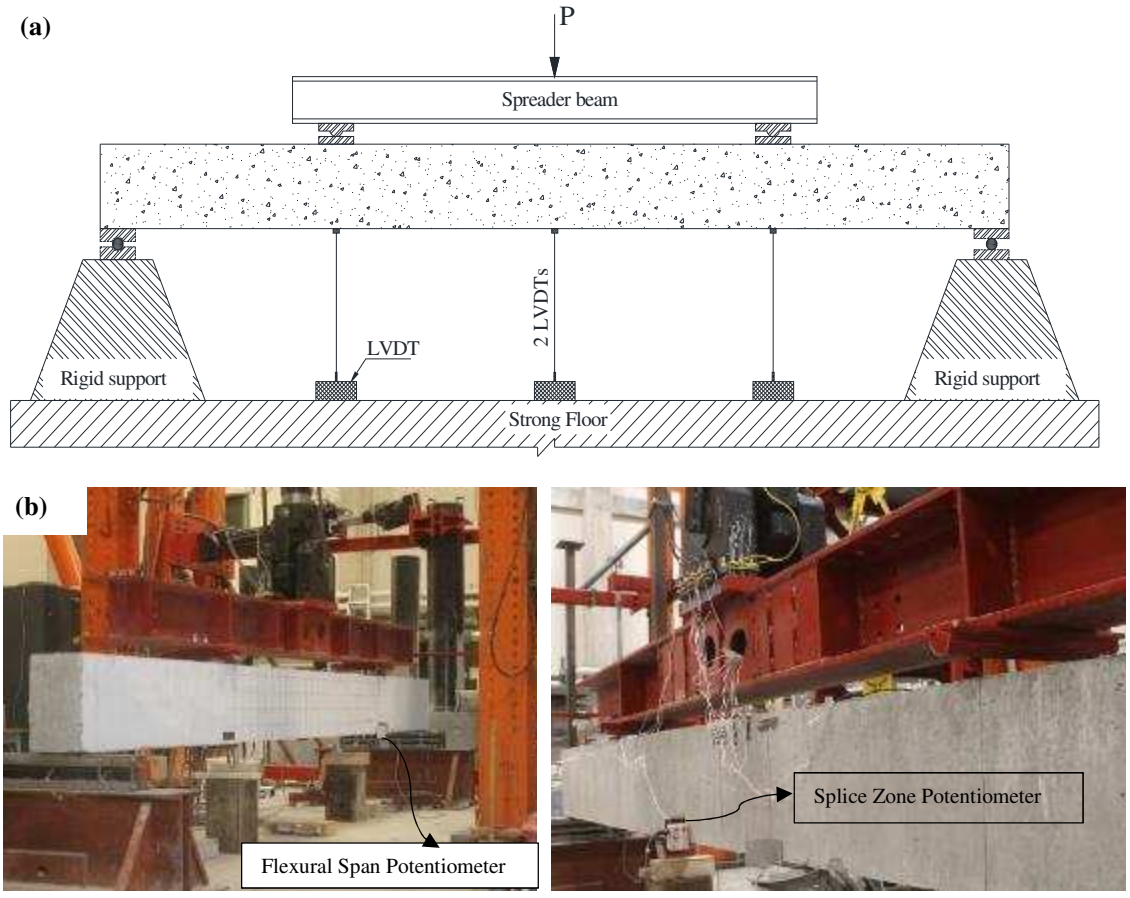

Figure 6-4: Illustration of: (a) test setup and location of LVDTs; (b) flexural span and splice zone potentiometers

The strain values in the reinforcing bars and stirrups were measured with a series of electrical resistance strain gages. The reinforcing bar strain gages, shown in Figure 6-5, were installed 20 mm from the ends of the splices to prevent any interruption in the bond between the reinforcing bar and the surrounding concrete due to installation. All the data obtained from testing including loads, displacements, crack widths and strain values were automatically recorded using a data logger system.

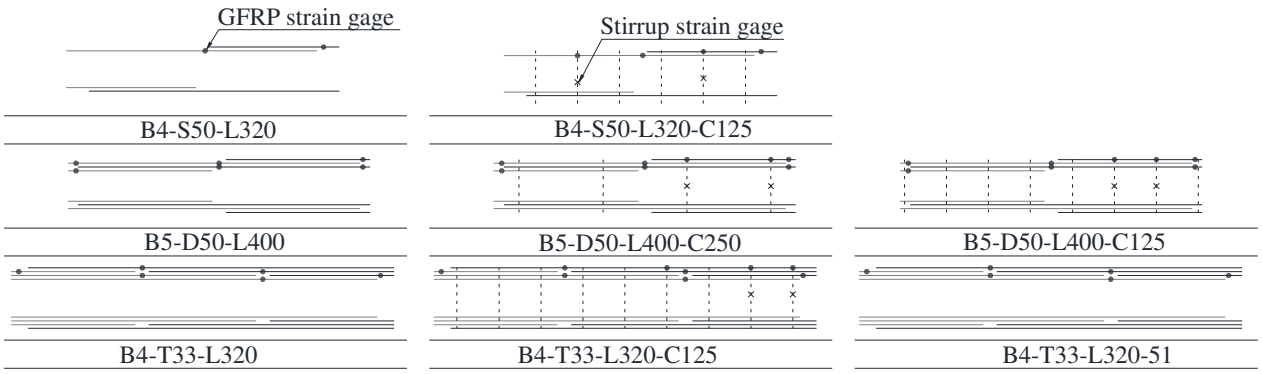

Figure 6-5: Illustration of the location of reinforcement strain gages

6.4. General Behavior and Test Results

6.4.1. Load-deflection Response

The mid-span deflection was recorded with two LVDTs attached at one-third of the beam width (Fig. 4 (a)). Similar values were recorded by those two LVDTs, confirming negligible torsion in the beams during testing. Thus, their average was recorded. Figure 6-6 shows the mid-span load-deflection response of the beams. As shown, prior to the initial cracking, the beams exhibited similar linear behaviors. Thereafter, the curves were roughly linear with a noticeable reduction in the stiffness up to their failure points.

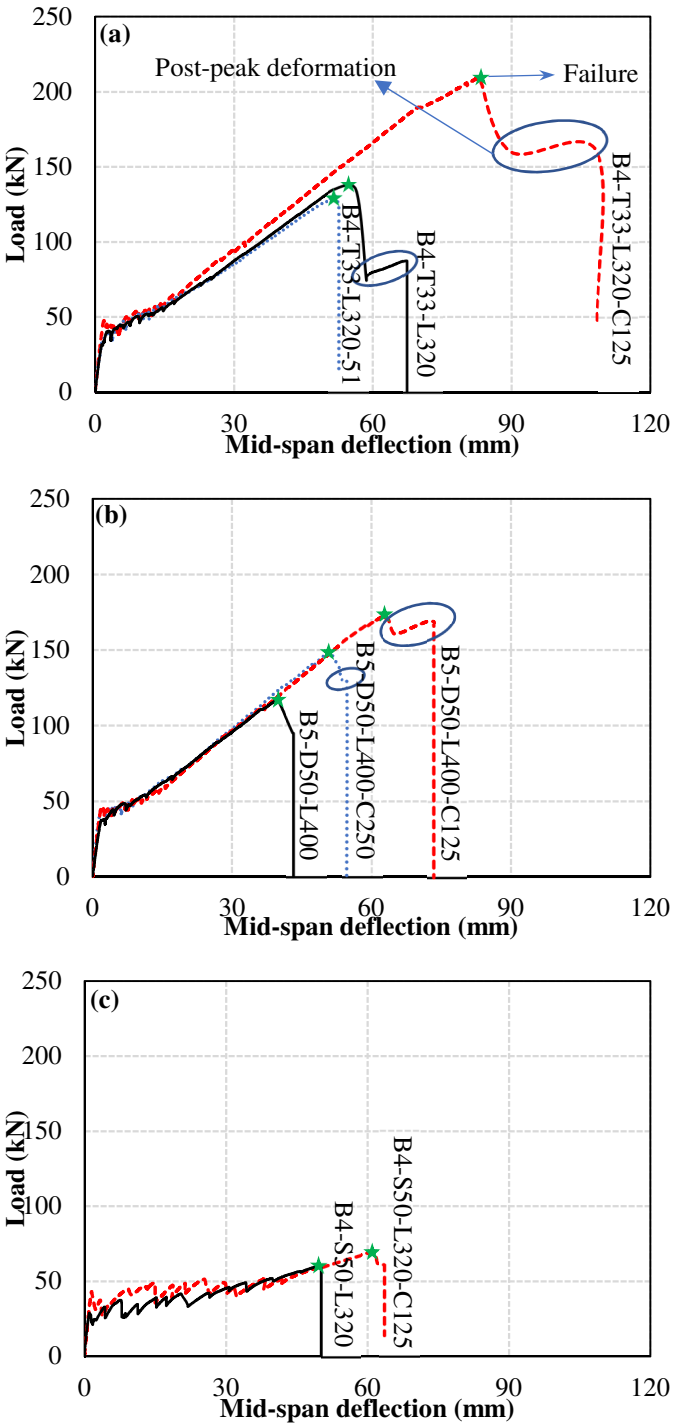

Figure 6-6: Load-deflection responses of beams reinforced with (a) No.4 three-bar bundles, (b) No.5 two-bar bundles, and (c) single No.4 bars

As evident in Figure 6-6, regardless of the confinement level provided by the transverse reinforcement and concrete cover, the companion beams with the same reinforcement size and configuration exhibited similar pre-cracking stiffness. Moreover, providing transverse reinforcement within the splice zone had negligible effect on the post-cracking stiffness, while it dramatically enhanced the failure load (P_u in Table 6-3). It should be mentioned that the enhancements in both post-cracking stiffness and failure load were observed for B4-T33-L320-C125. In addition, Figure 6-6 shows that all of the beams with bar bundles but no transverse reinforcement, except B4-T33-L320, experienced an immediate drop in load instantly upon reaching their peak value. In contrast, all the beams with bar bundles and transverse reinforcement exhibited some post-peak deformations, albeit they were negligible for B5-D50-L400-C250. As for post-peak behavior, the confined specimens withstood more than 75% of their maximum load after peak load.

Table 6-3: Summary of the experimental results

Specimen	P_{cr}	P_u	Tensile Strain	Tensile Stress	Tensile Force at Failure
	kN	*kN*	$\mu\varepsilon$	*MPa*	*kN*
B4-S50-L320	30	60.6	8048	416	53
B4-S50-L320-C125	43	69	9720	503	64
B5-D50-L400	37	116.6	5151	263	105
B5-D50-L400-C250	44	148.5	6789	347	138
B5-D50-L400-C125	47	172.8	7997	409	162
B4-T33-L320	34	134.6	6478	335	127
B4-T33-L320-C125	48	209.4	9558	494	179
B4-T33-L320-51	36	130.2	6293	325	124

Table 6-3 lists the cracking loads (P_{cr}) — the load at which the first flexural crack appeared — for each beam. As indicated, the cracking load (P_{cr}) increased with higher levels of confinement provided by transverse reinforcement. This improvement might be attributed to the enhancement provided by the confined concrete strength. Moreover, an increase in the longitudinal reinforcement ratio could slightly increase the cracking load in the specimens with the same level of confinement.

6.4.2. Crack Pattern and Failure Mode

During testing, the first flexural cracks commonly initiated inside the constant-moment region and usually outside the splice zone. With increased load, more cracks developed along the constant-moment zone. After stabilization of the flexural cracks, inclined flexural-shear cracks developed in the shear spans. At the higher load levels, longitudinal hairline splitting cracks developed on the bottom of the beams along the outline of the spliced bars. As anticipated in the initial design, sudden splitting of the concrete cover in the spliced region accompanied the failure of all beams except B4-S50-L320-C125, which exhibited pullout failure.

Figure 6-7 presents the crack pattern of the test beams. As shown, the splitting crack patterns were similar for the companion beams with different levels of transverse reinforcement. Visual inspection of the beams after failure revealed evidence of the formation of splitting cracks on the side and bottom of all beams, except for B4-S50-L320-C125. In the latter, hairline splitting cracks were observable only on the soffit tension surface of the beam with no sign of splitting cracks on the sides. Since no splitting cracks were observed during the testing of B4-S50-L320-C125, it is very likely that the hairline splitting cracks on the beam bottom occurred just after the peak load. These observations confirm the pullout failure mode of the spliced bars in B4-S50-L320-C125.

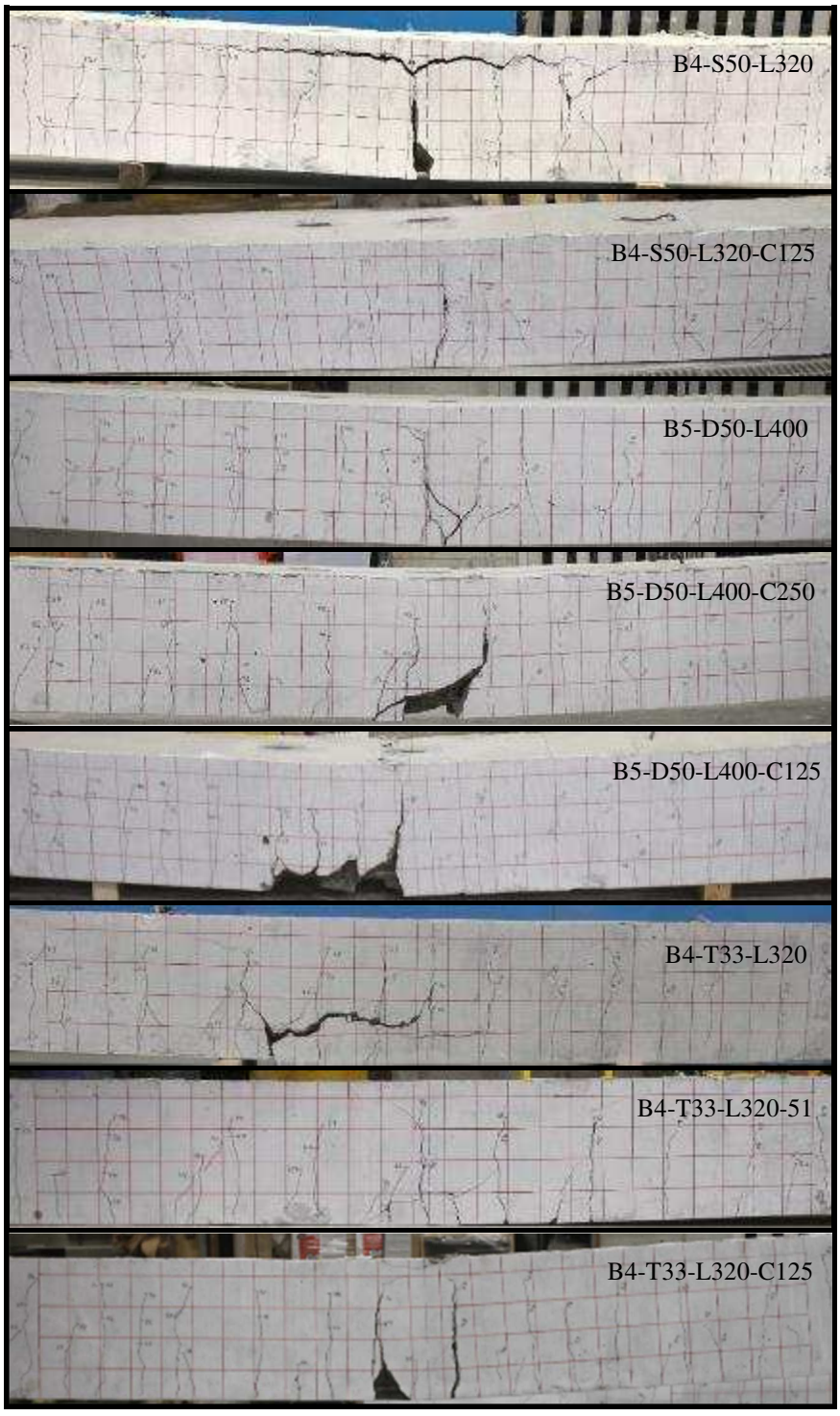

Figure 6-7: Crack patterns of beams at failure

Regardless of the amount of transverse reinforcement, the depths of flexural cracks in the companion beams with similar configurations of tension reinforcement were comparable. The beams with higher transverse reinforcement, however, developed a similar or greater

number of flexural cracks within the splice region and constant-moment zone. Moreover, increasing the reinforcement ratio always reduced the flexural-crack depth and added to the number of cracks in the constant-moment zone.

6.4.3. Maximum Crack Width

Wider cracks always progressed at the splice extremities. This is consistent with the initial expectation of the position of the maximum crack width measured during testing. Figure 6-8 presents the distributions of the maximum crack width versus applied load of the companion beams. As shown, the cracks widened gradually with increasing applied load throughout the test. Comparing the crack width data for the companion beams, it can be concluded that enhancing the level of confinement with transverse reinforcement decreased the maximum crack widths. For the same reinforcement ratio and surface treatment, the wider cracks could be considered as an indication of less slip and, therefore, superior bond behavior. It may also suggest that providing transverse reinforcement would be an effective means to reduce the maximum crack width at the end of splices of GFRP-reinforced beams at the serviceability limit state. In addition, as shown in Figure 6-8 (a), increasing the concrete cover had negligible effect on the maximum crack width.

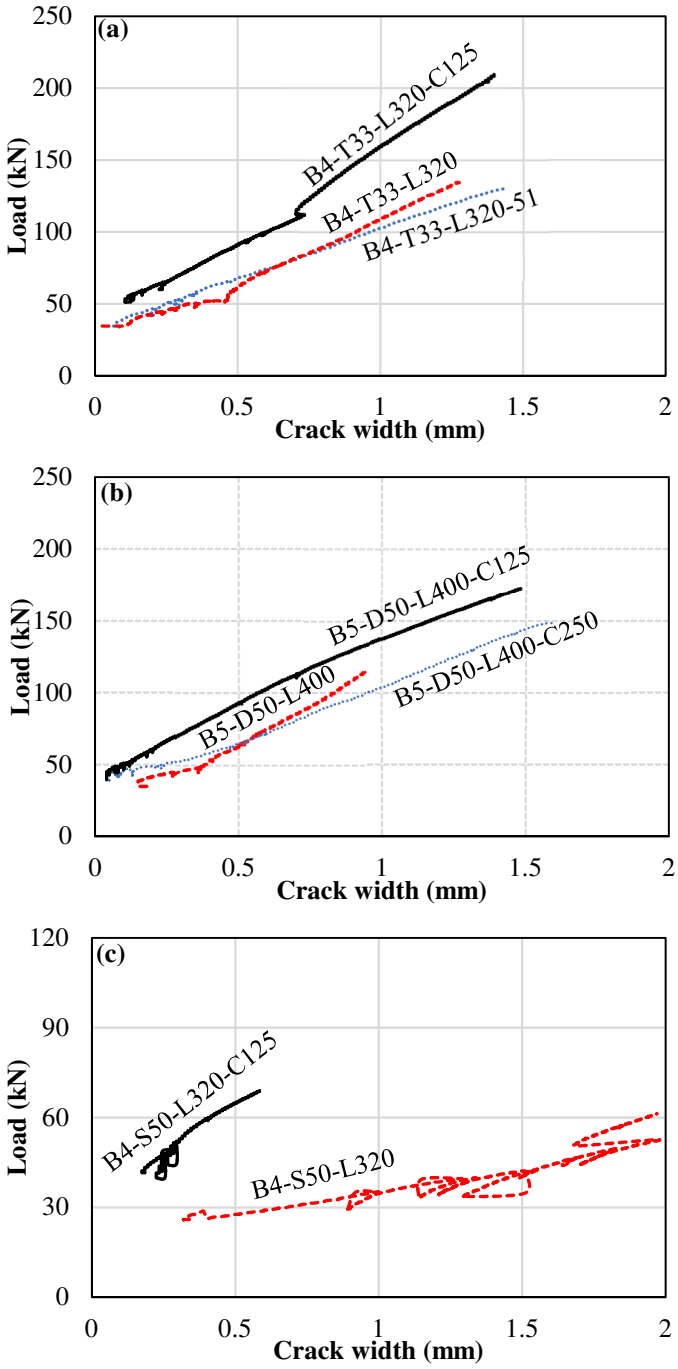

Figure 6-8: Distribution of the maximum crack width versus applied load; (a) No. 4 three-bar bundle, (b) No. 5 two-bar bundle, and (c) single No.4 bar

Note that, the crack widths presented in Figure 6-8 correspond to the crack developed at the extremities of a splice in beams designed with inadequate splice length. Consequently, it is

expected that the average crack width of the GFRP-reinforced beams without splices or with adequate splice length would be narrower in practice.

6.4.4. Elongation of Splice Length and Flexural Span

Figure 6-9 compares the elongation of the splice zone (indicated by solid lines) and the flexural span (shown in dashed lines) of beams reinforced with three-bar bundles of No. 4 rebar and two-bar bundles of No. 5 rebar. Since the cracks propagated causing the potentiometers in beams B4-S50-L320 and B5-D50-L400 to fall of, their elongation curves could not be obtained.

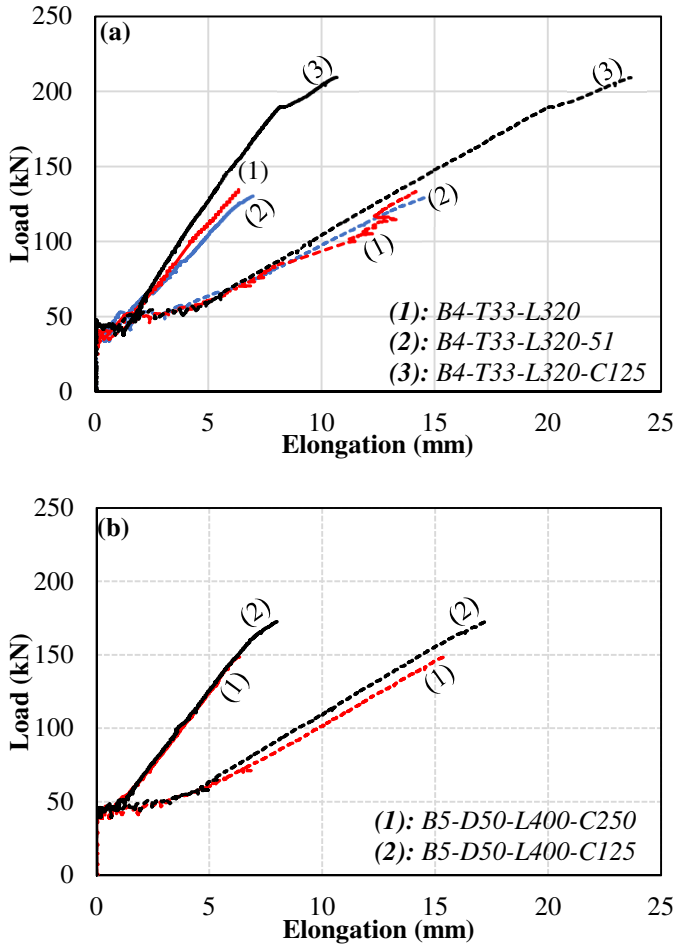

Figure 6-9: The total horizontal elongation of the splice zone (solid lines) and the flexural span (dashed lines); (a) No. 4 three-bar bundle, (b) No. 5 two-bar bundle

As shown, the increased concrete cover had a negligible effect on the horizontal elongation of the splice region and constant-moment zone, while increasing the level of confinement with transverse reinforcement generally reduced the elongation. The horizontal elongation is related to the crack-width development, horizontal curvature, and bar slippage within the splice length. As mentioned above, the beams with higher levels of confinement developed similar or higher numbers of flexural cracks within the constant-moment span and splice zone. This observation, together with shorter elongation in the beams with more confinement might indicate that providing confinement can reduce the average crack width. Lower average crack widths might be considered as an indication of improved bond strength between the longitudinal reinforcement and concrete as a result of providing transverse reinforcement.

6.5. Evaluation of the Splice Strength

6.5.1. Bond Strength

The average strain values developed in a spliced GFRP rebar at the peak load was considered as its failure strain (ε_{test}).The failure stress (f_{test}) was then calculated by multiplying the failure strain (ε_{test}) by the modulus of elasticity of the GFRP bars (E). Subsequently, the reinforcement force at failure was determined as $F_{test} = f_{test}A_b$, where Ab is the nominal cross-sectional area of an individual bar in the bundle. A few strain gages were inevitably damaged during either casting or testing, so they were discarded from the average values.

Past studies (ACI 408 Committee, 2003; Darwin et al., 2005) have shown that the bond strength of reinforcing bars is proportional to the fourth root of the concrete compressive strength of, f_c', for the longitudinal rebars not confined by transverse reinforcement. Moreover, it was found that the improvement in the bond strength due to the transverse reinforcement was related to $f_c'^{3/4}$ (ACI 408 Committee, 2003; Darwin et al., 2005). In the current study, due to the slight fluctuation of the concrete compressive strengths (from 40 to 42 MPa), the effects of variation in concrete strength on the calculated bond strengths and

on the additional bond provided by transverse reinforcement were neglected. Table 6-3 presents the experimental results for all the beam specimens.

6.5.2. Strain in the Reinforcing Bars

The load values were plotted against the strain measurements for all the test beams in Figure 6-10. As indicated, the strain values were small before flexural crack development. Thereafter, the strain values sharply increased. As loading progressed, the stresses consistently increased up to failure. The data presented in Figure 6-10 reveal that using transverse reinforcement within the splice zone was very effective in increasing the total developed stress at failure. It had, however, negligible effect on the rate of strain improvement in the cracking and post-cracking load regions.

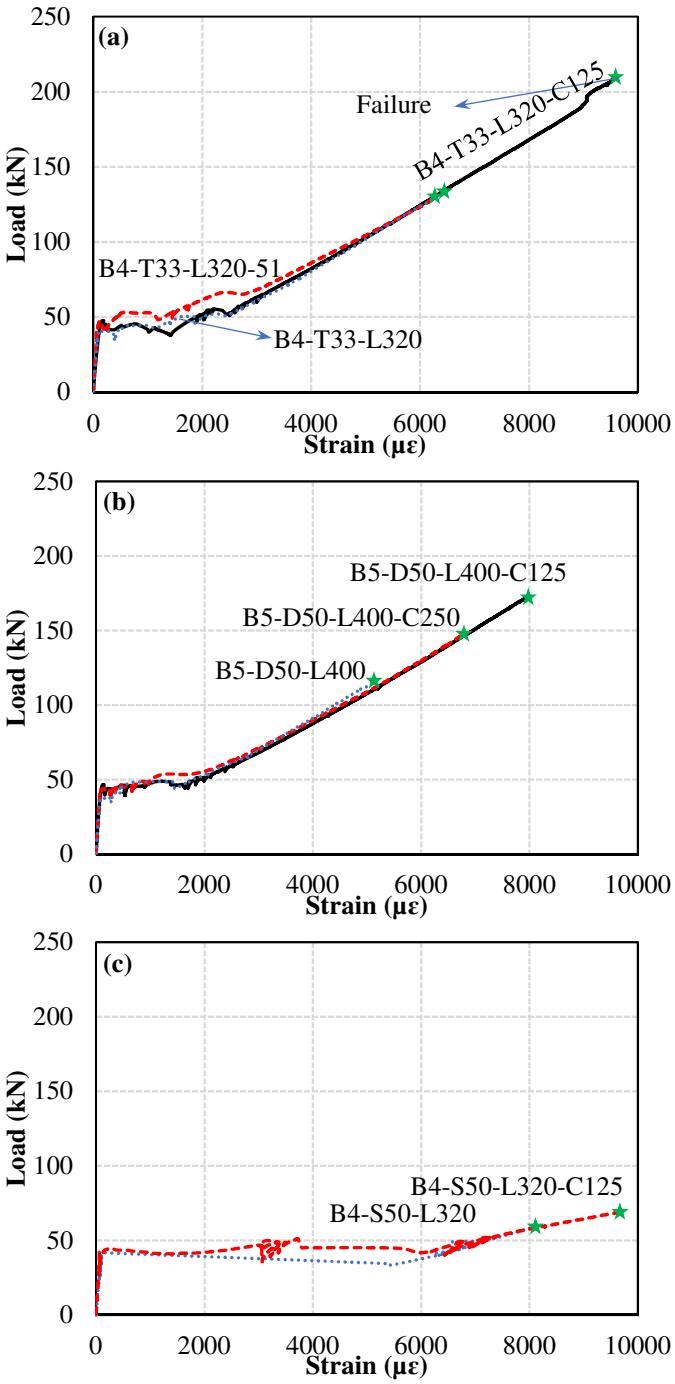

Figure 6-10: Mean strain in GFRP bars versus applied load; (a) No.4 three-bar bundle, (b) No.5 two-bar bundle, (c) No.4 single bar

6.5.3. Strain in the Transverse Reinforcement

Figure 6-11 plots the measured strains in the transverse reinforcement within the splice zone versus the average tensile strain developed by longitudinal reinforcement at the ends of a splice. As mentioned before, the strain measured by a strain gage is highly susceptible to its position with respect to nearby cracks. The evaluation provided in this section is, however, necessary to provide more insight into how steel stirrups and concrete collaborate to resist bursting bond forces.

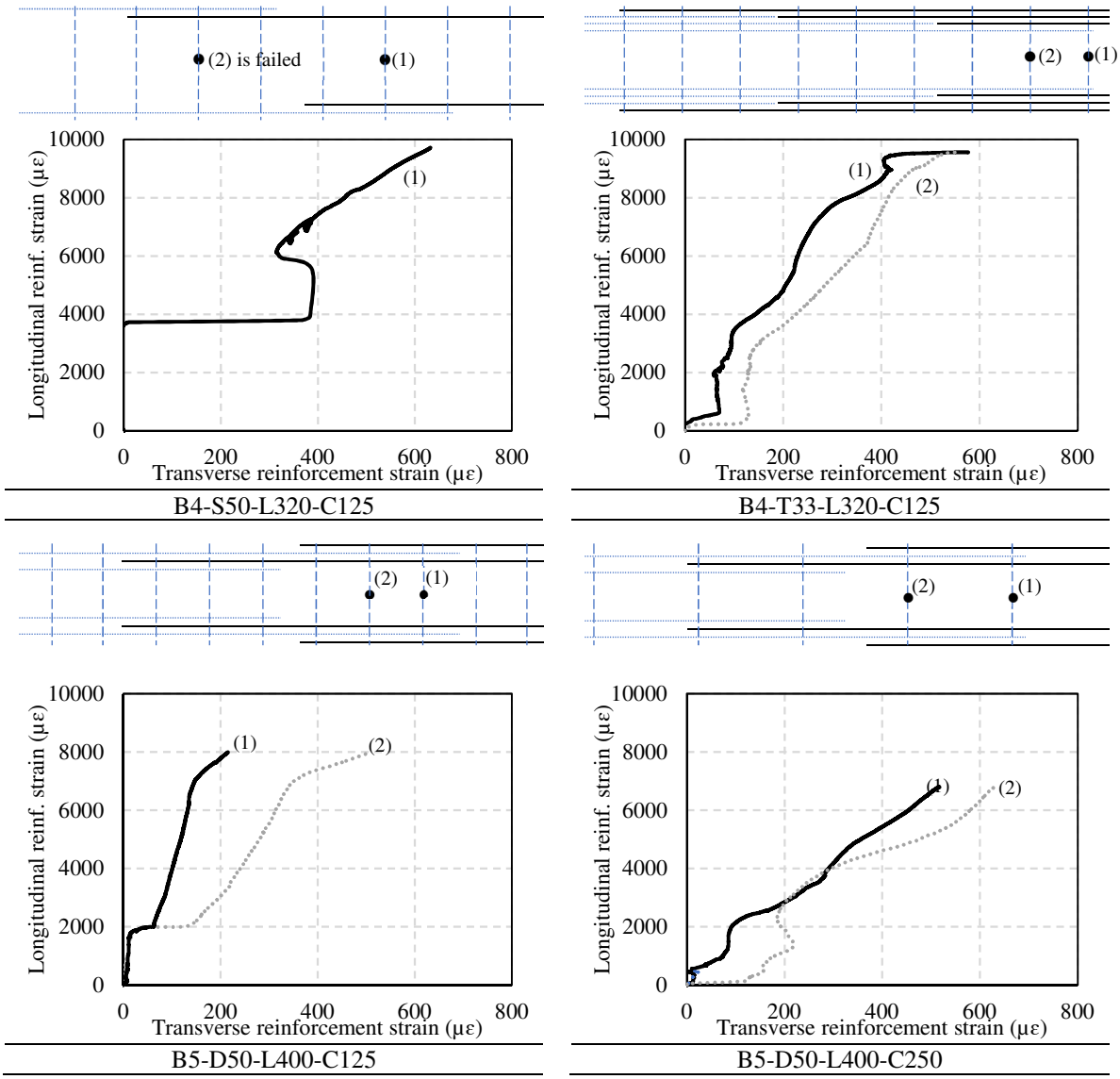

Figure 6-11: Strain in the transverse reinforcement versus the average strain in the longitudinal reinforcement

The data shown in Figure 6-11 indicate that stirrup strain values increased with an increase in the strain of longitudinal reinforcement until failure and that stirrup strain varied depending on stirrup location within the splice zone. This might be due to the fact that the bond stress is not linearly distributed over the splice length of GFRP bars (Aly et al., 2006b; Tekle et al., 2017; Zemour et al., 2018). Moreover, the rate of strain variation in the transverse reinforcement increased by increasing the strain values in the longitudinal reinforcement. This may suggest that the contribution of stirrups in resisting the bursting bond forces increases at higher load levels when the concrete clear cover contributes less. In addition, the stirrup strain could not reach its yield value. It can therefore be concluded that despite the contribution of steel transverse reinforcement to the splice strength of GFRP rebars, the role of its yield strength is not significant.

6.6. Effect of Test Parameters

6.6.1. Concrete Cover

The effect of concrete cover was investigated by comparing the bond strength of two companion specimens reinforced with three-bar bundle of No.4 rebar (B4-T33-L320 and B4-T33-L320-51). Increasing the concrete clear cover from 32 to 51 mm ($2.5d_b$ to $4.5d_b$) could hardly affect the splice strength because it decreased from 335 to 325 MPa (less than 3%). This observation might suggest that the splice strength of bundled GFRP bars is not dependent on concrete clear cover (c) for $c/d_b > 2.5$. Nonetheless, the influence of concrete cover in different ranges needs further investigation due to a very limited number of tests performed herein.

6.6.2. Transverse Reinforcement

It is believed that providing transverse reinforcement can not only delay the initiation of splitting cracks but it can change the failure mode and bond-slip relationship (Tepfers, 1973; Orangun et al., 1977; ACI 408 Committee, 2003). Moreover, it can control the width of splitting cracks and their propagation, thereby increasing the total force required for splitting failure (Tepfers, 1973; Orangun et al., 1977; ACI 408 Committee, 2003).

In this study, the effect of the confinement provided by the transverse reinforcement was investigated by comparing the splice strength of the companion specimens reinforced with a single No. 4 bar, a two-bar bundle of No.5 bars and a three-bar bundle of No. 4 bars (Table 6-3). The direct comparison between the specimens with transverse reinforcement and the reference specimens without transverse reinforcement indicates the positive effect of the transverse reinforcement on splice strength. In this regard, Figure 6-12 plots the average tensile stress at failure (f_{test}) of the companion specimens versus the ratio of the splice length to stirrup spacing (l_s/s). As depicted, increasing the level of confinement over the splice length could effectively improve the average tensile stress at failure (f_{test}) for splices of bundled and single GFRP bars of different sizes.

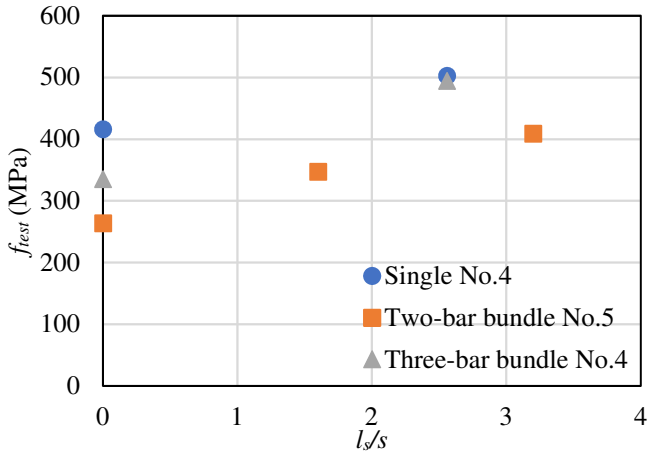

Figure 6-12: Effect of confinement provided by the transverse reinforcement on the splice strength

Considering the results for the three companion specimens reinforced with two-bar bundles of No.5 (B5-D50-L400, B5-D50-L400-C250, B5-D50-L400-C125), it can be concluded that providing 10M steel stirrups at 250 and 125 *mm* enhanced the splice strength by 32% and 55%, respectively. Moreover, providing 10M steel stirrups at 125 *mm* improved the splice strength in the case of splices with single bars and three-bar bundle of No.4 bars by 21% and 48%, respectively. Thus, providing stirrups over the splice length of GFRP bars can effectively increase the average tensile stress at failure (f_{test}) in spliced single and bundled bars. The same amount of confinement (10M stirrups at 125 *mm* on centers) had a greater

impact on the splice strength of three-bar bundles of No.4 bars than it did on single No.4 bars.

It is important to mention that increasing the splice strength was not the only advantage of confining the splice region. Another beneficial effect was the increased ratio of the splice strength of the bundled and single splices from 0.80 for the unconfined specimens to 0.98 for the confined specimens.

As discussed, bundled GFRP bars benefit greatly from the presence of transverse reinforcement. Although further study on the effectiveness of transverse reinforcement over the splice length of bundled GFRP bars is necessary, particularly with FRP stirrups a minimum amount of transverse reinforcement should be provided along the splices of bundled GFRP bars in practice to improve splice reliability.

6.7. Contribution of Transverse Reinforcement to the Splice Strength

The experimental results of the current study were used to derive an analytical model to predict the contribution of transverse reinforcement (T_s) to the splice strength of the bundled GFRP bars. This was achieved by implementing two well-known semi-empirical models proposed by Orangun et al. (1977) and Zuo and Darwin (2000). The contribution of transverse reinforcement was calculated by subtracting the experimental bond force of unconfined splices (T_c) from that of the companion confined ones (T_b). As discussed above, B4-S50-L320-C125 failed by tensile reinforcement pull-out. Therefore, the results for this specimen were not included in the analysis.

Orangun et al. (1977) proposed a semi-empirical model for determining the design development and splice lengths of steel reinforcing bars. This model has been endorsed by ACI 318 Code for the design development and splice lengths of steel bars in concrete. The model has also been used as the basis for proposing the design development and splice lengths of FRP bars in concrete (Wambeke & Shield, 2006). According to Orangun et al.

(1977), the average bond stress, u_b, of steel splices confined by transverse reinforcement at failure can be expressed as follows:

$$\frac{u_b}{\sqrt{f_c^{'}}} = \frac{A_b f_s}{\pi d_b l_s} = \frac{u_c + u_s}{\sqrt{f_c^{'}}} \tag{6-1}$$

where u_c and u_s are the contribution of concrete and transverse reinforcement to the bond strength, respectively. The latter may be represented in terms of bond force as follows:

$$\frac{T_s}{\sqrt{f_c^{'}}} = C_1 \frac{l_s A_{tr}}{sn} f_{yt} \tag{6-2}$$

where f_{yt} is the yield stress of transverse reinforcement, $f_c^{'}$ is the compressive strength of concrete, l_s is the splice length, A_{tr} is the area of each stirrup crossing the potential splitting plane, n is the number of reinforcing bars being spliced along the splitting plane, s is the maximum center-to-center spacing of stirrups over the splice length, and C_1 is a constant for regression analysis. ACI 318 code did not include f_{yt} in its 2008 and succeeding versions since Azizinamini et al. (1999) showed that transverse reinforcement rarely yields during the bond failure.

Linear regression analysis was performed to establish a predictive equation for the contribution of transverse reinforcement, T_s, normalized to $\sqrt{f_c^{'}}$ in the total splice force as a function of $l_s A_{tr}/sn$. The resulting equation producing the best fit to the experimental results of the current study (with $R^2 = 0.843$) expressed as follows:

$$\frac{T_s}{\sqrt{f_c^{'}}} = 13.57 \frac{l_s A_{tr}}{sn} \quad \text{(SI units).} \tag{6-3}$$

Figure 6-13 displays the variation in the bond force, T_s, normalized to $\sqrt{f_c^{'}}$ versus $l_s A_{tr}/sn$.

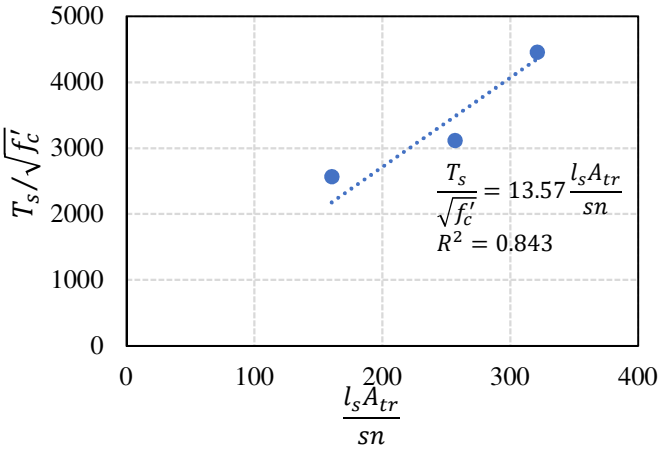

Figure 6-13: Variation of the bond force, T_s, normalized with respect to $\sqrt{f_c'}$ against $l_s A_{tr}/sn$

The second model considered in this study was proposed by Zuo and Darwin, (2000). This model was recalibrated and adopted by ACI 408-03 (ACI 408 Committee, 2003). According to Zuo and Darwin (2000), the total bond force, T_b, of steel splices confined by transverse reinforcement over the splice region can be represented by

$$T_b = T_c + T_s \tag{6-4}$$

where T_c and T_s are the contribution of concrete and transverse reinforcement to the bond strength, respectively. The latter is a function of concrete compressive strength, spliced-bar properties, and the area and spacing of transverse reinforcement in the splice region. The basic relationship for T_s is defined as follows:

$$\frac{T_s}{f_c'^{3/4}} = C_1 t_r t_d \frac{l_s A_{tr}}{sn} + C_2 \tag{6-5}$$

where f_c' is the concrete compressive strength, t_r is the relative rib area factor, t_d is the bar diameter factor, l_s is the splice length, A_{tr} is the area of each stirrup crossing the potential splitting plane, n is the number of reinforcing bars being spliced along the splitting plane, and s is the maximum center-to-center spacing of stirrups over the splice length. The term t_d, which represents the effect of bar diameter on T_s, can be calculated as follows:

$$t_d = 0.03 d_b + 0.22 \quad \text{in SI units} \tag{6-6}$$

where d_b is the diameter of the tensile reinforcing bar in mm (Darwin et al., 2005).

Linear regression analysis of the specimens was performed to establish a predictive equation for the contribution of transverse reinforcement ($T_s / f_c'^{3/4}$) to the total splice force as a function of $t_d (l_s A_{tr} / sn)$. The resulting equation (with $R^2 = 0.990$) is given as follows:

$$\frac{T_s}{f_c'^{3/4}} = 6.73 t_d \frac{l_s A_{tr}}{sn} + 227 \quad \text{(SI units).} \tag{6-7}$$

Figure 6-14 displays the correlation between the bond force T_s normalized to $f_c'^{3/4}$ and $t_d (l_s A_{tr} / sn)$. It should be mentioned that t_r is not an independent parameter herein as all the reinforcing bars had similar surface treatment (sand coating). Nonetheless, this equation could be calibrated for different surface conditions once corresponding experimental data becomes available.

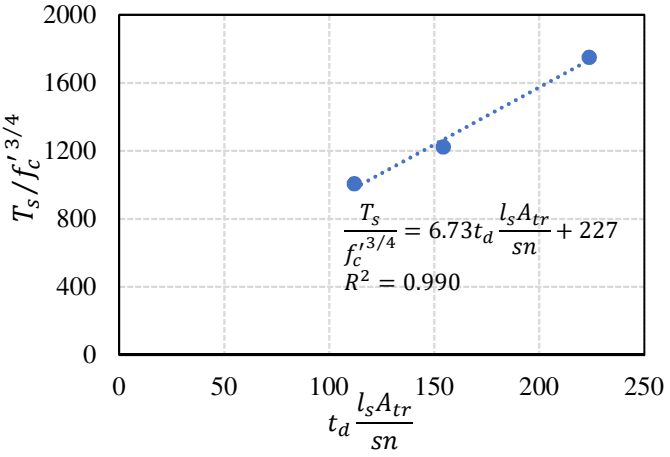

Figure 6-14: Variation of the bond force T_s normalized with respect to $f_c'^{3/4}$ against $t_d (l_s A_{tr} / sn)$

As indicated, Eq.(6-7) with $R^2 = 0.990$ was found to produce the best correlation for predicting the contribution of transverse reinforcement to the bond strength of bundled GFRP bars. The two main differences between the transverse reinforcement parameters in Eqns.(6-3) and (6-7) are: (a) Eq.(6-3) represents the contribution of the transverse

reinforcement T_s proportional to $\sqrt{f_c'}$ while it is in relation to $f_c'^{3/4}$ in Eq. (6-7); and (b) unlike Eq. (6-3), Eq. (6-7) considers a bar size factor, t_d. Given the same concrete compressive strength of the companion specimens, it can be concluded that inclusion of t_d will result in a more consistent predictive equation for evaluating the contribution of transverse reinforcement to the total bond force of the spliced bundled GFRP reinforcement.

As mentioned above, the effect of transverse reinforcement on the bond strength of bundled sand-coated GFRP bars was investigated solely using steel stirrups. The use of FRP stirrups is beyond the scope of this study. Therefore, Eq. (6-7) might be applicable to situations in which the longitudinal reinforcement is sand-coated GFRP and the transverse reinforcement is steel. In design practice, the use of conventional- or stainless-steel stirrups with GFRP as tensile reinforcement might become inevitable to avoid congestion of GFRP shear reinforcement in concrete bridge girders due to considerable shear forces.

As mentioned above, JSCE-97 and CSA S6-14, associate the increase in bond strength of FRP reinforcement due to transverse reinforcement with the ratio of elastic modulus of the confining reinforcement to that of steel (E_t/E_s , where E_t and E_s are moduli of elasticity of the transverse reinforcement and steel, respectively). In addition, Harajli et al., (2004) concluded that the increase in bond strength of steel reinforcement due to confining reinforcement is related to both the modulus of elasticity and the area of the confining material (steel or FRP). In view of these considerations, a plausible approach for design purposes could be introducing the E_t/E_s factor into Eq. (6-7), until more experimental data becomes available. Doing so and dropping the intercept 227 in Eq. (6-7), so as to err on the conservative side, yield:

$$\frac{T_s}{f_c'^{3/4}} = 6.73 t_d \frac{l_s A_{tr}}{sn} \frac{E_t}{E_s} \quad \text{(SI units).} \tag{6-8}$$

It is worth mentioning that providing additional transverse reinforcement above a certain limit might be ineffective in increasing the bond strength (Orangun et al., 1977). Therefore, the applicability of Eq. (6-8) for $t_d(l_s A_{tr}/sn)(E_t/E_s)$ values greater than 223 (SI units), which

is the maximum value of the horizontal axis in Fig. 6-14, needs to be confirmed by more experimental results. More experimental investigation is required to fully grasp the influence of the modulus of elasticity of the transverse reinforcement on the behavior of spliced GFRP bars.

6.8. Summary and Conclusions

A total of eight full-scale beam-spliced specimens were fabricated and tested to investigate the effects of concrete cover and transverse reinforcement on the splice strength of bundled GFRP bars. The failure mode, crack pattern and width, ultimate load, general load-deflection behavior and measured splice stress at failure were compared to the companion beams. The main conclusions from this study are as follows:

1. Providing transverse reinforcement along the splice zone improved the cracking and failure loads. It was, also, very effective in increasing the reinforcement stress at failure. It had negligible effect, however, on the pre- and post-cracking stiffness of the test beams.
2. Regardless of the amount of transverse reinforcement, the companion beams with identical configuration of tension reinforcement had flexural cracks on similar depth. The beams with increased transverse reinforcement, however, developed a similar or slightly greater number of flexural cracks within the splice zone and the constant-moment span.
3. Increasing the reinforcement ratio consistently reduced the depth of the flexural cracks and increased the number of cracks within the constant-moment span.
4. Providing transverse reinforcement effectively decreased the maximum crack width at the splice ends in GFRP-reinforced beams and the average crack width within the flexural span.
5. The splice strength of bundled GFRP bars was not dependent on the clear concrete cover (c) for $c/d_b > 2.5$.
6. Based on the strain measurements, the steel transverse reinforcement could effectively contribute to the splice strength. Providing 10M stirrups at 250 and 125 mm on centers enhanced the splice strength of two-bar bundles of No.5 bars by 32% and 55%,

respectively. Moreover, providing 10M stirrups at 125 mm on centers improved the splice strength of single bar and three-bar bundles of No.4 bars by 21% and 48%, respectively.

7. The yield strength of the steel transverse reinforcement did not, however, play a noticeable role in in improving splice strength.
8. The ratio of splice strength of bundled bars to single bars rose from 0.80 in the case of unconfined specimens to 0.98 in the case of specimens with transverse reinforcement.
9. Based on the experimental findings, the contribution of transverse reinforcement (T_s) to the total strength of spliced bundled GFRP bars, was predicted accurately using the semi-empirical model proposed by Zuo and Darwin (2000). Therefore, this model was used as the basis for proposing a relationship to account for the contribution of transverse reinforcement (GFRP and steel) to the overall bond strength of lap splices of bundled sand-coated GFRP bars.

Despite the contribution made by this study, further experimental investigation is needed to verify and strengthen the study's findings and to study the effect of other parameters, such as modulus of elasticity of transverse reinforcement, concrete cover ($c/d_b < 2.5$), bar size, and other bar-surface treatments.

CHAPTER 7 GENERAL CONCLUSIONS AND RECOMMENDATIONS

7.1. Summary

The focus of this project was to elaborate on the bond behavior of lap-spliced bundled GFRP bars. Pursuing this objective, a total of 22 full-scale beams were reinforced with different configurations of spliced bundled and single GFRP bars. The experimental parameters were comprised of splice length, bar diameter, confinement provided by transverse reinforcement, concrete cover, and bar staggering. The results were analyzed and described in terms of strain values developed in the reinforcing bars, crack width, number of cracks within the splice zone, cracking pattern, maximum load capacity, and mid-span deflection.

7.2. Conclusions

The following conclusions can be drawn based on the experimental and analytical investigations conducted in this research program:

- Staggering had negligible effect on the beam stiffness. It, however, could increase the splice strength, particularly in the case of three-bar bundles. It also reduced the maximum crack width.
- Based on the strain measurements, all bars in a bundle may not act as a single unit as there was a relative displacement between them.
- The elastic flexural theory could provide good predictions of the pre-cracking stiffness and cracking load. Moreover, determining the neutral-axis depth as well as the reinforcement and concrete strains based on the moment–curvature analysis demonstrated reliable results compared to those measured experimentally.

- The splice strength decreased as the number of bars in a bundle increased. On average, the ratios of the bond strength of bundled bars to that of their companion single bars were 85% and 82% for the two- and three-bar bundles, respectively.
- Although the bond strength of individual bars in a bundle was lower than that of single bars, their general behavior was similar, particularly in terms of splice length, bar diameter, and stress distribution over splice length.
- Increasing the bar diameter could increase the post-cracking stiffness of beams. Moreover, the splitting pattern of beams reinforced with No. 8 bars was different than that of the beams reinforced with No. 5 and No. 4 bars.
- Increasing the splice length can increase both the reinforcement stress and force at failure. The effect of splice length, however, decreased with increasing the splice length and bar diameter. This clearly confirms that using the design practice with the concept of a proportional relationship between the bond force and splice length would lessen the level of safety by increasing splice length. In addition, the patterns of splitting cracks were similar for specimens reinforced with bundled bars of the same diameter, but with different splice lengths. The cracking loads of specimens with longer splices were slightly higher than those with shorter splices. In addition, increasing the splice length had a negligible effect on the flexural stiffness of the beams.
- Beams reinforced with longer splices exhibited slightly narrower cracks compared to those with shorter splices. This finding might underline the lower slippage of the longer splices.
- For a given splice length and similar level of confinement by surrounding concrete, the total force required for splitting failure ($F_{test,n}$) was found to be a function of the area of bundled GFRP bars. However, the increase in $F_{test,n}$ was less than the increase in the bar area which might connote that a larger-diameter bar required a longer splice length to fully develop a given bar stress.
- Based on the outcomes of the experimental tests, it was recommended that the incremental factors could be applied to design stresses in order to compensate more

effectively for the nonlinear splice length–strength relationship. In lieu of the length modifier factors available in CSA S806-12 and until more experimental results become available, design-stress amplification factors of 1.2 and 1.33 may be used for two- and three-bar bundles, respectively. Note that, having the design equation that recognizes a nonlinear relationship between the design stress and splice length of single splices is a primary prerequisite of this recommendation. Considering design provisions stipulated in ACI 440.1R-15, it was found that the design of splice length of an individual bar within a bundle based on a design stress increased by 20% and 33% for two- and three-bar bundles, respectively, would provide reasonable results.

- Providing transverse reinforcement along the splice zone could improve the failure loads and the reinforcement stress at failure. In addition, the maximum crack width at the end of splice and the average crack width within the flexural span of GFRP RC beams were significantly reduced after implementing the transverse reinforcement.
- Regardless of the amount of transverse reinforcement, the companion beams with identical configurations of tension reinforcement had flexural cracks on similar depth. The beams with increased transverse reinforcement, however, developed a similar or greater number of flexural cracks within the splice zone and the constant-moment span.
- Increasing the reinforcement ratio always resulted in reducing the depth of flexural cracks and raising the number of cracks within the constant-moment span.
- The splice strength of bundled GFRP bars was not dependent on the clear concrete cover (c) for$c/d_b > 2.5$, where d_b is the bar diameter.
- Based on the strain measurements, the steel transverse reinforcement could effectively contribute to the splice strength. Providing 10M stirrups at 250 and 125 *mm* intervals enhanced the splice strength of two-bar bundles of No.5 bars by 32% and 55%, respectively. Moreover, providing 10M stirrups at 125 *mm* intervals improved the splice strength of single bars and three-bar bundles of No.4 bars by 21% and 48%, respectively.
- The ratio of splice strength of bundled bars to single bars rose from 0.80 in the unconfined specimens to 0.98 in the specimens with transverse reinforcement within spice zone.

- Based on the experimental findings, the contribution of transverse reinforcement (T_s) to the total strength of spliced bundled GFRP bars, was predicted accurately using the semi-empirical model proposed by Zuo and Darwin (2000). Therefore, this model was used as the basis for deriving a relationship to account for the contribution of transverse reinforcement (GFRP and steel) to the overall bond strength of lap splices of bundled sand-coated GFRP bars.

7.3. Recommendations for Future Work

Despite the contribution made by this research study, further experimental investigations should be carried out to elaborate the following remarks:

1. A finite element model should be developed using the obtained experimental results to evaluate the influence of various parameters.
2. As mentioned earlier, the staggered specimens were not completely in accordance with the recommendations stipulated in major design codes and guidelines as the minimum staggering space of $45d_b$ was not complied with in this study due to the limitations in specimen size. Although this configuration might lead to conservative results, considering the code recommendations might influence the ratio of the bond strength of single to bundled bars.
3. It is also recommended to conduct more experimental investigations on the splice strength of non-staggered splices due to the simplicity they can add to both detailing and caging of reinforcement in the real field applications.
4. FRP bars are being produced with different types of fibers (i.e., carbon, glass, aramid, and basalt) and surface deformations (e.g., sand coated, braided, helically wrapped, ribbed, and indented surfaces). Thus, future work should be directed toward understanding the effect of surface treatment and material properties on the bond behavior of bundled GFRP bars.
5. The applicability of the design recommendations made herein to the FRP bars should be evaluated for other surface treatments and types of fibers.
6. The effect of concrete type and strength also needs to be evaluated.

7. Further experimental investigation is needed to study the effect of modulus of elasticity of transverse reinforcement (GFRP, CFRP, and steel), and concrete cover ($c/d_b < 2.5$) on the splice strength of bundled GFRP bars.

7.4. Conclusions

Les conclusions suivantes peuvent être tirées sur la base des études expérimentales et analytiques menées dans le cadre de ce programme de recherche :

- Le décalage avait un effet négligeable sur la rigidité de la poutre. Cependant, il pourrait augmenter la résistance du chevauchement, en particulier dans le cas de trois barres groupées. Il a permis également de réduire l'ouverture maximale des fissures.
- Sur la base des mesures de déformations, toutes les barres groupées ne pouvaient pas agir comme une seule entité, car il y avait des déplacements relatifs entre elles.
- La théorie de la flexion élastique pourrait fournir de bonnes prévisions sur la rigidité avant la fissuration ainsi que la charge de fissuration. De plus, la détermination de la profondeur de l'axe neutre ainsi que les armatures et les déformations du béton sur la base d'une analyse moment-courbure ont montré des résultats fiables par rapport à ceux mesurés expérimentalement.
- La résistance du chevauchement diminuait avec l'augmentation du nombre de barres groupées. En moyenne, les rapports entre la résistance d'adhérence des barres groupées et celle des barres non groupées étaient respectivement de 85 % et 82 % pour les groupes de deux et trois barres.
- Bien que la résistance d'adhérence d'une seule barre du groupe de barres soit inférieure à celle d'une barre unique non groupée, leur comportement général était similaire, notamment en termes de longueur de chevauchement, de diamètre de barre et de répartition des contraintes sur la longueur de chevauchement.
- Une augmentation du diamètre de la barre pourrait augmenter la rigidité des poutres après fissuration. De plus, le patron de fendage des poutres renforcées avec des barres n° 8 était différent de celui des poutres avec des barres d'armature n° 5 et n° 4.

- L'augmentation de la longueur de chevauchement peut augmenter à la fois la contrainte dans les armatures et la charge de rupture. Cependant, l'effet de la longueur de chevauchement diminue avec l'augmentation de la longueur de chevauchement et du diamètre de la barre. Cela confirme clairement que l'utilisation de pratiques de conception reposant sur le concept d'une relation proportionnelle entre la force d'adhérence et la longueur de chevauchement impliquerait une diminution du niveau de sécurité en augmentant la longueur de chevauchement. De plus, les patrons de fissuration de fendage étaient similaires pour les spécimens renforcés avec des barres groupées de même diamètre, mais avec des longueurs de chevauchement différentes. Les charges de fissuration des spécimens avec des chevauchements plus longs étaient légèrement plus élevées à celles avec des chevauchements plus courts. De plus, l'augmentation de la longueur de chevauchement avait un effet négligeable sur la rigidité en flexion des poutres.
- Les poutres renforcées avec des barres ayant des chevauchements plus longs présentaient des fissures légèrement plus étroites que celles ayant des chevauchements plus courts. Ce constat pourrait révéler un glissement plus faible des barres dans le cas des chevauchements plus longs.
- Pour une longueur de chevauchement donnée et un niveau similaire de confinement par le béton environnant, la force totale requise pour la rupture par fendage ($F_{test,n}$) s'est avérée être fonction de l'aire des barres en PRFV groupées. Cependant, l'augmentation de $F_{test,n}$ était inférieure à l'augmentation de l'aire de la barre, ce qui pourrait indiquer qu'une barre de plus grand diamètre nécessitait une plus grande longueur de chevauchement pour développer pleinement une contrainte de barre donnée.
- Sur la base des résultats des essais expérimentaux, il a été recommandé l'application des facteurs incrémentaux aux contraintes de calcul afin de compenser plus efficacement la relation non linéaire longueur de chevauchement-résistance. Au lieu des facteurs de modification de longueur disponibles dans la norme CSA S806-12 et jusqu'à ce que davantage de résultats expérimentaux soient disponibles, les facteurs d'amplification de contrainte de calcul de 1,2 et 1,33 peuvent être utilisés respectivement pour des groupes

à deux et trois barres. Notez que disposer d'équation de conception qui prend en considération une relation non linéaire entre la contrainte de conception et la longueur de chevauchement dans le cas de jonctions simples est une condition préalable essentielle de cette recommandation. En tenant compte des dispositions de conception de l'ACI 440.1R-15, il a été constaté que la conception de la longueur de chevauchement d'une barre individuelle dans un groupe de barres basée sur la contrainte de conception augmentait respectivement de 20 % et de 33 % pour les groupes de deux et trois barres, fournissant ainsi des résultats raisonnables.

- La présence d'armatures transversales le long de la zone de chevauchement pourrait augmenter les charges de rupture et la contrainte dans les armatures lors de la rupture. En outre, l'ouverture maximale des fissures à la fin du chevauchement et l'ouverture moyenne des fissures dans la travée de flexion des poutres en béton armé de PRFV ont été considérablement réduites après la mise en place d'armatures transversales.
- Indépendamment de la quantité des armatures transversales, les profondeurs des fissures de flexion apparaissant sur les poutres ayant une configuration identique de renforcement en traction étaient similaires. Cependant, les poutres ayant plus d'armatures transversales ont développé un nombre similaire ou un nombre plus grand de fissures de flexion dans la zone de chevauchement et dans la zone moment constant.
- L'augmentation du taux d'armature a toujours entraîné une réduction de la profondeur des fissures de flexion et une augmentation du nombre de fissures dans la zone de moment constant.
- La résistance de chevauchement des barres en PRFV groupées ne dépendait pas de l'enrobage du béton (c) pour $c/d_b > 2.5$, où d_b est le diamètre de la barre.
- Sur la base des mesures de déformations, les armatures transversales en acier pourraient contribuer efficacement à la résistance du chevauchement. L'utilisation d'étriers 10M espacés de 250 mm et 125 mm améliorait la résistance du chevauchement du groupe de deux barres n° 5 de 32 % et 55 %, respectivement. De plus, l'utilisation d'étriers 10M à intervalles de 125 mm améliorait la résistance de chevauchement d'une barre unique non groupée et de trois barres groupées n° 4 respectivement de 21 % et 48 %.

- Le rapport entre la résistance de chevauchement des barres groupées et des barres individuelles non groupées a été amélioré, passant de 0,80 dans les spécimens non confinés à 0,98 dans les spécimens avec armatures transversales dans la zone de recouvrement.
- Sur la base des résultats expérimentaux, la contribution des armatures transversales (T_s) à la résistance totale des barres de PRFV groupées avec chevauchement a été prédite avec précision à l'aide du modèle semi-empirique proposé par Zuo et Darwin (2000). Ce modèle a ainsi été utilisé comme base pour établir une relation tenant compte de la contribution des armatures transversales (PRFV et acier) à la force d'adhérence globale des jonctions par chevauchement de barres groupées en PRFV revêtues de sable.

7.5. Recommandations pour des travaux futurs

En dépit de la contribution apportée par cette étude, des recherches expérimentales supplémentaires devraient être menées pour étudier les remarques suivantes:

1. Un modèle d'éléments finis devrait être développé en utilisant les résultats expérimentaux obtenus pour évaluer l'influence de divers paramètres.
2. Comme mentionné précédemment, les spécimens décalés n'étaient pas complètement conformes aux recommandations stipulées dans les principaux codes et directives de conception, car le décalage minimal de $45d_b$ n'était pas respecté dans cette étude en raison des limitations de la taille de l'échantillon. Bien que cette configuration puisse conduire à des résultats conservateurs, le fait de respecter les recommandations des codes pourrait influer sur le rapport entre la résistance d'adhérence des barres uniques non groupées et celle des barres groupées.
3. Il est également recommandé de mener davantage d'études expérimentales sur la résistance de chevauchement non décalés en raison de la simplicité qu'ils peuvent ajouter aux détails et à la mise place des armatures dans des applications réelles sur le terrain.
4. Les barres en PRF sont produites avec différents types de fibres (carbone, verre, aramide et basalte) et de finis de surface (surfaces revêtues de sable, tressées,

enveloppées en hélice, nervurées et dentelées). Ainsi, les travaux futurs devraient viser à comprendre l'effet du fini de surface et des propriétés des matériaux sur l'adhérence des barres en PRFV groupées.

5. L'applicabilité des recommandations de conception formulées ici aux barres en PRF doit être évaluée pour d'autres finis de surface et types de fibres.
6. L'effet du type et de la résistance du béton doit également être évalué.
7. Une étude expérimentale supplémentaire est nécessaire pour étudier l'effet du module d'élasticité des armatures transversales (PRFV, PRFC et acier) et de l'enrobage du béton ($c/d_b < 2.5$) sur la résistance du chevauchement des barres en PRFV groupées.

REFERENCES

AASHTO-LRFD. (2012). Bridge design specifications: American Association of State Highway and Transportation Officials, Washington, DC.

Achillides, Z., & Pilakoutas, K. (2004). Bond Behavior of Fiber Reinforced Polymer Bars under Direct Pullout Conditions. *Journal of Composites for Construction, 8*(2), 173-181. doi:10.1061/(ASCE)1090-0268(2004)8:2(173)

ACI 408 Committee. (2003). Bond and Development of Straight Reinforcing Bars in Tension (ACI 408R-03). *American Concrete Institute, Detroit, Michigan, US*.

ACI Committee 318. (1963). Building Code Requirements for Reinforced Concrete (ACI 318-63) (pp. 144). Farmington Hills, Mich.: American Concrete Institute.

ACI Committee 318. (2014). Building Code Requirements for Structural Concrete (ACI 318-14) and Commentary (ACI 318R-14). Farmington Hills, Mich.: American Concrete Institute.

ACI Committee 440. (2006). Guide for the design and construction of structural concrete reinforced with FRP bars (ACI 440.1R-06). Farmington Hills, Michigan, USA: American Concrete Institute.

ACI Committee 440. (2015). Guide for the Design and Construction of Structural Concrete Reinforced with Fiber-Reinforced Polymer (FRP) Bars (ACI 440.1R-15). Farmington Hills, Michigan, USA: American Concrete Institute.

Aly, R. (2005). *Experimental and analytical studies on bond behaviour of tensile lap spliced FRP reinforcing bars in concrete.* (PhD), University of Sherbrooke, Sherbrooke, QC, CA.

Aly, R., Benmokrane, B., & Ebead, U. (2006a). Tensile Lap Splicing of Bundled CFRP Reinforcing Bars in Concrete. *Journal of Composites for Construction, 10*(4), 287-294. doi:10.1061/(asce)1090-0268(2006)10:4(287)

Aly, R., Benmokrane, B., & Ebead, U. (2006b). Tensile Lap Splicing of Fiber-Reinforced Polymer Reinforcing Bars in Concrete. *ACI Structural Journal, 103*(6), 857-864. doi:10.14359/18239

Atorod Azizinamini, Pavel, R., Hatfield, E., & Ghosh, S.K. (1999). Behavior of Lap-Spliced Reinforcing Bars Embedded in High-Strength Concrete. *ACI Structural Journal, 96*(5). doi:10.14359/737

Bashandy, T.R. (2009). Evaluation of Bundled Bar Lap Splices. *ACI Structural Journal, 106*(2), 215-221. doi:10.14359/56360

BS EN 1992-1-1:2004. (2004). Eurocode 2: Design of Concrete Structures-Part 1-1: General Rules and Rules for Buildings, (pp. 225). British Standards Institution, London, UK: British Standards Institution.

Cairns, J. (2013). Lap Splices of Bars in Bundles. *ACI Structural Journal, 110*(2). doi:10.14359/51684399

Canadian Standards Association. (2012). Design and Construction of Building Structures with Fiber Reinforced Polymers (CAN/CSA S806-12). Ontario, Canada: Canadian Standards Association.

Canadian Standards Association. (2014a). Canadian Highway Bridge Design (CAN/CSA S6-14) (pp. 875). Ontario, Canada: CSA Group.

Canadian Standards Association. (2014b). Design of concrete structures (CAN/CSA A23.3-14). Ontario, Canada: Canadian Standards Association.

Choi, D.-U., Chun, S.-C., & Ha, S.-S. (2012). Bond strength of glass fibre-reinforced polymer bars in unconfined concrete. *Engineering Structures, 34*(0), 303-313. doi:10.1016/j.engstruct.2011.08.033

Darwin, D., Dolan, C.W., & Nilson, A.H. (2011). *Design of concrete structures*: McGraw-Hill, New York.

Darwin, D., L. McCabe, S., K. Idun, E., & P. Schoenekase, S. (1992). Development Length Criteria: Bars Not Confined by Transverse Reinforcement. *ACI Structural Journal, 89*(6). doi:10.14359/4158

Darwin, D., Lutz, L.A., & Zuo, J. (2005). Recommended Provisions and Commentary on Development and Lap Splice Lengths for Deformed Reinforcing Bars in Tension. *ACI Structural Journal, 102*(6), 892-900. doi:10.14359/14798

Darwin, D., Tholen, M.L., K. Idun, E., & Zuo, J. (1996). Splice Strength of High Relative Rib Area Reinforcing Bars. *ACI Structural Journal, 93*(1). doi:10.14359/9680

Darwin, D., Zuo, J., L. Tholen, M., & K. ldun, E. (1996). Development Length Criteria for Conventional and High Relative Rib Area Reinforcing Bars. *ACI Structural Journal, 93*(3). doi:10.14359/9694

El-Nemr, A., Ahmed, E.A., El-Safty, A., & Benmokrane, B. (2018). Evaluation of the flexural strength and serviceability of concrete beams reinforced with different types of GFRP bars. *Engineering Structures, 173*, 606-619. doi:10.1016/j.engstruct.2018.06.089

Esfahani, M.R., Rakhshanimehr, M., & Mousavi, S.R. (2013). Bond Strength of Lap-Spliced GFRP Bars in Concrete Beams. *Journal of Composites for Construction, 17*(3), 314-323. doi:10.1061/(asce)cc.1943-5614.0000359

Hadley, H.M. (1952). "Bundled" Reinforcement. *Journal of the American Concrete Institute, 49*, 157-159.

Hanson, N.W., & Reifenstuhl, H. (1958). Concrete Beams and Columns with Bundled Reinforcement. *Journal of the Structural Division, 84*(6), 1-23.

Harajli, M., & Abouniaj, M. (2010). Bond Performance of GFRP Bars in Tension: Experimental Evaluation and Assessment of ACI 440 Guidelines. *Journal of Composites for Construction, 14*(6), 659-668. doi:10.1061/(asce)cc.1943-5614.0000139

Harajli, M.H., Hamad, B.S., & Rteil, A.A. (2004). Effect of Confinement on Bond Strength between Steel Bars and Concrete. *ACI Structural Journal, 101*(5). doi:10.14359/13381

Hognestad, E. (1951). *Study of combined bending and axial load in reinforced concrete members*. Retrieved from http://hdl.handle.net/2142/4360

Japan Society of Civil Engineers. (1997). Recommendation for Design and Construction of Concrete Structures Using Continuous Fiber Reinforcing Materials (pp. 1-64).

Jirsa, J.O., Chen, W.-L., Grant, D., & Elizondo, R. (1995). *Development of bundled reinforcing steel*. Retrieved from Report No.1363-2F, Center for Transportation Research, University of Texas at Austin, Austin, TX,:

Larralde, J., & Silva-Rodriguez, R. (1993). Bond and slip of FRP rebars in concrete. *Journal of Materials in Civil Engineering, 5*(1), 30-40.

Martí-Vargas, J.R. (2015). Bond Strength of Spliced Fiber-Reinforced Polymer Reinforcement. *ACI Structural Journal, 112*(1), 115.

Mazaheripour, H., Barros, J.A., Sena-Cruz, J., Pepe, M., & Martinelli, E. (2013). Experimental study on bond performance of GFRP bars in self-compacting steel fiber reinforced concrete. *Composite Structures, 95*, 202-212.

Mosley, C.P., Tureyen, A.K., & Frosch, R.J. (2008). Bond Strength of Nonmetallic Reinforcing Bars. *ACI Structural Journal, 105*(5), 634-642. doi:10.14359/19947

Nanni, A. (1993). Flexural Behavior and Design of RC Members Using FRP Reinforcement. *Journal of Structural Engineering, 119*(11), 3344-3359. doi:10.1061/(asce)0733-9445(1993)119:11(3344)

Orangun, C., Jirsa, J., & Breen, J. (1975). *The Strength of Anchor Bars: A Reevaluation of Test Data on Development Length and Splices*. Retrieved from The University of Texas at Austin, Austin, Texas:

Orangun, C.O., Jirsa, J.O., & Breen, J.E. (1977). A Reevaulation of Test Data on Development Length and Splices. *ACI Journal Proceedings, 74*(3), 114-122. doi:10.14359/10993

Pay, A.C., Canbay, E., & Frosch, R.J. (2014). Bond Strength of Spliced Fiber-Reinforced Polymer Reinforcement. *ACI Structural Journal, 111*(2). doi:10.14359/51686519

Pecce, M., Manfredi, G., Realfonzo, R., & Cosenza, E. (2001). Experimental and Analytical Evaluation of Bond Properties of GFRP Bars. *Journal of Materials in Civil Engineering, 13*(4), 282-290. doi:10.1061/(ASCE)0899-1561(2001)13:4(282)

Retika, A.C., Shield, C., & French, C. (1997). Thermal and Mechanical Fatigue Effects On GFRP Rebar-Concrete Bond.

Tekle, B.H., Khennane, A., & Kayali, O. (2017). Bond of spliced GFRP reinforcement bars in alkali activated cement concrete. *Engineering Structures, 147*(Supplement C), 740-751. doi:10.1016/j.engstruct.2017.06.040

Tepfers, R. (1973). *A Theory of Bond Applied to Overlapped Tensile Reinforcement Splices for Deformed Bars*. Goteborg: Chalmers University of Technology, Division of Concrete Structures.

Tepfers, R. (1979). Cracking of Concrete Cover along Anchored Deformed Reinforcing Bars. *Magazine of Concrete Research, 31*(106), 3-12.

Tepfers, R. (1982). Lapped Tensile Reinforcement Splices. *Journal of the Structural Division, 108*(1), 283-301.

Tepfers, R., & De Lorenzis, L. (2003). Bond of FRP Reinforcement in Concrete - a Challenge. *Mechanics of Composite Materials, 39*(4), 315-328. doi:10.1023/A:1025642411103

Tepfers, R., Hedlund, G., & Rosinski, B. (1998). Pull-out and tensile reinforcement splice tests with GFRP bars. *Second International Conference on Composites in Infrastructure, 2*.

Tighiouart, B., Benmokrane, B., & Gao, D. (1998). Investigation of bond in concrete member with fibre reinforced polymer (FRP) bars. *Construction and Building Materials, 12*(8), 453-462. doi:10.1016/s0950-0618(98)00027-0

Tighiouart, B., Benmokrane, B., & Mukhopadhyaya, P. (1999). Bond strength of glass FRP rebar splices in beams under static loading. *Construction and Building Materials, 13*(7), 383-392. doi:10.1016/s0950-0618(99)00037-9

Wambeke, B.W., & Shield, C.K. (2006). Development Length of Glass Fiber-Reinforced Polymer Bars in Concrete. *ACI Structural Journal, 103*(1). doi:10.14359/15081

Wight, J.K., & MacGregor, J.G. (2011). *Reinforced Concrete: Mechanics and Design (Sixth Edition)*: Pearson Education, Inc., Upper Saddle River, New Jersey 07458.

Zemour, N., Asadian, A., Ahmed, E.A., Khayat, K.H., & Benmokrane, B. (2018). Experimental study on the bond behavior of GFRP bars in normal and self-consolidating concrete. *Construction and Building Materials, 189*, 869-881. doi:10.1016/j.conbuildmat.2018.09.045

Zuo, J., & Darwin, D. (2000). Splice strength of conventional and high relative rib area bars in normal and high-strength concrete. *ACI Structural Journal, 97*(4). doi:10.14359/7428